Multiresolution Modeling for Traffic Analysis: Case Studies Report

PUBLICATION NO. FHWA-HRT-22-054

FEBRUARY 2022

U.S. Department of Transportation
Federal Highway Administration

Research, Development, and Technology
Turner-Fairbank Highway Research Center
6300 Georgetown Pike
McLean, VA 22101-2296

FOREWORD

Multiresolution modeling (MRM) is capable of producing great insights into the complex mobility challenges associated with surface transportation. However, the lack of available case studies may present a barrier to MRM adoption by transportation agencies. This case studies report provides a blueprint of the successful pilot studies conducted during and within the MRM project. This report also provides lessons learned for agencies to overcome barriers to MRM adoption. These findings will provide an important point for future advancement in the research, development, and application of MRM in transportation engineering. This case studies report is a precursor to the final MRM report, which will propose a recommended MRM methodology. Ultimately, both reports will be of interest to State and local departments of transportation that are interested in advancing their traffic analysis capabilities.

Brian P. Cronin, P.E.
Director, Office of Safety and Operations
Research and Development

Notice

This document is disseminated under the sponsorship of the U.S. Department of Transportation in the interest of information exchange. The U.S. Government assumes no liability for the use of the information contained in this document.

The U.S. Government does not endorse products or manufacturers. Trademarks or manufacturers' names appear in this report only because they are considered essential to the objective of the document.

Quality Assurance Statement

The Federal Highway Administration (FHWA) provides high-quality information to serve Government, industry, and the public in a manner that promotes public understanding. Standards and policies are used to ensure and maximize the quality, objectivity, utility, and integrity of its information. FHWA periodically reviews quality issues and adjusts its programs and processes to ensure continuous quality improvement.

Recommended citation: Federal Highway Administration, *Multiresolution Modeling for Traffic Analysis: Case Studies Report* (Washington, DC: 2022) https://doi.org/10.21949/1521855

TECHNICAL REPORT DOCUMENTATION PAGE

1. Report No. FHWA-HRT-22-054	2. Government Accession No.	3. Recipient's Catalog No.
4. Title and Subtitle Multiresolution Modeling for Traffic Analysis: Case Studies Report		5. Report Date February 2022
		6. Performing Organization Code
7. Author(s) Mohammed Hadi (0000-0003-2233-8283), Xuesong (Simon) Zhou (0000-0002-9963-5369), David Hale (0000-0001-5486-9367)		8. Performing Organization Report No.
9. Performing Organization Name and Address		10. Work Unit No. (TRAIS)
Leidos Inc. 11251 Roger Bacon Drive Reston, VA 20190		11. Contract or Grant No. DTFH6116D00030-693JJ319F000376
12. Sponsoring Agency Name and Address U.S. Department of Transportation Federal Highway Administration 1200 New Jersey Avenue, SE Washington, DC 20590		13. Type of Report and Period Covered Report; September 2020–July 2021
		14. Sponsoring Agency Code HRSO-50
15. Supplementary Notes The government task manager was Hyungjun Park (0000-0002-6627-6857).		
16. Abstract The Federal Highway Administration (FHWA) and Traffic Analysis and Simulation Pooled Fund Study sponsored a research project on multiresolution modeling (MRM). The project intends to develop consistent definitions and a unified modeling framework for transportation professionals to help them better understand the opportunities and challenges associated with MRM. During the early stages of the project, stakeholders reported that the lack of available case studies presented a barrier to MRM adoption by transportation agencies. This case studies report provides a blueprint of the successful pilot studies conducted during and within the MRM project. The report also provides lessons learned for agencies to overcome barriers to MRM adoption. These findings will provide an important point for future advancement in the research, development, and application of MRM in transportation engineering.		
17. Key Words Multiresolution modeling, microscopic simulation, microsimulation, mesoscopic simulation, dynamic traffic assignment, travel demand model, activity-based model, simulation-based assignment, static assignment, traffic assignment, origin-destination matrix estimation		18. Distribution Statement No restrictions. This document is available to the public through the National Technical Information Service, Springfield, VA 22161. http://www.ntis.gov

19. Security Class if. (of this report) Unclassified	20. Security Class if. (of this page) Unclassified	21. No. of Pages 101	22. Price n/a

Form DOT F 1700.7 (8-72) Reproduction of completed page authorized

SI* (MODERN METRIC) CONVERSION FACTORS

APPROXIMATE CONVERSIONS TO SI UNITS

Symbol	When You Know	Multiply By	To Find	Symbol
		LENGTH		
in	inches	25.4	millimeters	mm
ft	feet	0.305	meters	m
yd	yards	0.914	meters	m
mi	miles	1.61	kilometers	km
		AREA		
in^2	square inches	645.2	square millimeters	mm^2
ft^2	square feet	0.093	square meters	m^2
yd^2	square yard	0.836	square meters	m^2
ac	acres	0.405	hectares	ha
mi^2	square miles	2.59	square kilometers	km^2
		VOLUME		
fl oz	fluid ounces	29.57	milliliters	mL
gal	gallons	3.785	liters	L
ft^3	cubic feet	0.028	cubic meters	m^3
yd^3	cubic yards	0.765	cubic meters	m^3
		NOTE: volumes greater than 1,000 L shall be shown in m^3		
		MASS		
oz	ounces	28.35	grams	g
lb	pounds	0.454	kilograms	kg
T	short tons (2,000 lb)	0.907	megagrams (or "metric ton")	Mg (or "t")
		TEMPERATURE (exact degrees)		
°F	Fahrenheit	5 (F-32)/9 or (F-32)/1.8	Celsius	°C
		ILLUMINATION		
fc	foot-candles	10.76	lux	lx
fl	foot-Lamberts	3.426	$candela/m^2$	cd/m^2
		FORCE and PRESSURE or STRESS		
lbf	poundforce	4.45	newtons	N
lbf/in^2	poundforce per square inch	6.89	kilopascals	kPa

APPROXIMATE CONVERSIONS FROM SI UNITS

Symbol	When You Know	Multiply By	To Find	Symbol
		LENGTH		
mm	millimeters	0.039	inches	in
m	meters	3.28	feet	ft
m	meters	1.09	yards	yd
km	kilometers	0.621	miles	mi
		AREA		
mm^2	square millimeters	0.0016	square inches	in^2
m^2	square meters	10.764	square feet	ft^2
m^2	square meters	1.195	square yards	yd^2
ha	hectares	2.47	acres	ac
km^2	square kilometers	0.386	square miles	mi^2
		VOLUME		
mL	milliliters	0.034	fluid ounces	fl oz
L	liters	0.264	gallons	gal
m^3	cubic meters	35.314	cubic feet	ft^3
m^3	cubic meters	1.307	cubic yards	yd^3
		MASS		
g	grams	0.035	ounces	oz
kg	kilograms	2.202	pounds	lb
Mg (or "t")	megagrams (or "metric ton")	1.103	short tons (2,000 lb)	T
		TEMPERATURE (exact degrees)		
°C	Celsius	1.8C+32	Fahrenheit	°F
		ILLUMINATION		
lx	lux	0.0929	foot-candles	fc
cd/m^2	candela/m2	0.2919	foot-Lamberts	fl
		FORCE and PRESSURE or STRESS		
N	newtons	2.225	poundforce	lbf
kPa	kilopascals	0.145	poundforce per square inch	lbf/in^2

*SI is the symbol for International System of Units. Appropriate rounding should be made to comply with Section 4 of ASTM E380. (Revised March 2003)

TABLE OF CONTENTS

CHAPTER 1. INTRODUCTION 1
Scope 2
Identified Gaps 2
Report Structure 7
CHAPTER 2. WEST PALM BEACH DOWNTOWN CASE STUDY 9
Network Description 9
Model Overview 10
Data Description 12
Analysis Details 13
O-D Demand Estimation (Gap 2.3 and Gap 3.2) 13
Performance Measure Definitions (Gap 2.1 and Gap 2.2) 24
Performance Measure Consistency (Gap 2.4 and Gap 3.6) 27
Benefit of MRM (Gap 3.6 and Gap 6.1) 37
Cost and Time Requirements (Gap 1.3) 42
Model Archiving and Maintenance (Gap 1.4) 43
Model Conversion Effectiveness (Gap 3.1) 43
Impacts of Advanced Applications (Gap 3.4) 43
Collaboration Assessment (Gap 5.1 and Gap 5.2) 43
Summary 43
Demand Estimation 44
Impact of Assignment Method 44
Performance Measure Consistency 45
CHAPTER 3. PHOENIX METROPOLITAN AREA CASE STUDY 47
Network Description 47
Model Overview 49
Integration of ABM and Regional Traffic Assignment 49
Traffic Assignment Periods 51
Data Description 51
Analysis Details 52
Model Conversion Effectiveness (Gap 3.1) 53
Performance Measure Consistency (Gap 2.4) 53
Performance Measure Definitions (Gap 2.1 and Gap 2.2) 54
Feedback Loop (Gap 3.6) 59
Cost and Time Requirements (Gap 1.3) 59
Analysis Results 61
Summary 68
CHAPTER 4. MARYLAND I–95 NETWORK 69
Network Description 69
Model Overview 70
Data Description 70
Analysis Details 70
Model Conversion Effectiveness (Gap 3.1) 71

Enhancement of Tools (Gap 3.2) 75
Performance Measure Consistency (Gap 2.4 and Gap 3.6) 76
Signal Timing Methods and Tools (Gap 3.1 and Gap 3.2) 77
Benefit of MRM (Gap 3.6 and Gap 6.1) 78
Multimodal Modeling (Gap 3.3) 78
Cost and Time Requirements (Gap 1.3) 79
Analysis Results 79
Summary 80
CHAPTER 5. CONCLUSION 81
West Palm Beach Lessons Learned 81
Phoenix Lessons Learned 82
Maryland Lessons Learned 82
ACKNOWLEDGMENTS 83
REFERENCES 85

LIST OF FIGURES

Figure 1. Map. Expanded Palm Beach area (OpenStreetMap A). 10
Figure 2. Bar Chart. Link and turn deviations with different weight ratios..... 16
Figure 3. Graph. Turn volume deviation when putting no weight on the counts. 17
Figure 4. Graph. Link volume deviation when putting no weight on the counts. 17
Figure 5. Graph. Turn volume deviation when putting no weight on the seed matrix. 18
Figure 6. Graph. Link volume deviation when putting no weight on the seed matrix. 18
Figure 7. Graph. Turn volume deviation when putting 0.5 weight ratio on the seed matrix. 19
Figure 8. Graph. Link volume deviation when putting 0.5 weight ratio on the seed matrix. 19
Figure 9. Graph. Turn volume deviation when putting a weight ratio of 10 on the seed matrix. 20
Figure 10. Graph. Link volume deviation when putting a weight ratio of 10 on the seed matrix. 20
Figure 11. Scatterplot. Examination of volumes to the top 10 destinations for zone 40. 24
Figure 12. Equation. BPR volume-delay function. 25
Figure 13. Scatterplot. Comparison of the BPR curve derived from simulation models with those used in the demand forecasting model and base macroscopic model. 29
Figure 14. Graph. V/c ratio versus delay for Okeechobee Boulevard at South Tamarind Avenue intersection (EB approach). 31
Figure 15. Graph. V/c ratio versus delay for Okeechobee Boulevard at South Tamarind Avenue intersection (WB approach) 32
Figure 16. Graph. V/c ratio versus delay for Okeechobee Boulevard at South Tamarind Avenue intersection (SB approach)..... 32
Figure 17. Graph. V/c ratio versus delay for Okeechobee Boulevard at South Tamarind Avenue intersection (NB approach). 33
Figure 18. Graph. V/c ratio versus delay for Okeechobee Boulevard at South Tamarind Avenue intersection after extending the left-turn bay length (NB direction). 33
Figure 19. Graph. Relationship between the major street movement volume and minor street capacity according to different models. 35
Figure 20. Graph. Relationship between the minor street v/c ratio and delay according to different models. 35
Figure 21. Bar Chart. Total travel time in the critical links for static assignment with and without BPR model calibration. 36
Figure 22. Bar Chart. Critical link average travel time for static assignment with and without BPR model calibration. 37
Figure 23. Maps. Paths resulting from static traffic assignment with and without development (OpenStreetMap B). 39
Figure 24. Maps. Paths resulting from SBA with and without development (OpenStreetMap B). 40
Figure 25. Bar Chart. Network-wide travel time for STAs and SBAs with and without development. 41
Figure 26. Bar Chart. Changes in average travel time on critical links due to new development. 41
Figure 27. Bar Chart. Comparison of network-wide latent demands with and without new development. 42

Figure 28. Map. GMNS for the Phoenix area (OpenStreetMap C). 48
Figure 29. Map. Observed link volume for the Phoenix network. 52
Figure 30. Flowchart. Integrated supply-side calibration process. 54
Figure 31. Graph. Regimes in the speed versus v/c ratio coordinate plane. 55
Figure 32. Graph. Derived queued demand when congestion duration is less than 1 h. 56
Figure 33. Graph. Derived queued demand when congestion duration exceeds 1 h. 57
Figure 34. Equation. QDF formula. 57
Figure 35. Scatterplot. Volume-delay function calibration results for the Phoenix network. 58
Figure 36. Flowchart. ABM and DTA integration. 59
Figure 37. Graph. Calibrated speed-density relationship using data from freeways in the CBD (dataset 1). 61
Figure 38. Graph. Calibrated volume-density relationship using data from freeways in the CBD (dataset 1). 62
Figure 39. Graph. Calibrated speed-volume relationship using data from freeways in the CBD (dataset 1). 62
Figure 40. Graph. Calibrated speed-density relationship using data from freeways in the CBD (dataset 2). 63
Figure 41. Graph. Calibrated volume-density relationship using data from freeways in the CBD (dataset 2). 63
Figure 42. Graph. Calibrated speed-volume relationship using data from freeways in the CBD (dataset 2). 64
Figure 43. Graph. Comparison of observations and assignment results to assess possible demand-side or supply-side estimation errors. 68
Figure 44. Map. Maryland I–95 network (OpenStreetMap D). 69
Figure 45. Map. Mesoscopic network representation near node 10643 (OpenStreetMap E). 71
Figure 46. Map. Microscopic network representation near node 10643 (OpenStreetMap E). 72
Figure 47. Illustration. Automated consolidation of complex intersections from OpenStreetMap. 73
Figure 48. Map. Maryland network with points of interest (OpenStreetMap D). 73
Figure 49. Illustrations. Multiresolution network representations. 75
Figure 50. Screenshot. Field-measured speed heat map in the CBI tool. 77
Figure 51. Equation. WMSE formula. 79

LIST OF TABLES

Table 1. Overview of case study information. 4
Table 2. Comparison of Tamarind–Okeechobee intersection volumes with different ODME parameters. 22
Table 3. Comparison of Banyan–Tamarind intersection volumes with different ODME parameters. 22
Table 4. Comparison of Banyan Boulevard at North Dixie Highway intersection volumes with different ODME parameters. 23
Table 5. Comparison of Lakeview Avenue at North Dixie Highway intersection volumes with different ODME parameters. 23
Table 6. Comparison of capacities derived from simulation with those used in the demand forecasting models and the base macroscopic model. 29
Table 7. Estimated capacities of Okeechobee Boulevard at South Tamarind Avenue intersection using different methods. 30
Table 8. Impact of conflicting flow rate on minor-street capacity for a two-way, stop-controlled intersection. 34
Table 9. Default and updated gap acceptance parameter values in the SBA model. 34
Table 10. Volume-delay function codes with AT and FT for a systematic assessment of data availability and data needs (gap 2.3). 48
Table 11. Inputs and outputs of activity-based and DTA models in the MAG case study. 49
Table 12. Travel activity characteristics produced by the ABM. 50
Table 13. Calibrated traffic stream model parameters for different datasets. 64
Table 14. MAPE of volume for dataset 1. 65
Table 15. MAPE of volume for dataset 2. 65
Table 16. MAPE of speed for dataset 1. 66
Table 17. MAPE of speed for dataset 2. 66
Table 18. Suggested performance measures for the traffic assignment validation step. 67
Table 19. Maryland traffic network statistics for different modeling resolutions. 70
Table 20. AMS workflow process involving the GMNS. 76
Table 21. Traffic count calibration results for the Maryland case study. 80
Table 22. Travel time calibration results for the Maryland case study. 80

LIST OF ABBREVIATIONS AND ACRONYMS

α	alpha
.mtx	matrix
a.m.	ante meridiem
ABM	activity-based model
AMS	analysis, modeling, and simulation
AT	area type
AV	automated vehicle
Ave	avenue
β	Bureau of Public Roads exponential coefficient
B	beta
Blvd	boulevard
BPR	Bureau of Public Roads
c	link capacity
C/D	collector-distributor
CBD	central business district
CBI	congestion and bottleneck identification
CMM	capability maturity model
CSV	comma-separated values
D	volume within the congestion period
D_h	volume within the peak hour
Dr	drive
D/C	demand-over-capacity
DTA	dynamic traffic assignment
EB	eastbound
EBL	eastbound left
EBR	eastbound right
EBT	eastbound through
FDOT	Florida Department of Transportation
FHWA	Federal Highway Administration
FT	facility type
GMNS	General Modeling Network Specification
GPS	Global Positioning System
GTFS	General Transit Feed Specification
h	hour
HCM	Highway Capacity Manual
HCS™	Highway Capacity Software™
HOV	high-occupancy vehicle
Hwy	highway
i	index number
ITC	Intermodal Transit Center
I–95	Interstate 95
L	congestion period
LOS	level of service
m	observed point

MAG	Maricopa Association of Governments
MAPE	mean absolute percentage error
min	minute
mph	miles per hour
MRM	multiresolution modeling
N	total number of sensors
n	derived point
NA	not addressed
N/A	not applicable
NB	northbound
NBL	northbound left
NBR	northbound right
NBT	northbound through
NeXTA	Network EXplorer for Traffic Analysis
O-D	origin-destination
ODME	origin-destination matrix estimation
OSM	OpenStreetMap®
p.m.	post meridiem
QBM	queue-based method
QDF	queue demand factor
R^2	coefficient of determination
RMSE	root mean square error
RTOR	right-turn-on-red
s	second
S	south
SB	southbound
SBA	simulation-based assignment
SBL	southbound left
SBR	southbound right
SBT	southbound through
SERPM	Southeast Florida Regional Planning Model
STA	static traffic assignment
St	street
t	time
T	total number of time intervals
t_0	start of congested period
t_3	end of congested period
t_i	congested travel time for link *i*
TAZ	traffic analysis zone
u	speed
u_c	speed at capacity
u_{min}	minimum speed during the assignment period
v	observable volume
v^*	unobservable demand
v/c	volume-to-capacity
VDF	volume-delay function

vph	vehicles per hour
vphpl	vehicles per hour per lane
W/O	without
WB	westbound
WBL	westbound left
WBR	westbound right
WBT	westbound through
WMSE	weighted mean squared error
$y_{i,t}$	observed traffic volume or travel time for link *i* at time *t*
$y^*_{i,t}$	simulated traffic volume or travel time for link *i* at time *t*

CHAPTER 1. INTRODUCTION

This project aims to develop consistent definitions and a unified modeling framework on the application of multiresolution models for traffic simulation and modeling. Microscopic models simulate the realistic movement of individual vehicles through the network. These extremely detailed models enable analysis and comparison of project alternatives, but they are limited in spatial and temporal scope given the high-resolution representation. Macroscopic models are the most aggregated form of traffic modeling and reflect the well-established relationships among traffic flow, density, and speed. These models assign flow to vehicles but do not simulate flow. Mesoscopic models exhibit properties of both microscopic and macroscopic models. The study authors have separately published a state-of-practice and gap analysis report, which provides a comprehensive set of terms and definitions associated with multiresolution models (Zhou, Hadi, and Hale 2021).

Over the years, traffic analysts have considered the benefits of applying multiple modeling resolutions to the same project or analysis. Increasing computer speeds and traffic network complexities have further motivated the use of such multiresolution analyses. Analysts have used combinations of models with different resolutions to complement each other's in providing the required functionalities. Analysts have also successfully used the outputs of one modeling resolution to verify, calibrate, and validate the results of other modeling resolutions. With these applications, multiresolution analyses have expanded the number of things that a single project can model and consider. These sorts of modeling upgrades have allowed analyses to become more defensible and have improved confidence between stakeholders and decisionmakers.

Despite the evident benefits, traffic modeling experts think that practitioners are underutilizing multiresolution analysis largely because of the lack of well-documented case studies and pilot projects. This report aims to fill that gap by providing three real-world case studies. These case studies help demonstrate popular yet fundamentally different types and scales of traffic analysis. This variety of analysis types and conditions helps to illustrate multiresolution challenges and benefits across typical work tasks, such as scoping, data collection, model development, model calibration, and alternatives analysis. The case studies also demonstrate fundamentally different traffic problems and conditions from different parts of the United States.

Specifically, the downtown West Palm Beach, FL, case study, which used commercial simulation tools, demonstrates a detailed traffic impact study for a relatively small urban area. In contrast, the Phoenix, AZ, metropolitan area case study, which used public domain simulation tools, demonstrates a much larger regional analysis. Finally, the Maryland Interstate 95 (I–95) case study, which used a common data format to seamlessly represent all three levels of analysis (i.e., macroscopic, mesoscopic, and microscopic), demonstrates a next-generation traffic model development procedure. The authors hope that this variety of case studies, along with the resulting discussion of lessons learned, will provide helpful information to enable more transportation agencies to adopt multiresolution analysis.

SCOPE

This report describes three case studies that demonstrate the challenges with, and value of, multiresolution modeling (MRM) on real-world, complex transportation networks: West Palm Beach downtown network, Phoenix metropolitan area, and Maryland I–95 network. The authors previously developed a state-of-the-practice review. That review was based on the information available in the literature on MRM in transportation system modeling and findings from the teleconferences that were conducted with users and vendors of MRM tools and other transportation system modelers and analysts. The authors also conducted a gap analysis based on the aforementioned activities. They combined the state-of-practice review and gap analysis into a single summary report that was published separately from this report. The authors selected research activities for the case studies by mapping these activities to the gaps identified during tasks that were completed earlier in the project. This mapping activity ensured that the case studies would address the gaps identified in previous research. The next section provides a summary of the identified gaps.

IDENTIFIED GAPS

The previously conducted gap analysis identified gaps associated with the adoption of MRM by transportation agencies (Zhou, Hadi, and Hale 2021). The research team based the gap analysis on a review of literature and outreach with 19 simulation model users. Some of the constraints and limitations are associated with the methodologies, guidance, procedures, data, and tools available to transportation agencies. Other issues related to policies, staffing, training, collaboration, information sharing, and attitudes toward simulation modeling have affected the adoption and effectiveness of MRM.

Given the several dimensions and subdimensions of the gaps associated with MRM, the research team utilized the six dimensions of the capability maturity model (CMM) framework in the gap analysis (FHWA 2012). The six dimensions of the CMM are the business processes, performance measurement, system and technologies, organization and workforce, collaboration, and culture. The team designed the case studies to address some of the identified gaps in MRM practice. Table 1 presents the identified gaps and summarizes the extent to which the case studies address these gaps. A more detailed explanation of information in each column of table 1 is as follows:

- Dimension: Documents each of the six CMM dimensions.
- Gap: Documents the identified gaps in MRM practice (Zhou, Hadi, and Hale 2021).
- West Palm Beach downtown: Documents the section, within chapter 2 of this report, which discusses how the West Palm Beach downtown case study fills the gaps listed in the previous column.
- Phoenix metropolitan area: Documents the section, within chapter 3 of this report, which discusses how the Phoenix metropolitan area case study fills the gaps listed in the Gap column.

- Maryland I–95: Documents the section, within chapter 4 of this report, which discusses how the Maryland I–95 case study fills the gaps listed in the Gap column.

- MRM Methodology Steps: Documents the major step numbers of the proposed MRM methodology as presented in the companion *Multiresolution Modeling for Traffic Analysis Guidebook* (*MRM Guidebook)*,[1] which address the gaps listed in the gap column. Chapter 2 of the guidebook devotes a section to each step of the MRM methodology.

[1]Zhou, X., M. Hadi, and D. Hale. Forthcoming. *Multiresolution Modeling for Traffic Analysis Guidebook*. Washington, DC: Federal Highway Administration.

Table 1. Overview of case study information.

Dimension	Gap	West Palm Beach Downtown	Phoenix Metropolitan Area	Maryland I–95	MRM Methodology Steps
Business process	1.1 Institutionalization of MRM use for certain types of analysis	IA	IA	IA	Step 1 (planning/scoping)
	1.2 Development and provision of methodology and guidance	IA	IA	IA	Step 1 (planning/scoping)
	1.3 Allocation of funding and project time to meet MRM requirements	Refer to the "Cost and Time Requirements" section	Refer to the "Cost and Time Requirements" section	Refer to the "Cost and Time Requirements" section	Step 1 (planning/scoping)
	1.4 Adoption of processes for model archiving and maintenance	Refer to the "Model Archiving and Maintenance" section	NA	NA	Step 1 (planning/scoping)
	1.5 Enhancement of contracting and procurement practices	IA	IA	IA	Step 1 (planning/scoping)
Performance measurement	2.1 Variations in the definitions of measures	Refer to the "Performance Measure Definitions" section	Refer to the "Performance Measure Definitions" section	NA	Step 1 (planning/scoping)
	2.2 Variations in the methods used in estimation of various performance metrics	Refer to the "Performance Measure Consistency" section	Refer to the "Performance Measure Consistency" section	NA	Step 2 (data collection/analysis)
	2.3 Data needs	Refer to the "Origin-Destination Demand Estimation" section	NA	NA	Step 2 (data collection/analysis)

Dimension	Gap	West Palm Beach Downtown	Phoenix Metropolitan Area	Maryland I–95	MRM Methodology Steps
	2.4 Types and resolutions of measures used in model calibration and validation	Refer to the "Performance Measure Consistency" section	Refer to the "Performance Measure Consistency" section	Refer to the "Performance Measure Consistency" section	Step 2 (data collection/analysis)
Systems and Technology	3.1 Methods and tools that support integration and data conversion between different modeling levels	Refer to the "Model Conversion Effectiveness" section	Refer to the "Model Conversion Effectiveness" section	Refer to the "Model Conversion Effectiveness" section	Step 3 (model development), Step 6 (alternatives analysis)
	3.2 Enhancement of MRM tools	Refer to the "Origin-Destination Demand Estimation" section	NA	Refer to the "Enhancement of Tools" section	Step 3 (model development), Step 6 (alternatives analysis)
	3.3 Multimodal modeling	NA	NA	Refer to the "Multimodal Modeling" section	Step 1 (planning/scoping), Step 3 (model development)
	3.4 Behavioral responses to advanced technologies and strategies	Refer to the "Impacts of Advanced Applications" section	NA	NA	Step 1 (planning/scoping), Step 3 (model development), Step 5 (model calibration), Step 6 (alternatives analysis)
	3.5 Simulation/model coupling for real-time management applications	NA	NA	NA	Step 1 (planning/scoping)

Dimension	Gap	West Palm Beach Downtown	Phoenix Metropolitan Area	Maryland I–95	MRM Methodology Steps
	3.6 Feedback loop in internally consistent cross-resolution traffic representation	Refer to the "Performance Measure Consistency" section and the "Benefit of MRM" section	Refer to the "Feedback Loop" section	Refer to the "Performance Measure Consistency" section and the "Benefit of MRM" section	Step 1 (planning/scoping), Step 3 (model development), Step 5 (model calibration), Step 6 (alternatives analysis)
Organization and Workforce	4.1 Acquisition of MRM experience and background	IA	IA	IA	Step 1 (planning/scoping)
	4.2 Recruitment, retention, and training of staff to support MRM	IA	IA	IA	Step 1 (planning/scoping)
	4.3 Qualified staff members who can develop, calibrate, and peer-review models	IA	IA	IA	Step 1 (planning/scoping)
Collaboration	5.1 Interagency collaboration	Refer to the "Collaboration Assessment" section	IA	IA	Step 1 (planning/scoping)
	5.2 Intra-agency collaboration	Refer to the "Collaboration Assessment" section	IA	IA	Step 1 (planning/scoping)
Culture	6.1 The transportation agency values the MRM implementation benefits	Refer to the "Benefit of MRM" section	IA	Refer to the "Benefit of MRM" section	Step 1 (planning/scoping)

IA = institutional activities; NA = not addressed.

*In most cases, the case studies and the proposed methodology do not address high-level IAs such as procurement, staff training, and shifting the culture.

REPORT STRUCTURE

The organization of the MRM case studies report is as follows: Chapter 1 provides an introduction. Chapters 2 through 4 provide details for each of the three case studies: the West Palm Beach downtown MRM in chapter 2, the Phoenix metropolitan area MRM in chapter 3, and the Maryland I–95 MRM in chapter 4. For the individual case study chapters 2 through 4, each chapter provides a traffic network description, model overview, data description, and analysis details. Chapter 5 then summarizes the main outcomes, lessons learned, and conclusions from these MRM case studies.

CHAPTER 2. WEST PALM BEACH DOWNTOWN CASE STUDY

The research team designed the case studies to address some of the identified gaps in MRM practice, as documented in chapter 1. To complement the other two case studies, this study focuses on a relatively small urban area and uses commercial simulation tools. This chapter describes the effort to model the downtown Palm Beach network using three different levels. The three levels include an unrefined subnetwork model extracted from a regional demand forecasting model, a macroscopic model-based static assignment model combined with an origin-destination matrix estimation (ODME) procedure in a macroscopic modeling tool, and a microscopic simulation model with static routing between origins and destinations.

As part of the project summarized in *Intermodal Transit Center (ITC) Relocation—West Palm Beach Traffic Modeling and Analysis* (Palm Beach County 2020), the project team modeled the West Palm Beach downtown subarea network in a commercial demand forecasting tool (Bentley Systems 2021), a commercial macroscopic and mesoscopic modeling tool, (PTV Group 2021a), and a commercial microscopic simulation tool (PTV Group 2021b). The ITC project developed the West Palm Beach downtown network model geometry and traffic demands for the year 2020, 2025, and 2045. The purpose of the study is to evaluate the impacts of the ITC relocation on traffic and transit mobility. However, the study also includes the impacts of many other major developments and geometry changes in the downtown area. Several major developments will result in a significant increase in demands. In addition, the team expects geometric improvements to result in traffic diversion. Drawbridge preemptions, caused by trains on two north–south tracks, are a significant source of traffic congestion in the network. The network, shown in figure 1, includes 48 signalized and 52 unsignalized intersections.

The upcoming sections present descriptions of the West Palm Beach network used as a case study in this project. The sections include overviews of the downtown model, existing conditions in the downtown area, the existing year model calibration process, future conditions modeled in the case study, mapping of the case study research activities to identified gaps, and the case study research activities.

NETWORK DESCRIPTION

The study area includes 35 signalized and 38 unsignalized intersections. The research team modeled additional roadway networks outside the study area for completeness and future use, but did not calibrate these additional segments in detail, as part of this study. Figure 1 shows the expanded area that includes 48 signalized and 52 unsignalized intersections.

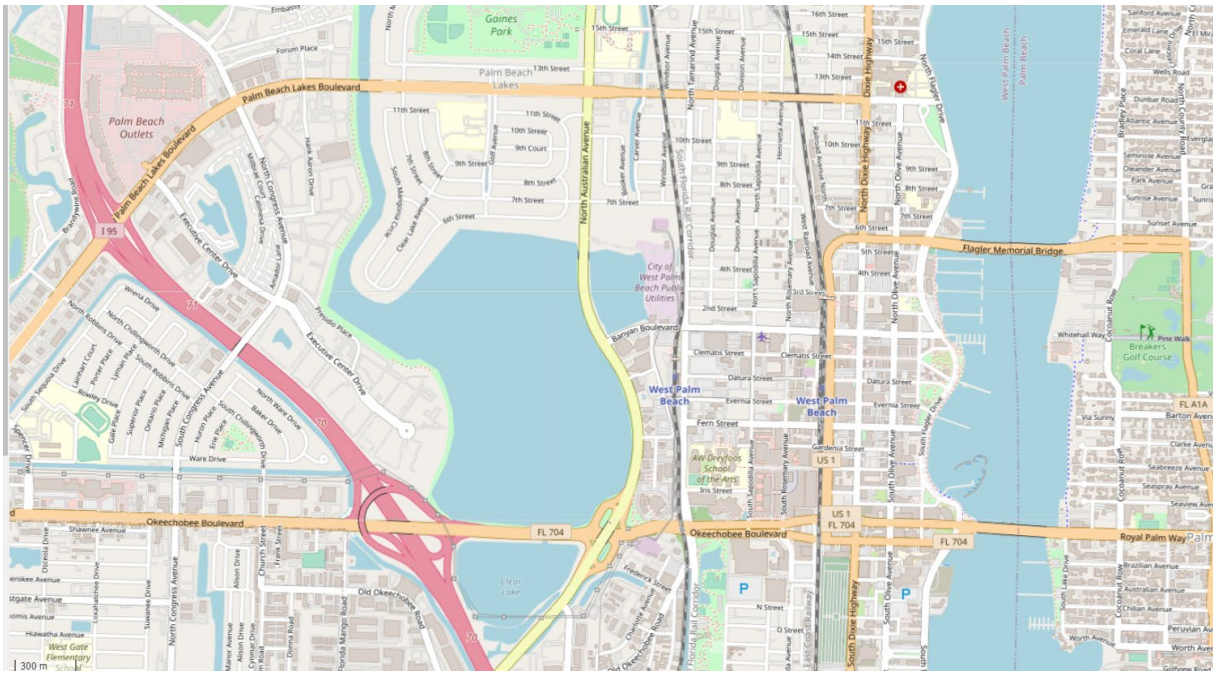

© 2021 OpenStreetMap contributors.

Figure 1. Map. Expanded Palm Beach area (OpenStreetMap A).

MODEL OVERVIEW

The developed models are for the morning peak period (7–10 a.m.) and afternoon period (4–7 p.m.) for the build and no-build scenarios. The model includes passenger cars, heavy vehicles, buses (Palm Tran), and trains (Tri-Rail, Brightline, and freight). The research team used the demand forecasting tool to extract a Palm Beach downtown transportation network as a subnetwork from the regional demand forecasting model. This process provided base geometry, initial origin-destination (O-D) matrices, and a loaded network (with link volumes for the modeled periods). The team extracted this base network from the regional demand model for the Southeast Florida Tri-County region, which includes Palm Beach County, Broward County, and Miami-Dade County. Transportation professionals refer to this regional southeast model, which exists in the commercial demand forecasting tool format, as the Southeast Florida Regional Planning Model (SERPM) (FSUTMSOnline 2021).

The project collected the following data for use in model development and calibration:

- Network geometry data.
- Intersection control data (e.g., signal timing plans, signal layouts, and signal split history).
- Available traffic counts (e.g., turning movement and tube counts).
- The network data, demand data, and assignment results for the years 2015 and 2045 from SERPM.

- Third-party vendor travel time data.
- Transit data (10 transit routes from the Palm Tran website), including route data, stop data, and schedule data (Palm Tran 2021).
- Transit ridership.
- Tri-Rail commuter train, Brightline commuter train, and freight train schedule data.

The research team updated the macroscopic network based on OpenStreetMap®, which is built into the macroscopic modeling tool (OpenStreetMap Contributors 2021). The team further validated the network using an online commercial mapping tool. In this manner, the team added and corrected detailed geometric features, control, parking lots/internal zones and associated zones, and approach counts and link counts. For the signalized intersections, the team added signal timing data for both the morning and afternoon periods to the network using the ring barrier controller feature. In addition to the nodes connecting to the external and internal zones utilized in the regional demand forecasting model, the project team identified public parking spaces within the study area. The research team modeled these parking spaces as production and attraction points to achieve more realistic O-D patterns. The county project team also coded the public transit network details. The research team estimated dwell (service) times, including boarding, alighting, and clearance times, based on automatic passenger counter data provided by the county. The team used an ODME model and static assignment model in the utilized tool to estimate the O-D matrices and assign traffic between each O-D pair. The team used a utility within the tool to produce the inputs to the utilized microscopic tool, including network geometry, signal control, volumes at network entry points, and static paths between O-D pairs in the microscopic simulation tool input format.

The analysis of the existing conditions indicates that the congestion mainly occurs on Banyan Boulevard and Okeechobee Boulevard, two major east-west arterials in the downtown area. The congestion occurs on the eastbound (EB) arterial in the morning, on the westbound (WB) arterial in the afternoon, and on the cross streets and feedings links to these two facilities in the north-south direction. In addition to high demands, major contributors to the congestion in the network are the rail preemptions that occur at two north-south tracks and drawbridge preemptions. The west train track mainly serves the Tri-Rail commuter trains and Amtrak trains. The east train track serves the Brightline commuter trains and freight trains. The main bottleneck locations in the morning peak and associated queues replicated in the model include the following:

- Okeechobee Boulevard and Tamarind Avenue EB approach.
- Okeechobee Boulevard EB between Tamarind Avenue and Flagler Drive.
- Northbound (NB) South Dixie Highway approach at Okeechobee Boulevard Intersection.
- NB right at Australian Avenue and Banyan Boulevard.
- EB through at Banyan Boulevard and Tamarind Avenue.

The main bottleneck locations and associated queues in the evening peak replicated in the model include the following:

- Southbound (SB) approach at Okeechobee Boulevard and Tamarind Avenue.
- WB Okeechobee Boulevard between Flagler Drive and Tamarind Avenue.
- SB approach of Quadrille at Lakeview Avenue/Okeechobee Boulevard.
- WB approach to Banyan Boulevard Intersection with Tamarind Avenue.

DATA DESCRIPTION

This section describes data items that the research team collected and used in the development and calibration of the West Palm Beach network. The team calibrated microscopic simulation models based on the available turning movement counts, travel times, and observations. The team calibrated traffic volumes using the criteria presented in the *Florida Department of Transportation Traffic Analysis Handbook: A Reference for Planning and Operations* (FDOT 2014). The criteria are as follows:

- For more than 85 percent of the links, the simulated and measured link volumes must be:
  - Within 100 vehicles per h (vph) for volumes less than 700 vph.
  - Within 15 percent for volumes between 700 vph and 2,700 vph.
  - Within 400 vph for volumes greater than 2,700 vph.

- The sum of link volumes from the simulation within the calibration area must be within 5 percent of the sum of the link volume counts based on real-world measurements.

The study calibrated the travel times by considering the criteria used in a number of States, including Florida (Florida Department of Transportation 2014), Virginia (Virginia Department of Transportation 2020), and Wisconsin (Wisconsin Department of Transportation 2018, 2019). The utilized criteria are as follows:

- Simulated travel time is within plus or minus 1 min for routes with observed travel times less than 7 min for all routes identified in the data collection plan.
- Simulated travel time is within plus or minus 15 percent for routes with observed travel times greater than 7 min for all routes identified in the data collection plan.

The research team downloaded travel time measurements available from a third-party vendor (CATT Lab 2021). The team's adjusted model parameters as part of the microsimulation calibration process included the following:

- Lane change distance.
- Driver behavior.
- Conflict areas and priority rules.
- Railroad crossing and preemption interval.
- Lane utilization.
- Police car lane blockage.
- Bus stop dwell time.

Several major developments will result in a significant increase in demands. This study models one of the major approved new developments to determine the model assignment of the generated traffic under different modeling configurations and parameters.

ANALYSIS DETAILS

This section describes the research activities that are conducted as part of the case study task to satisfy the gaps, as identified in table 1. First, this section discusses research related to ODME, including comparisons of the performance of different O-D estimation methods, associated parameters, and algorithms. Then, this section addresses differences in the definitions of performance measures in the three utilized tools. It further investigates the use of a feedback loop from the lower resolution level (microscopic simulation) to the upper levels (macroscopic and mesoscopic models) to increase the consistency between these models in terms of capacity and travel time assessment. This section then discusses the benefits and costs of utilizing MRM, and it provides additional information to address other identified gaps in table 1.

O-D Demand Estimation (Gap 2.3 and Gap 3.2)

This section addresses issues related to gap 2.3 (data availability and needs) and gap 3.2 (MRM needs and capabilities). O-D demand estimation is key to the success of MRM because static and dynamic assignment models require O-D matrices as inputs. Some assignment models also accept individual vehicle-level origins and destinations in lieu of O-D matrices. The simplest method to obtain the demands for traffic assignment is to import the O-D demands directly from a subarea network extracted for the project from the regional demand model. However, modelers have found that O-D demand matrices obtained from demand forecasting models may result in large errors in comparison to real-world counts when used in assignment procedures (Zhou, Hadi, and Hale 2021). The occurrence of these errors implies the need for further refinement of regional demand forecasting models to allow these models to produce results that are acceptable for simulation modeling.

Given the aforementioned issue, most existing commercial and open-source demand forecasting and assignment tools have ODME procedures to update the O-D demands generated by the demand forecasting models. These procedures allow for better correspondence with real-world traffic counts and sometimes other measures, such as travel times. These procedures generally use optimization algorithms to estimate the O-D matrices by minimizing errors between the model outputs and inputs, resulting in improved O-D demand matrices in comparison to those produced by the demand forecasting models. The existing ODME vary in the type of input variables utilized in the estimation. These input variables can include the segment counts, turning movement counts, initial O-D matrices used to seed the optimization, attractions per zone, and production demands per zone. Some tools also allow the use of additional measures as inputs to the O-D estimation process, including travel time measurements, queue lengths, and densities. However, practitioners have not widely used these additional measures, despite their proven ability to improve the results (Hadi et al. 2013).

Modelers also currently perform ODME procedures with or without a seed O-D demand matrix. In some cases, modelers completely ignore the provision of the seed matrix and only use count data to obtain the network's time-varying O-D demand. However, the quality of ODME results

depends on the availability of high-quality initial O-D demand matrices (Lin 2006). In most applications, analysts have used volume measurements combined with seed matrices based on demand model results as inputs to the ODME estimation algorithms. Practitioners are also using partial O-D demand matrices, which are based on roadside reader data, vehicle tracking using Global Positioning System (GPS) data, and third-party vendor data, as seed matrices to the O-D demand estimation (Zhou, Hadi, and Hale 2021). The ODME algorithms produce O-D demands that minimize deviations from the counts and seed matrices. In the optimization objective function used to estimate the O-D matrices, analysts can assign weights on different variables to reflect the level of confidence in the data. For example, in the utilized tool in this case study, the analyst can assign a weight ratio that reflects the relative weight of the seed matrix to traffic volume measurements in the optimization. For example, the analyst may assign a lower weight ratio if there is a higher confidence in traffic volume measurements in comparison to the seed O-D demand matrix.

This section discusses various aspects of O-D demand estimation and the application of ODME in the West Palm Beach case study. The following list shows the subsections sequentially:

- *Network Preparation:* This subsection describes the extraction of the network and associated demands from the demand forecasting modeling tool. Analysts can use these as inputs to the tool that allows both macroscopic model-based static assignment, and mesoscopic model-based dynamic traffic assignment (DTA).

- *Comparison of O-D Estimation Algorithms:* This subsection discusses the results from the use of two ODME algorithms built in the macroscopic modeling tool utilized in this case study.

- *Effect of the Utilization of Seed O-D Matrix:* This subsection compares the results of applying an ODME algorithm with different weight ratios (relative weight as discussed in the previous paragraph) on the seed matrix from the demand forecasting model.

Network Preparation

As previously noted, this study investigates the impact of utilizing O-D matrix data obtained from the regional planning model, which is the SERPM model for the case study region. MRM users often view obtaining defensible O-D matrix data as an important component of an MRM study that includes demand forecasting models as one of the resolutions (Zhou, Hadi, and Hale 2021). This subsection describes how the research team extracted the network and associated demands from the demand forecasting modeling tool. It also describes how the team used these as inputs to the lower-level tools, which allow both macroscopic model-based static assignment and mesoscopic model-based DTA.

For the West Palm Beach downtown case study area, the total number of traffic analysis zones (TAZ) in the study area is approximately 100, whereas the total number of TAZ in SERPM is more than 4,500. This network includes all streets of facility type (FT) collector and higher capacity (i.e., high-occupancy vehicle lanes, freeways, and expressways; see table 10). The research team extracted a subarea network from the SERPM that matched the West Palm Beach study area. The subnetwork generator in the demand forecasting tool allowed cutting the subarea

of interest for detailed analysis without losing reference to the original regional model. The subarea network is a shapefile with spatial references. In the second step, the team performed a subarea analysis technique to get the O-D data for the area. To accomplish the analysis, the team executed the demand forecasting tool's highway assignment module. The inputs were the O-D matrix for all zones, and the output was the O-D matrix for zones present in the subarea. Finally, the team used a utility in macroscopic modeling tool to import both the network and the O-D matrix to the macroscopic modeling tool's subarea network.

Comparison of Algorithms

In this study, the research team first considered two ODME procedures that are built into the macroscopic modeling tool. These procedures are the least-squares method and the TFlowfuzzy method (PTV Group 2021a). The team conducted sensitivity analyses during this case study, which showed that the least-squares method produced better results (in terms of the deviation of link/turn counts and O-D trip values) than the TFlowfuzzy procedure. Other advantages of the least-squares method is that it always delivers a solution and its run time is significantly lower than other methods available in the tool. Analysts can also use the least squares method in large networks that contain many count locations. Thus, the team used the least squares method for the remainder of the analysis.

The least-squares method minimizes the squared distance between the assignment value and the count value. Analysts can also minimize the deviation from the initial O-D matrix that is used as an input to the ODME process by minimizing the squared distance between the old and new trip values at the same time as the count values.

Effect of the Seed Matrix

With the least-squares method, analysts can define weighting factors for count locations to reflect their importance. Analysts can also specify another weighting factor, which is the weight ratio of matrix deviations versus count deviations. A weight smaller than 1.0 means the procedure will give count deviations higher importance than matrix deviations. Weight ratios higher than 1.0 indicate that the procedure will put a higher weight on the seed matrix than on count value deviations, resulting in smaller deviations in the O-D trip values.

This subsection discusses the impacts of using the O-D matrix produced by the demand forecasting model as an input to the utilized ODME algorithm (seed matrix). The subsection compares the updated O-D demands produced by the utilized ODME algorithm with different weight ratios assigned to the seed matrix relative to the turning movement counts in the ODME algorithm. The subsection examines several relative weights of the seed matrix, ranging from zero (no consideration of the seed matrix) to a very high number (no consideration of the traffic counts in the optimization).

Figure 2 shows an overall comparison between the use of different weight ratios on the seed matrix and the counts when using the least squares method. Figure 2 shows that as the weight ratio defined in the least squares ODME procedure increases, the O-D trips deviation became smaller. The link volume deviation and turn volume deviation changed only slightly with the change in the weight ratio, even when increasing the weight ratio on the matrix up to 10.

However, deviations of the link and turning volumes increased significantly when using a weight of 100. These deviations became very high when entering the maximum value for the weight ratio into the utilized tool, which is equivalent to using the matrix produced by the demand forecasting model with no consideration of the link or turn counts. Figure 2 shows that the use of ODME with a weight ratio of 10 on the demand matrix reduced the mean absolute deviation of turn movement volume and link volumes from 38 to 13 percent and from 46 to 13 percent, respectively. The O-D matrix resulting from the ODME had 20 percent deviation from the initial O-D matrix. It is notable that the magnitude of deviation from the original seed matrix depends on the quality of the matrix.

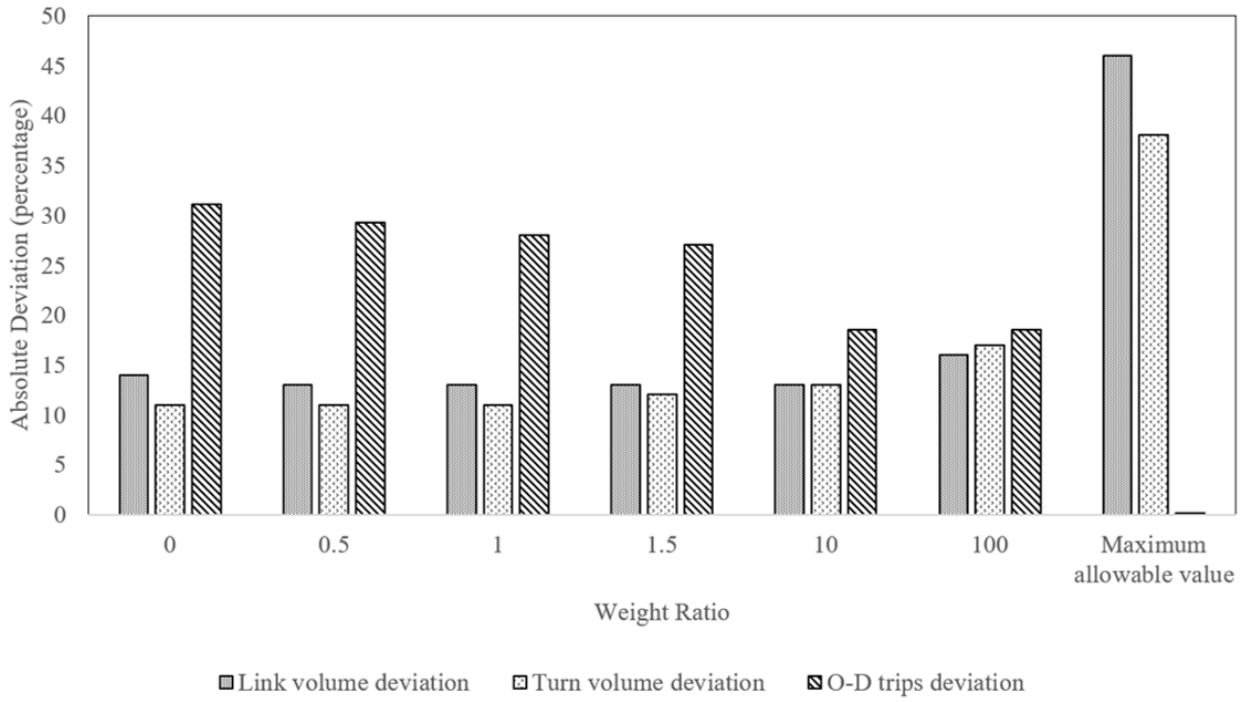

Source: FHWA.
Weight ratio = ratio of weights for demand deviation relative to count weights.

Figure 2. Bar Chart. Link and turn deviations with different weight ratios.

Figure 3 and figure 4 present the deviation of the turn volumes and link volume counts when using the demand forecasting model O-Ds. As can be seen from these figures, the coefficient of determination (R^2), is 0.719 for the turn volume deviation and 0.527 for the link volume deviation. Figure 5 and figure 6 show that these improve to 0.929 and 0.913, respectively, with use of the ODME without the seed matrix. However, as will be explained in more details later, this option also results in a large deviation from the regional demand model O-D matrix. Figure 7, figure 8, figure 9, and figure 10 show that the values are approximately 0.97 and 0.92 when using a weight ratio of 0.5 or 10, respectively, which are comparable to the solution with no weight on the seed matrix. These solutions also produced less deviation from the regional model O-D matrix, in particular, with the weight ratio of 10.

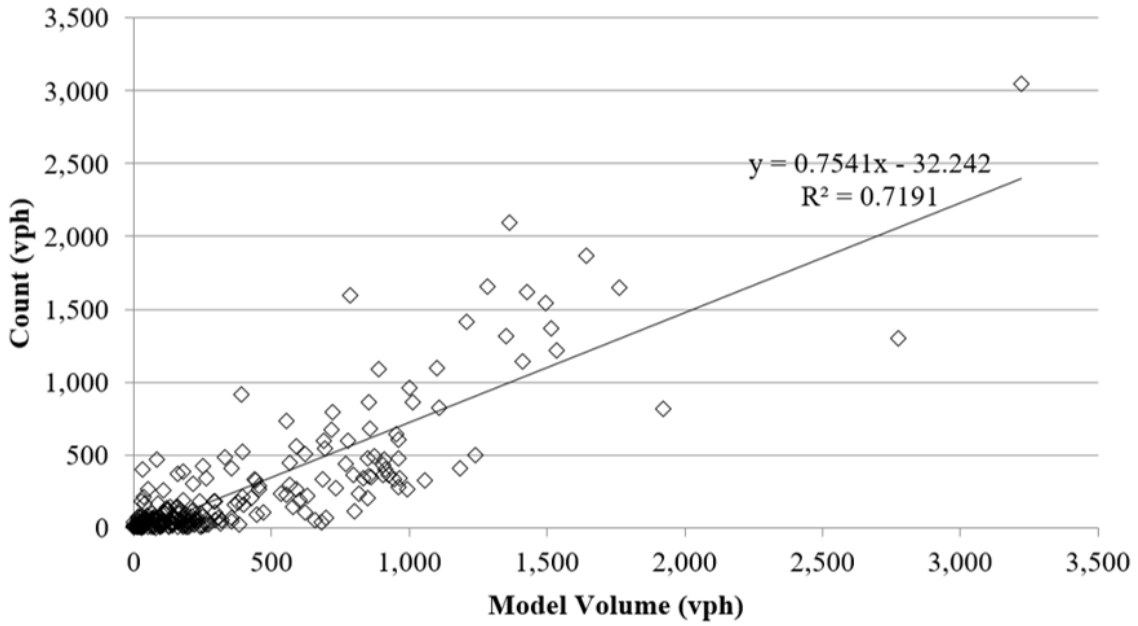

Source: FHWA.
R^2 = coefficient of determination; vph = vehicles per hour; x = model volume variable; y = count variable.

Figure 3. Graph. Turn volume deviation when putting no weight on the counts.

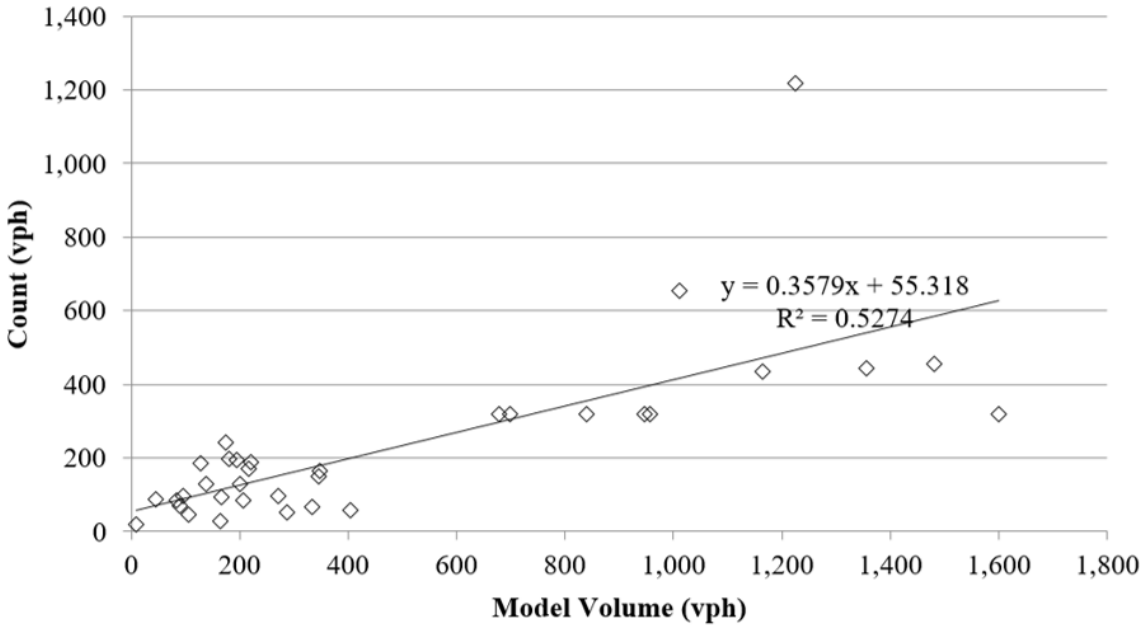

Source: FHWA.

Figure 4. Graph. Link volume deviation when putting no weight on the counts.

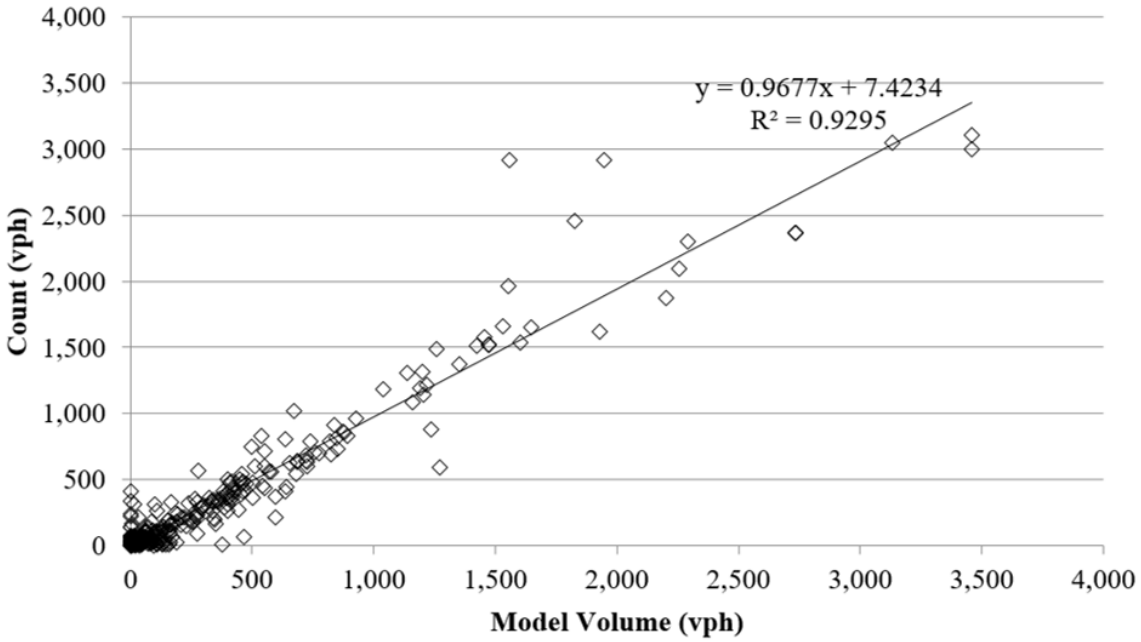

Source: FHWA.

Figure 5. Graph. Turn volume deviation when putting no weight on the seed matrix.

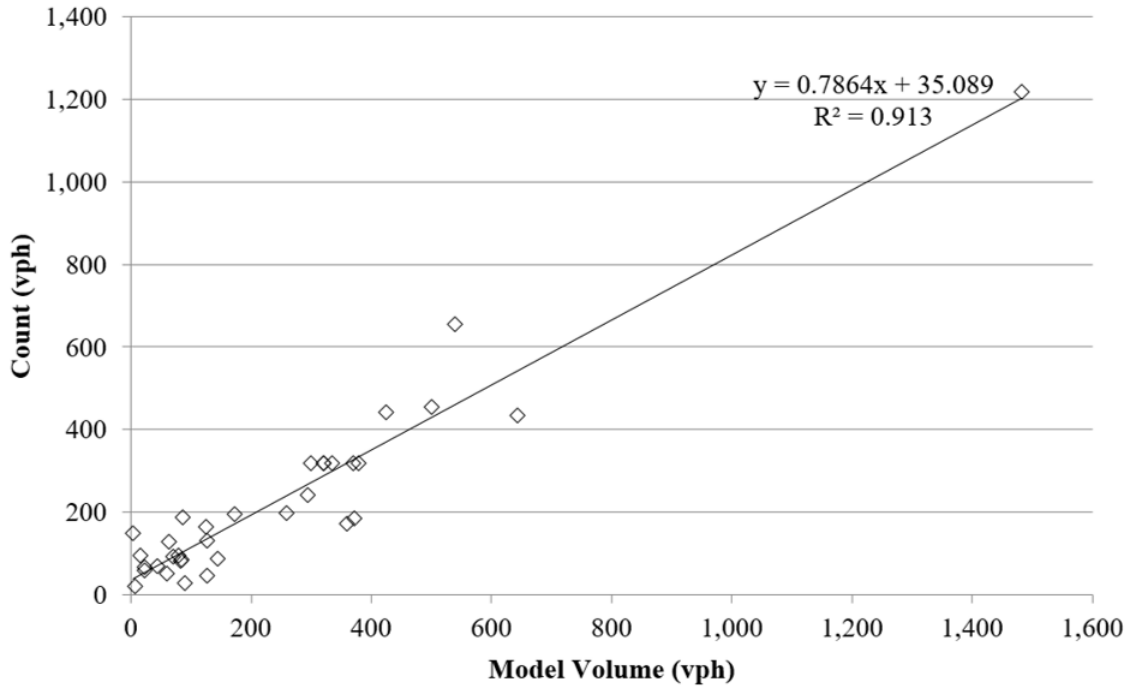

Source: FHWA.

Figure 6. Graph. Link volume deviation when putting no weight on the seed matrix.

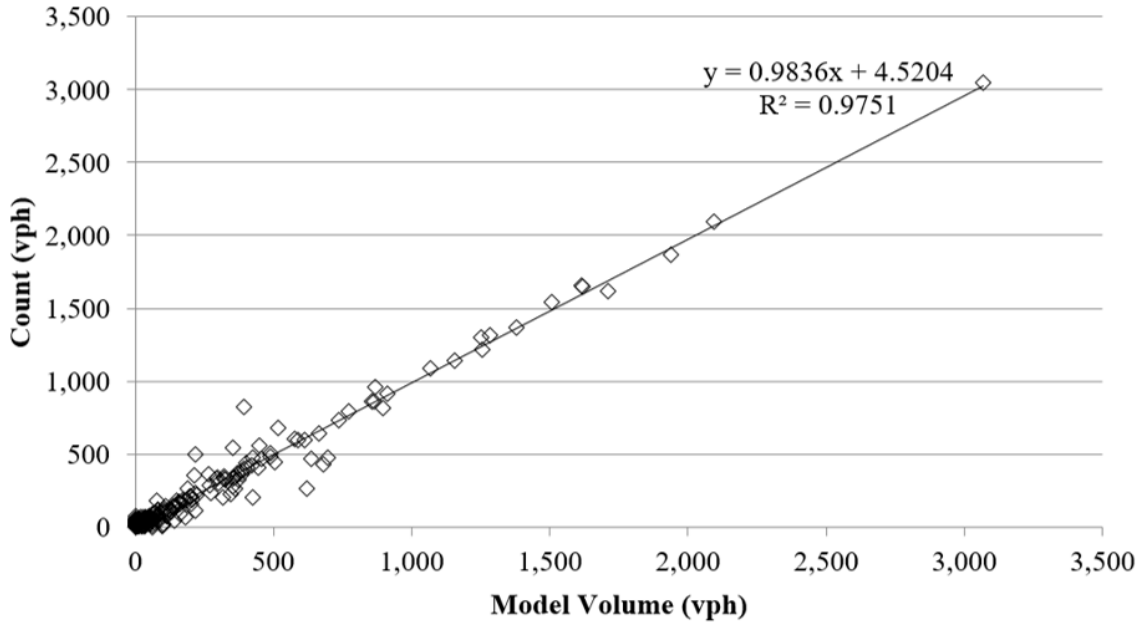

Source: FHWA.

Figure 7. Graph. Turn volume deviation when putting 0.5 weight ratio on the seed matrix.

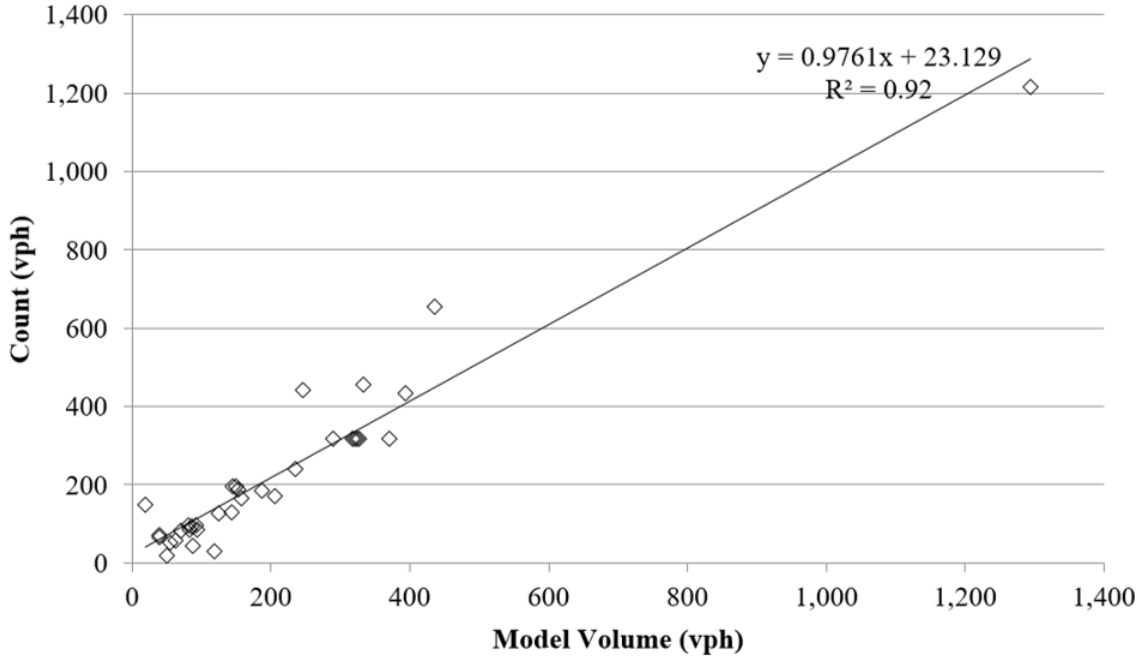

Source: FHWA.

Figure 8. Graph. Link volume deviation when putting 0.5 weight ratio on the seed matrix.

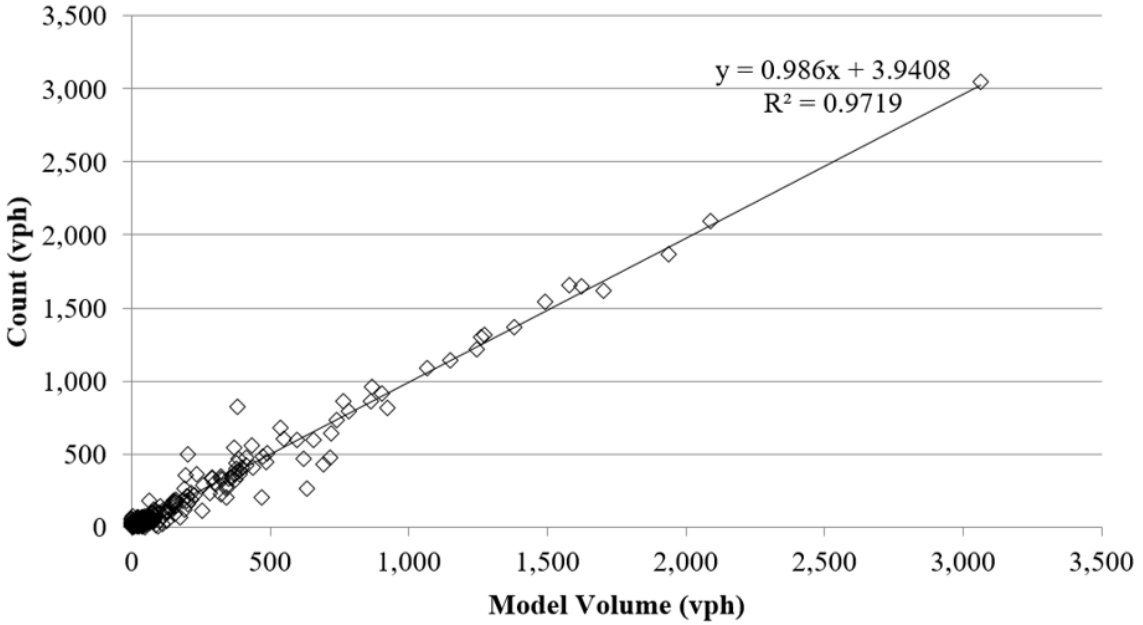

Source: FHWA.

Figure 9. Graph. Turn volume deviation when putting a weight ratio of 10 on the seed matrix.

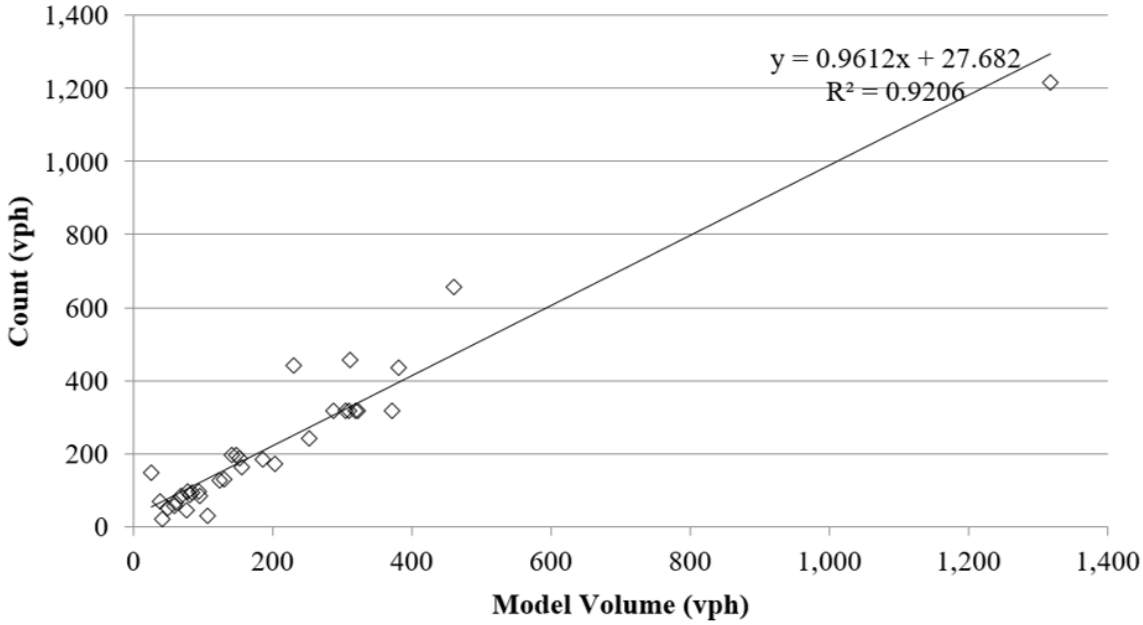

Source: FHWA.

Figure 10. Graph. Link volume deviation when putting a weight ratio of 10 on the seed matrix.

Table 2, table 3, table 4, and table 5 show the resulting turning movement volumes from different ODME setups for four critical intersections. These tables further show how the results are different with different setups. In particular, the resulting volumes from assigning the regional model O-D matrix without ODME (zero weight on the counts in table 2, table 3, table 4,

and table 5) are very different from real-world counts. For example, the real-world WB left-turn volume at Tamarind-Okeechobee is 122 vph, while the volume resulting from assignment is 706 vph, as shown in table 2. The real-world eastbound through volume at Tamarind-Okeechobee is 1,369 vph, while the volume resulting from assignment is 2,347 vph, as shown in table 2. The use of ODME significantly reduced deviations between the real-world and the modeled volume. Even with the use of 0.5 weight ratio on the seed matrix that produced good overall deviation statistics, there are movements such as the WB through for Banyan at Tamarind that have high deviations from the real-world counts, as shown in table 3 (1,656 vph in the real world versus 1,344 vph in the model). A closer examination of the counts could determine whether this results from imbalance in the traffic counts or extremely unrealistic demands, according to the regional demand forecasting model for a TAZ near the intersection. Fine-tuning the seed matrix base, possibly with the help of real-world partial O-D data, and putting a weight on some of the important movements in the optimization process, might also help. This process can be iterative. The authors also strongly recommend that the simulation modelers work with demand forecasting modelers to improve the demand forecasting model results to increase its applicability for use as a seed matrix in ODME.

Table 2. Comparison of Tamarind–Okeechobee intersection volumes with different ODME parameters.

Scenario	Volume (vph)													
	Weight	WBL	WBT	WBR	SBL	SBT	SBR	EBL	EBT	EBR	NBL	NBT	NBR	Total
Real-world turning movement counts	N/A	112	2,096	51	47	596	913	382	1,369	303	103	177	106	6,255
Zero weight on seed matrix	0	91	2,256	125	48	727	839	394	1,350	303	121	187	105	6,546
Regional model (zero weight on counts)	9,999	706	2,536	135	381	924	679	579	2,347	161	625	240	517	9,830
ODME with 0.5 and 10 weight ratios	0.5	77	2,105	52	61	597	911	383	1,368	302	103	178	111	6,248
	10	85	2,095	55	80	601	902	390	1,381	296	128	184	129	6,326

EBL = eastbound left; EBR = eastbound right; EBT = eastbound through; N/A = not applicable; NBL = northbound left; NBR = northbound right; NBT = northbound through; SBL = southbound left; SBR = southbound right; SBT = southbound through; WBL = westbound left; WBR = westbound right; WBT = westbound through.

Table 3. Comparison of Banyan–Tamarind intersection volumes with different ODME parameters.

Scenario	Volume (vph)													
	Weight	WBL	WBT	WBR	SBL	SBT	SBR	EBL	EBT	EBR	NBL	NBT	NBR	Total
Real-world turning counts	N/A	178	1,656	14	10	503	146	66	472	50	141	399	40	3,675
Zero weight on seed matrix	0	85	1,530	15	0	447	230	58	409	102	71	399	11	3,357
Regional model (zero weight on counts)	9,999	123	1,082	13	68	591	58	17	609	407	164	69	125	3,326
ODME with 0.5 and 10 weight ratios	0.5	117	1,209	0	6	490	133	46	452	41	527	390	15	3,426
	10	79	1,344	0	6	491	134	38	438	70	336	371	15	3,322

Table 4. Comparison of Banyan Boulevard at North Dixie Highway intersection volumes with different ODME parameters.

Scenario	Volume (vph)										
	Weight	WBL	WBT	WBR	SBL	SBT	SBR	EBL	EBT	EBR	Total
Real-world turning counts	N/A	68	263	18	32	354	338	62	95	42	1,272
Zero weight on seed matrix	0	36	338	74	76	263	332	55	160	45	1,379
Regional model (zero weight on counts)	9,999	204	1,007	299	151	572	149	81	536	133	3,132
ODME with 0.5 and 10 weight ratios	0.5	90	468	79	29	258	82	58	66	32	1,162
	10	94	430	92	41	219	100	55	69	33	1,133

Table 5. Comparison of Lakeview Avenue at North Dixie Highway intersection volumes with different ODME parameters.

Scenario	Volume (vph)						
	Weight	WBL	WBT	SBT	SBR	NBL	Total
Real-world turning counts	N/A	237	1,086	543	208	327	2,401
Zero weight on seed matrix	0	195	1,159	680	242	359	2,635
Regional model (zero weight on counts)	9,999	474	1,011	798	146	546	2,975
ODME with 0.5 and 10 weight ratios	0.5	216	1,068	449	199	325	2,257
	10	217	1,065	444	201	325	2,252

Figure 2 shows that analysts could reduce the mean absolute deviation of turning movement volumes and link volumes, from 38 to 13 percent and from 46 to 13 percent, respectively, with the use of ODME. This section further analyzes O-D volume changes under different ODME setups by examining the trip destinations generated from several critical zones. For each of these generation zones, the study estimates the number of trips to the 10 destination zones with the highest number of trips. Figure 11 shows the results for one of these zones, while other zones exhibit a similar pattern. The results show how different ODME parameters can produce different results, but they indicate that the ODME with a weight on the seed matrix (the matrix from the demand forecasting model) can result in lower deviation from the seed matrix. Still, the results show large differences between the regional model O-D demands and the O-D demands resulting from the ODME with different parameters. These results indicate the need for better calibration of the regional models, possibly based on real-world partial O-D matrices. The results also show that performing the ODME with no seed matrix results in a small number of destinations and higher deviations from other setups of the ODME procedure.

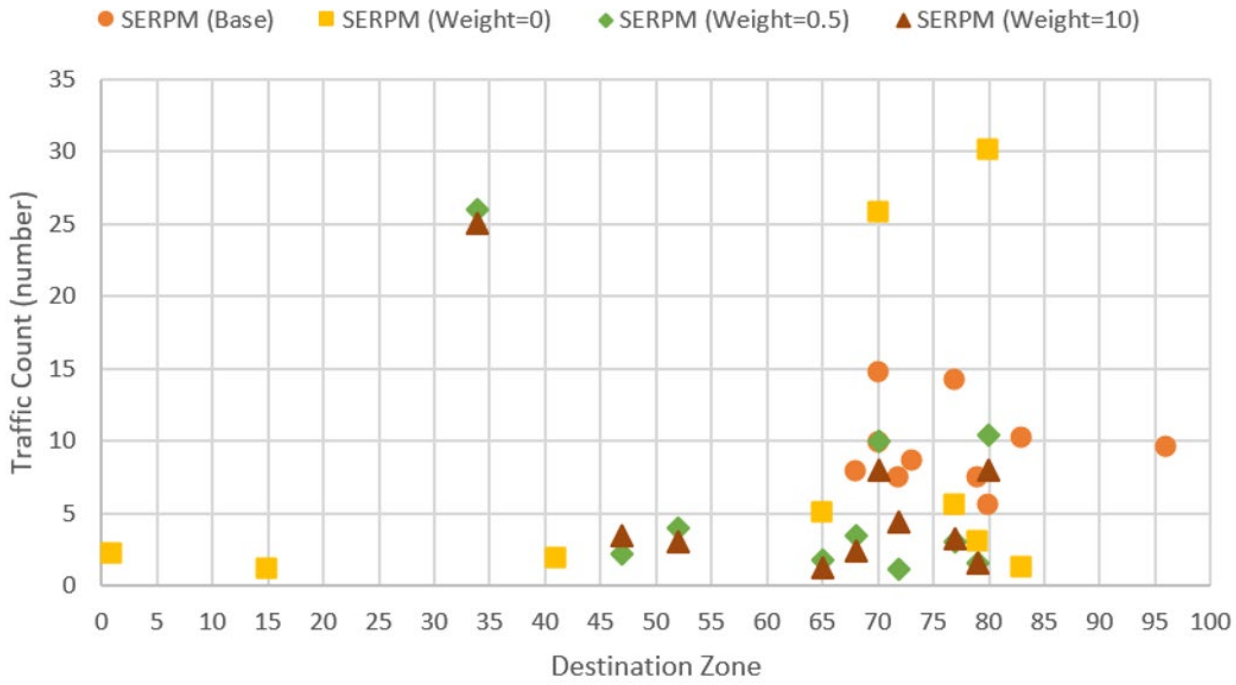

Source: FHWA.

Figure 11. Scatterplot. Examination of volumes to the top 10 destinations for zone 40.

Performance Measure Definitions (Gap 2.1 and Gap 2.2)

A key aspect of MRM is to ensure consistency between the performance measures at different levels. However, before addressing these issues, it is helpful to understand fundamental differences in the definitions of metrics at different levels. Measures such as travel time, delays, stops, queues, and density, have the same name in different tools, but are defined and calculated differently. Thus, analysts should understand these differences. The discussion in this section addresses gap 2.1 (variations in the definitions of measures) and gap 2.2 (variations in the methods used in estimation of various performance metrics).

The Federal Highway Administration (FHWA) *Traffic Analysis Toolbox Volume VI: Definition, Interpretation, and Calculation* addressed differences in the definition, interpretation, and computation of measures in different modeling levels and tools (Dowling 2007). One example given in the toolbox is that some simulation tools compute vehicle-miles traveled only for vehicles that enter the link during the analysis period, while others include the vehicles present on the link at the start of the period. Another example is that some tools include second-by-second calculation of the measures, while others only calculate measures for vehicles able to exit the link during the analysis period. Another example is the computation of vehicle hours traveled (Dowling 2007). Some simulation tools include the delay incurred by vehicles denied entry to the system. Most others do not. Most tools calculate delay using free-flow speed as a basis. The report concluded that the measures from simulation model tools are usually not directly translatable into *Highway Capacity Manual* (*HCM*) measures and level of service (LOS) (Dowling 2007; Transportation Research Board 2010). The report recommended the use of measures calculated in a consistent manner based on vehicle trajectories for comparison of results between tools and methods. Such computation is possible with mesoscopic and microscopic models. The remainder of this section describes how the macroscopic, mesoscopic, and microscopic models consider movement capacity and calculate the travel time or delay.

Utilized Macroscopic Traffic Model

Most demand forecasting models apply volume-delay functions (VDF), which are the relationship between speed and the volume-to-capacity (v/c) ratio such as the Bureau of Public Roads (BPR) equation (Bureau of Public Roads 1964), Akçelik equation (Akçelik 1991), modified Davidson equation (Tisato 1991), and conical equation (Spiess 1984). For this case study, the macroscopic modeling tool uses the BPR equation for static assignment. Figure 12 shows the expression of the BPR curve, which has been widely used in travel demand models to calculate link travel time.

$$t_i = t_0 \left[1 + \alpha \left(\frac{v}{c} \right)^{\beta} \right]$$

Figure 12. Equation. BPR volume-delay function.

Where:

- α = coefficient.
- β = BPR exponential coefficient.
- c = link capacity.
- t_i = congested travel time for link *i*.
- t_0 = free-flow travel time for link *i*.
- v = traffic volume on link *i*.

Analysts usually calibrate these parameter values by FT based on local conditions, using real-world traffic data. Analysts have also used microscopic simulation modeling to estimate these parameter values.

VDFs like the BPR require capacity and free-flow speed as inputs. They calculate delay as the difference between the free-flow travel time and the calculated travel time, using the equation in figure 12. Although the BPR curves are very popular in static route choice assignment as part of demand forecasting, modelers often criticize it for underperforming in congested traffic conditions where demand exceeds capacity. The BPR relationship suggests that if volume (or flow) increases relative to the capacity, the speed decreases (or the travel time increases). By definition, the BPR curve defines delay as a function of link length instead of the number of vehicles in the queue (Dowling, Horowitz, and McShane 1999). Thus, the shorter the coded link is with the higher v/c ratio, the lower the delay is. No spillback of congestion projected to upstream links is considered. In addition, the model allows for having v/c ratios higher than 1.0 (Hadi et al. 2019). The aforementioned discussion indicates that there are major deficiencies in the BPR curve and similar VDF relationships.

The traditional values for α and β are 0.15 and 4, respectively (Martin 1998). However, the value of α could vary from 0.1 to 1.0, and the value of β could vary from 4 to 11, according to Dowling (1997). Different studies have calibrated the BPR equation for various conditions and found different sets of values for the parameters (Dowling et al. 1997; Martin 1998; Moses et al. 2013; Horowitz et al. 2014).

Utilized Mesoscopic Simulation

Simulation-based assignment (SBA) is a DTA procedure that uses network loading based on mesoscopic simulation. The utilized algorithms in the SBA reflect the work of Mahut (Mahut 2001). The simulation model in the SBA of the utilized mesoscopic modeling tool simulates individual vehicles with a simplified car-following model and simplified assumptions regarding lane changing. The car-following model keeps a temporal distance to the rear end of the leading vehicle based on the reaction time plus the time required by the vehicle to stop. The lane selection procedure accounts for the lanes and turns that allow the vehicle to follow its route. Intersection modeling accounts for signal control and gap acceptance. SBA assumes a fixed-time traffic signal control. SBA accounts for conflicts between turning flows in a similar manner to the *HCM* (Transportation Research Board 2010).

The default values for time gaps are from the *HCM*, but the analyst can overwrite these if desired (Transportation Research Board 2010). The critical gap defines the time headway between two vehicles of the higher ranked traffic stream that allows one vehicle from a lower ranked movement to turn into the desired direction (PTV Group 2021a). The critical gap determines how the capacity of the lower ranked movement changes, depending on the higher ranked traffic stream with the right of way. The followup gap in the utilized SBA is the time headway between the departures of two consecutive vehicles from the same lower ranked approach. Consequently, the followup gap determines the saturation flow rate of the minor flow. Followup gaps only have an impact on vehicle behavior if they lead to a longer minimum time headway than defined by the car-following model (PTV Group 2021a).

In the SBA, capacity is an output of the model rather than an input as in the BPR. The capacity is a function of the reaction time and effective vehicle length per link using the corresponding link attributes “SBA reaction time factor” and “SBA effective vehicle length factor.” SBA calculates delay time from the loaded travel times on the network object (links/turns) minus the unloaded

travel times. In the calculation, loaded travel time implies the travel time with traffic assigned to the network, while the unloaded travel time is with no traffic assigned to the network. Other important parameters that affect capacity for opposed movements (at unsignalized intersections or permissive movements at signalized intersections) are those related to gap acceptance, which are the critical gap and followup gap.

Utilized Microscopic Simulation

The traffic flow model in the utilized microscopic simulation tool contains a detailed car-following model, lane-changing model, and gap-acceptance model. The tool uses the psychophysical perception model developed by Wiedemann (1974). In addition to the car-following model parameters that affect capacity (which is also an output rather than an input to the model) and performance, many other parameters have significant impacts. Analysts usually fine-tune these during the calibration process.

The utilized microscopic simulation tool calculates delay as the difference between individual vehicle travel time and its desired travel time (PTV Group 2021b). This calculation tool is different from other models, such as the SBA, which calculates the delay as the difference between the loaded and unloaded travel time, as described in the "Utilized Mesoscopic Simulation" section. In addition, the utilized microscopic simulation tool accounts for reduced turn speeds in the ideal travel time. The travel times and delays are computed from the actual travel times of all vehicles passing the destination point (PTV Group 2021b).

Performance Measure Consistency (Gap 2.4 and Gap 3.6)

As mentioned in the previous section, a key aspect of MRM is to ensure consistency between the performance measures at different levels. This section discusses the feedback loop that can improve consistency. The section addresses gaps 2.4 and 3.6 by examining the impact of more consistent measures among levels on assignment results and the impact of a feedback loop that improves consistency on MRM performance.

Different model resolutions calculate the performance measures differently, as described in the "Utilized Microscopic Simulation" section. The utilized macroscopic model requires capacity as an input and calculates delay as the difference between travel time calculated by the BPR equation and free-flow travel time. The utilized mesoscopic model calculates capacity based on parameters such as the reaction time, effective vehicle length, and gap acceptance parameters. The utilized mesoscopic model calculates delay as the difference between loaded and unloaded travel times. The capacity in the utilized microscopic model results from the simulation of individual vehicles with the specified microscopic traffic flow model parameters. The utilized microscopic simulation tool calculates delay as the difference between each individual vehicle's actual travel time and its desired travel time.

Thus, the three levels of resolutions assess capacity and delay utilizing different definitions and methods. However, fine-tuning the specific parameters of the traffic flow models in each resolution can result in comparable estimates of capacity and delay in the three resolutions. This fine-tuning process is key to the success of MRM, because the ODME and assignment conducted at the macroscopic and mesoscopic levels produce demands used as inputs to the microscopic

level. If the macroscopic and mesoscopic models underestimate delay on a given path, the heavy assigned traffic might produce unrealistic gridlock in the microscopic network. This study used a precalibrated microscopic simulation model (Palm Beach County 2020). Thus, the researcher investigated fine-tuning model parameters in the macroscopic and mesoscopic models to produce capacities and travel times consistent with those produced by the microscopic model.

Volume-Delay Function Calibration

This study examined the impact of utilizing the microscopic simulation model at the lower level of MRM to calibrate the BPR curve used in static assignment at the upper macroscopic level. The research team compared the calibrated curves with the curves utilized in the regional demand model (SERPM) and those used in the base macroscopic model from Palm Beach County. Figure 13 shows a comparison of the SERPM curve ($\alpha = 0.35$ and $\beta = 4.05$), the base curve used in the original macroscopic network ($\alpha = 0.15$ and $\beta = 5$), and the developed evening period model considering all critical network links ($\alpha = 0.8$ and $\beta = 2.0$). The regional demand model showed a range in travel time between 29.4 and 22.2 mph for v/c ratios ranging from 0.5 to 1.0. The range in travel time in the utilized macroscopic modeling tool model was between 29.9 and 26.1 mph for v/c ratios ranging from 0.5 to 1.0. This range was between 25.0 and 16.7 mph for the calibrated model based on the simulation results. This calibration used data from all critical links in the network under different demand levels. It is possible to calibrate the BPR curve for individual links in the network at higher spatial resolution (shorter links) if the analyst can extract sufficient data from the simulation model for a more accurate representation of the BPR curve. Using shorter links would likely decrease the speed at higher v/c ratios than those achieved by using longer links as was done in the network-wide BPR calibration.

In addition to the BPR calibration, the research team also used capacity from the microsimulation model as an input to the BPR curve. As stated in the Performance Measure Definitions (Gap 2.1 and Gap 2.2) section, capacity is an input to the macroscopic model in the demand forecasting tools, but it is output from the microscopic simulation model. Table 6 compares the capacities used in the demand forecasting model and the base macroscopic model to those obtained from the microscopic simulation model. The research team used the calibrated BPR curve and capacities in an updated version of the macroscopic modeling tool for use in the static assignment. The team examined the impacts on results, as described in the "Impact of Feedback Loop on Assignment Results" section later in this report.

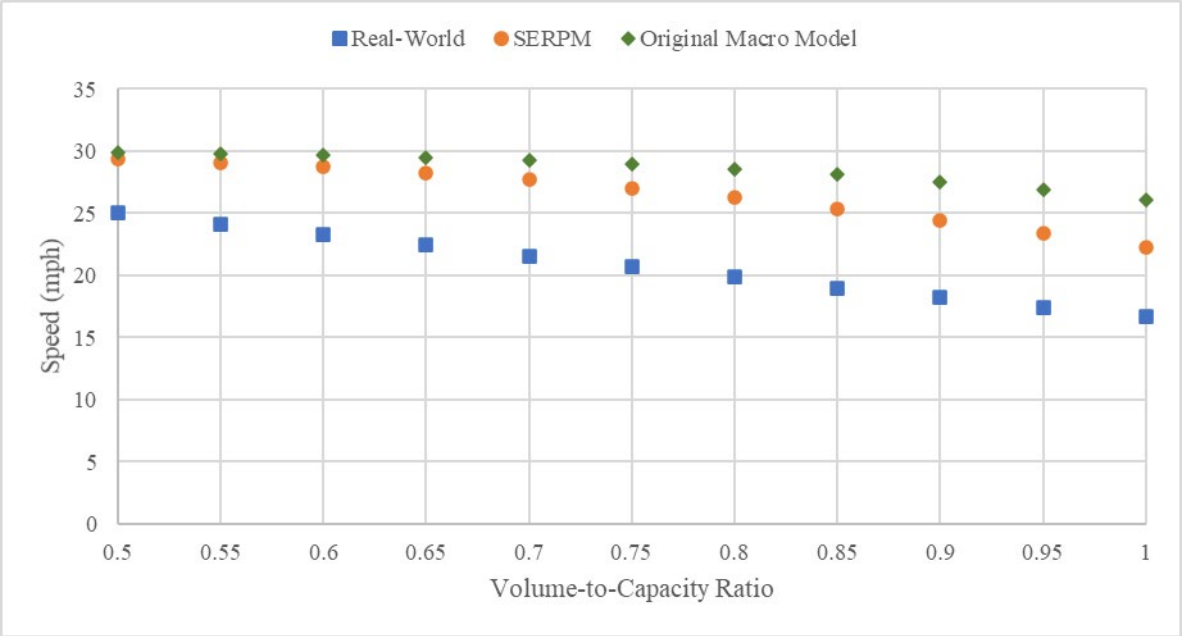

Source: FHWA.
mph = miles per hour.

Figure 13. Scatterplot. Comparison of the BPR curve derived from simulation models with those used in the demand forecasting model and base macroscopic model.

Table 6. Comparison of capacities derived from simulation with those used in the demand forecasting models and the base macroscopic model.

Critical Links	Capacity Per Lane Per Hour		
	Measured from Micromodel	Default in Macromodel	Default in Demand Model
Okeechobee Boulevard	850	1,715	1,035
South Tamarind Avenue	650	1,470	1,035
Banyan Boulevard	400	1,470	1,035
South Australian Boulevard	850	2,205	1,902

Calibration of the SBA Model

The next step was to examine the capacity and travel time/delays outputs from the utilized mesoscopic model (the SBA model). As described in the previous section, unlike the utilized macroscopic model, capacity is an output rather than an input from the SBA. The research team performed this examination for both signalized and unsignalized intersections.

Signalized Intersections

Table 7 shows a comparison among capacities estimated by the SBA mesoscopic model, the microsimulation model, and the *HCM* signalized intersection procedure within the Highway Capacity Software™ (HCS™) (Transportation Research Board 2010; McTrans 2021). The results indicate that capacities between the three models are comparable, although both the

mesoscopic and microscopic model could be further calibrated to better match the HCS estimated capacities or real-world measured capacities.

Table 7. Estimated capacities of Okeechobee Boulevard at South Tamarind Avenue intersection using different methods.

Approach	Movement	Mesomodel Capacity (vphpl) (default reaction time)	Mesomodel Capacity (vphpl) (fine-tuned reaction time)	Micromodel Capacity (vphpl)	HCS Capacity (vphpl)
EB	Left	503	495	411	369
	Through	835	774	655	638
	Right	1,117	818	794	637
WB	Left	390	375	326	278
	Through	765	592	664	558
	Right	830	753	720	558
NB	Left	386	367	339	304
	Through	487	421	390	326
	Right	1,118	881	686	552
SB	Left	325	320	289	253
	Through	470	388	342	291
	Right	958	843	559	528

vphpl = vehicles per hour per lane.

Analysts can calibrate protected movement capacities by varying the reaction time and vehicle length in the mesoscopic model. However, the research team found a larger deviation between the capacities of the SB right-turn and NB movements in SBA in comparison to those estimated by the other two models. The team attributed this deviation to the right-turn-on-red (RTOR) gap acceptance algorithm in the SBA. The capacity for the NB right-turn movement (exclusive right turn with RTOR) in the SBA was initially 1,118 vehicles per h per lane (vphpl), compared to 686 vphpl according to microscopic simulation, and 552 vph according to the *HCM* (Transportation Research Board 2010). The team increased critical gap and followup gap times from the default values of 5.5 and 3.3 s to 7.0 and 5.0 s, respectively, resulting in a capacity of 881 vph. The resulting capacity is closer, but still higher than the other capacities, indicating the need for further examination of gap acceptance models in the SBA. The team performed the aforementioned comparisons assuming no spillback from downstream intersections or from other activities such as railroad and drawbridge preemptions. The calibration of specific movement capacities can account for these impacts too.

The next step was to examine consistency of the relationship between average delay and v/c ratio. The team compared the microscopic, mesoscopic, noncalibrated macroscopic BPR, and calibrated macroscopic BPR models at a critical intersection in the network (Okeechobee Boulevard/South Tamarind Avenue). Figure 14, figure 15, figure 16, and figure 17 show the results. These figures show that although the BPR model calibration improved the results slightly, the BPR curve underestimates the delays, in particular, for v/c ratios higher than 0.9.

As shown in figure 14, figure 15, and figure 16, the variations of delay versus v/c ratio are similar in the microscopic and mesoscopic simulation models. However, figure 17 shows that on the NB approach, there is a large difference in delays for v/c ratios higher than 0.8. Further examination indicates that this difference was attributable to spillover from the left-turn bay to the through movement lanes. The research team performed further exploration by assuming that the left-turn is a full lane rather than a turn bay. The results shown in figure 18 indicate that the difference decreases significantly, but there is still a difference. Further examination indicates that this difference between mesoscopic and microscopic models is due to a large number of vehicles changing lanes in the microscopic model, because a large number of vehicles change lanes from the right lane to the left lane to make a left turn, considering that the left-turn movement is heavy. This finding indicates that lane-changing behavior in microscopic models can produce capacity drops that are difficult to account for in mesoscopic models. One option is to adjust the capacity or the BPR curve parameter for the segment, to consider such impacts.

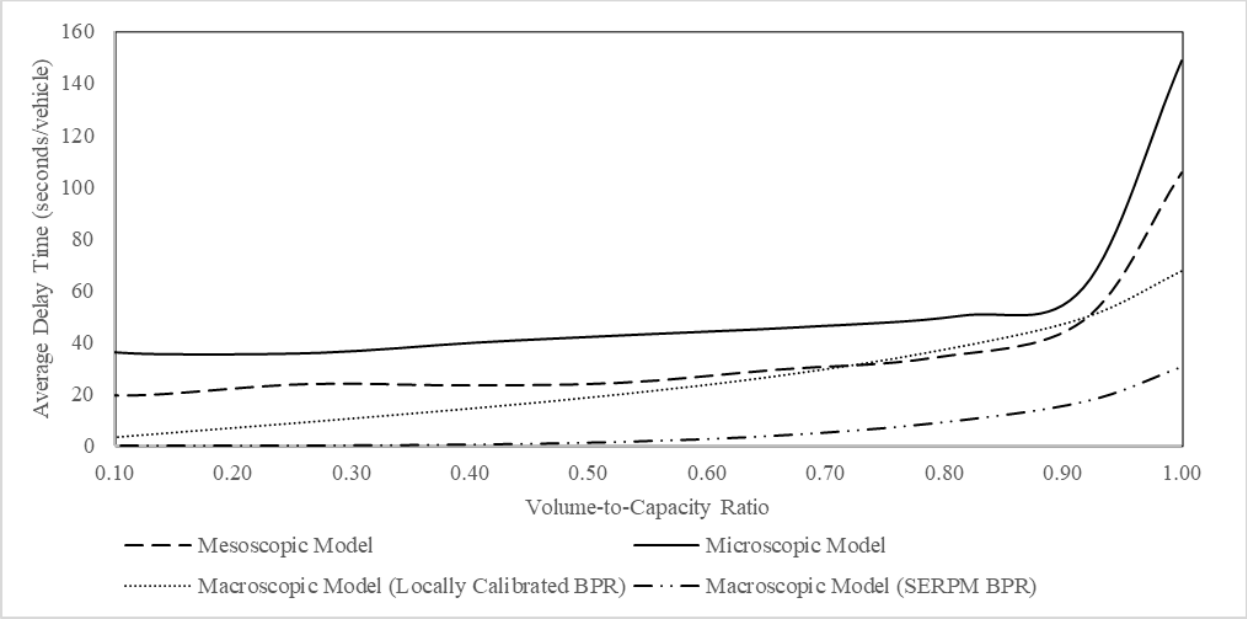

Source: FHWA.

Figure 14. Graph. V/c ratio versus delay for Okeechobee Boulevard at South Tamarind Avenue intersection (EB approach).

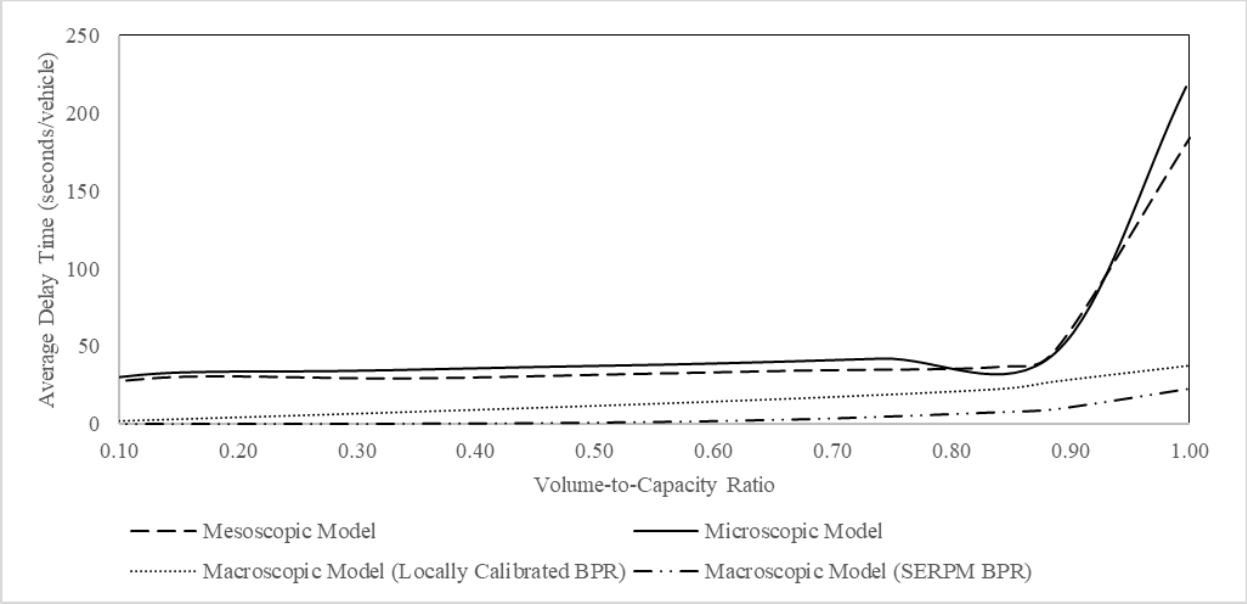

Source: FHWA.

Figure 15. Graph. V/c ratio versus delay for Okeechobee Boulevard at South Tamarind Avenue intersection (WB approach)

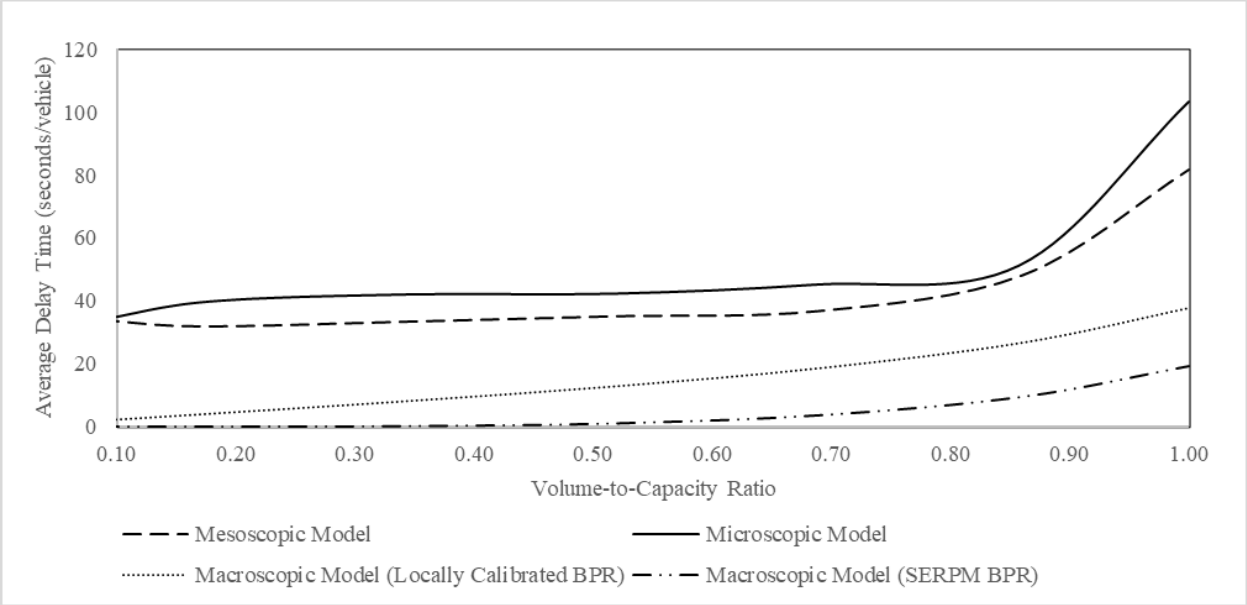

Source: FHWA.

Figure 16. Graph. V/c ratio versus delay for Okeechobee Boulevard at South Tamarind Avenue intersection (SB approach)

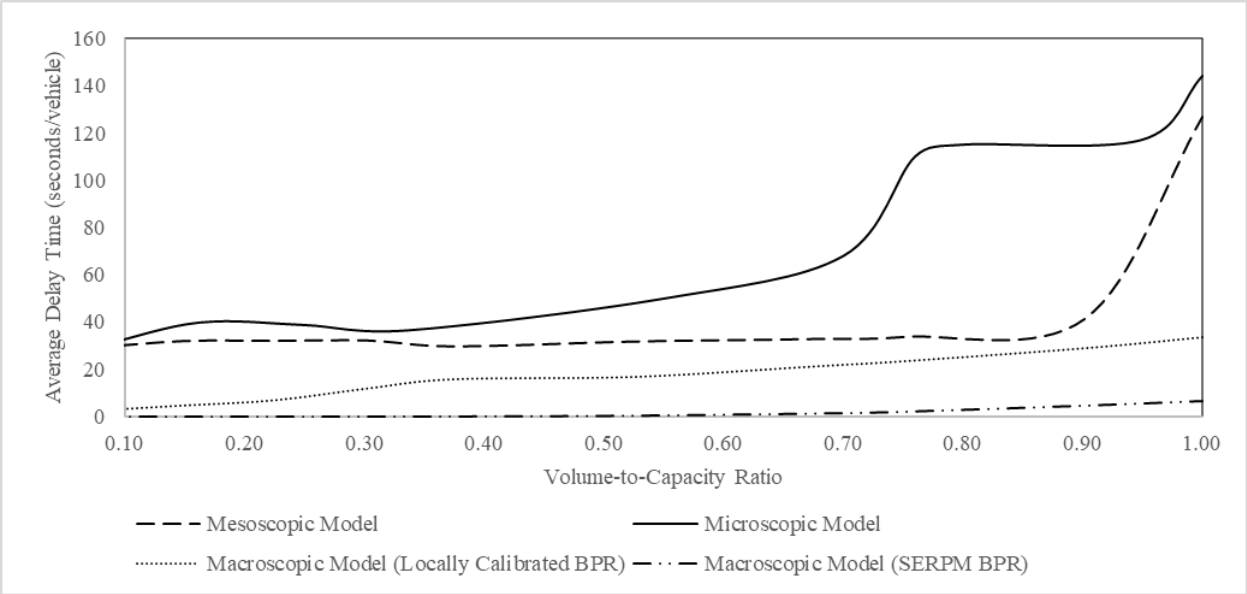

Source: FHWA.

Figure 17. Graph. V/c ratio versus delay for Okeechobee Boulevard at South Tamarind Avenue intersection (NB approach).

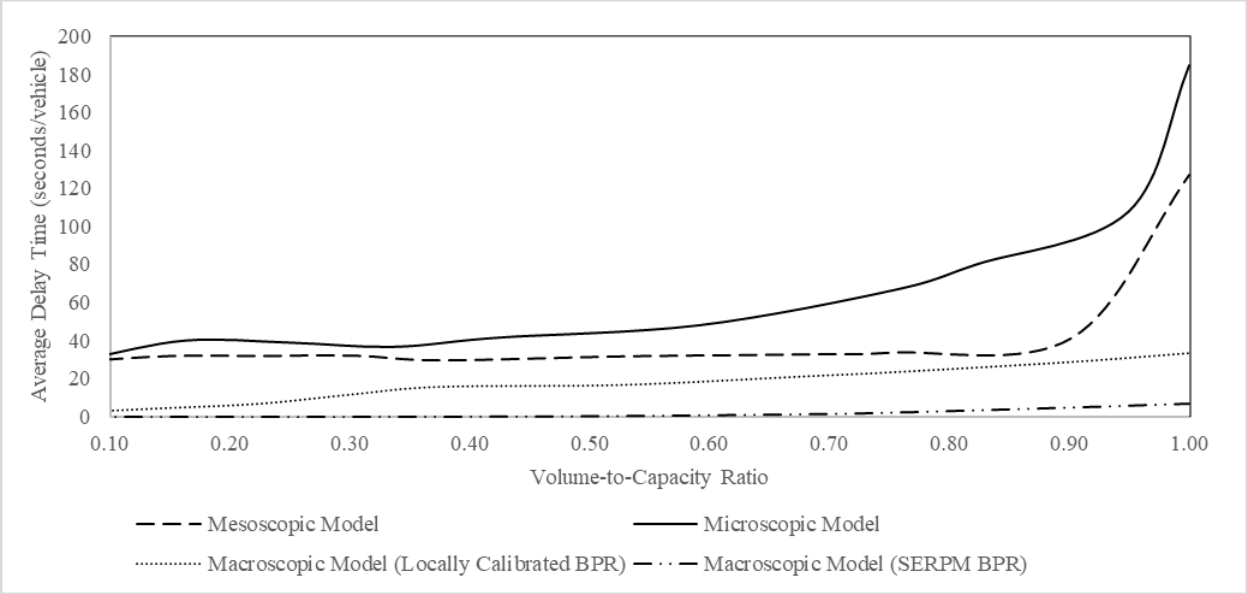

Source: FHWA.

Figure 18. Graph. V/c ratio versus delay for Okeechobee Boulevard at South Tamarind Avenue intersection after extending the left-turn bay length (NB direction).

Stop-Controlled Intersections

Table 8 shows the capacities according to the microscopic and mesoscopic models of the minor streets of a two-way, stop-controlled intersection in the network. The results show that with no calibration, there are large differences in the capacities. However, after the calibration of the gap acceptance parameters, as shown in table 9, the results in table 8 indicate that the differences in capacities between the two models are significantly smaller. Figure 19 shows the relationship between the major-street movement volume and minor-street capacity according to the calibrated SBA model. The results show a good correspondence in the capacity, in particular, for high conflicting major street volumes. It is notable that this comparison uses the calibrated SBA with updated gap acceptance parameters. However, figure 20 shows that the estimated delays are higher in microscopic simulation than the estimated delays in the SBA for the same v/c ratio.

Table 8. Impact of conflicting flow rate on minor-street capacity for a two-way, stop-controlled intersection.

Conflicting Flow Rate on Major Road (vphpl)		Mesomodel Minor-Road Capacity (vphpl)*		Mesomodel Minor-Road Capacity (vphpl)**		Micromodel Minor-Road Capacity (vphpl)	
NB	**SB**	**EBL**	**EBR**	**EBL**	**EBR**	**EBL**	**EBR**
65	212	378	446	195	219	156	287
128	423	259	305	140	169	125	219
194	634	179	212	113	133	97	140
258	845	91	111	93	103	83	114
323	1056	43	51	73	98	68	102

*With default values of gap acceptance parameters. **With calibrated gap acceptance parameters.

Table 9. Default and updated gap acceptance parameter values in the SBA model.

Gap Acceptance Parameters	Default Value		Used Value	
	Left Turn	**Right Turn**	**Left Turn**	**Right Turn**
Critical gap time	6.5	5.5	7.5	6.0
Followup time	3.5	3.3	5.0	4.5

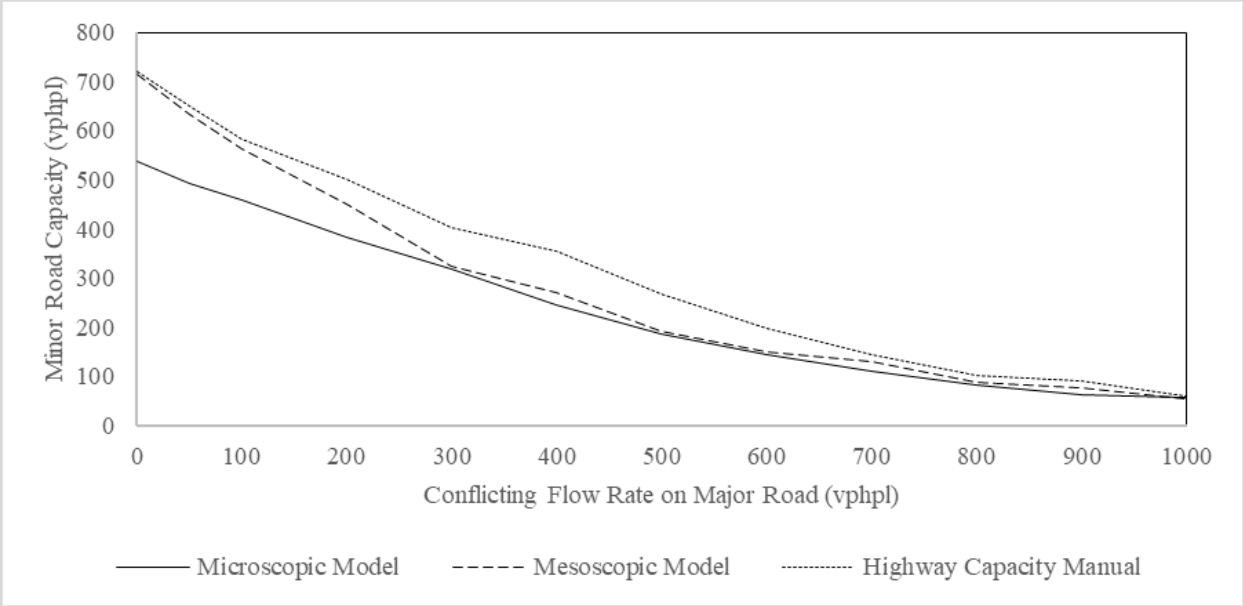

Source: FHWA.

Figure 19. Graph. Relationship between the major street movement volume and minor street capacity according to different models.

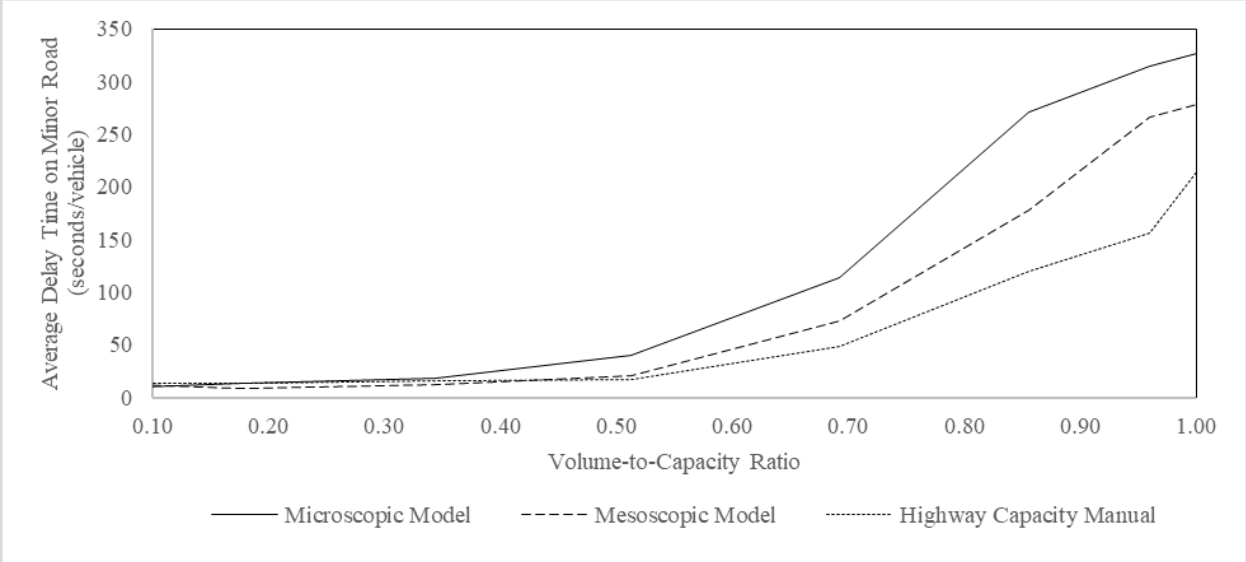

Source: FHWA.

Figure 20. Graph. Relationship between the minor street v/c ratio and delay according to different models.

Impact of Feedback Loop on Assignment Results

The previous sections discussed fine-tuning of the upper-level model parameters based on microscopic model results to improve the consistency between the models. This section compares the results of the assignment with and without this feedback loop when exported to the microscopic model. The objective of the assignment is to minimize travel times on selected routes between each O-D pair in the network. Thus, a better assignment procedure should result in lower overall travel times when analysts import assignment results into a microscopic simulation model. Figure 21 shows that the sum of travel time on the critical links is lower after fine-tuning the traffic assignment BPR curve (1,334 versus 1,667 s per vehicle, or 20 percent improvement). Figure 22 shows that critical link travel times (as assessed by microscopic simulation) dropped after fine-tuning traffic flow model parameters in the assignment stage, some of them significantly.

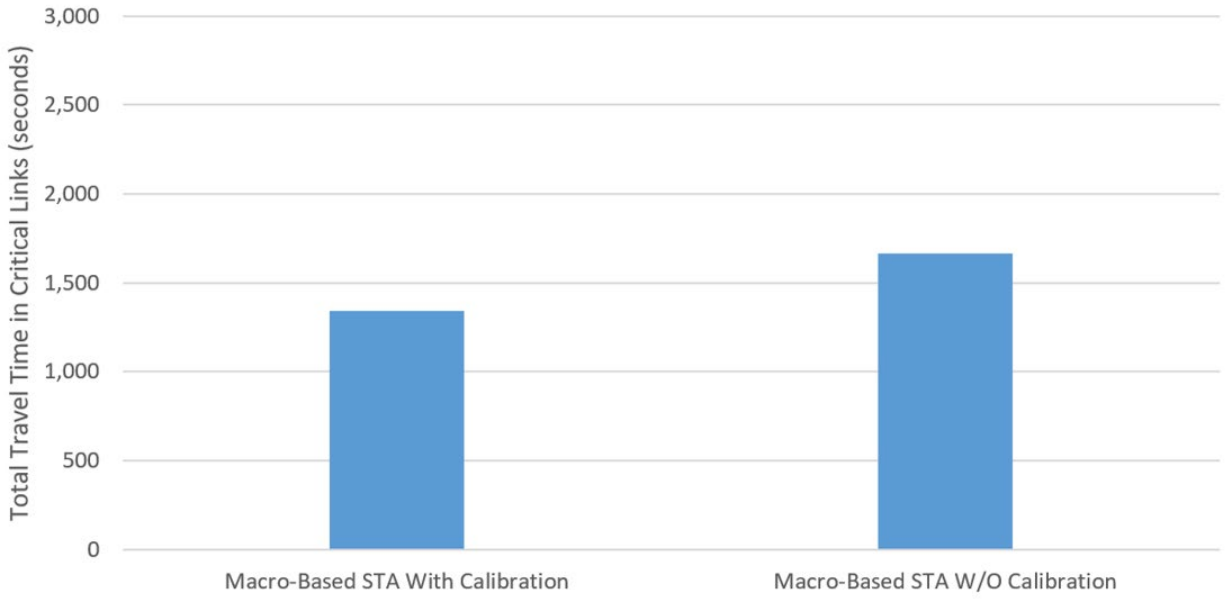

Source: FHWA.
STA = static traffic assignment; W/O = without.

Figure 21. Bar Chart. Total travel time in the critical links for static assignment with and without BPR model calibration.

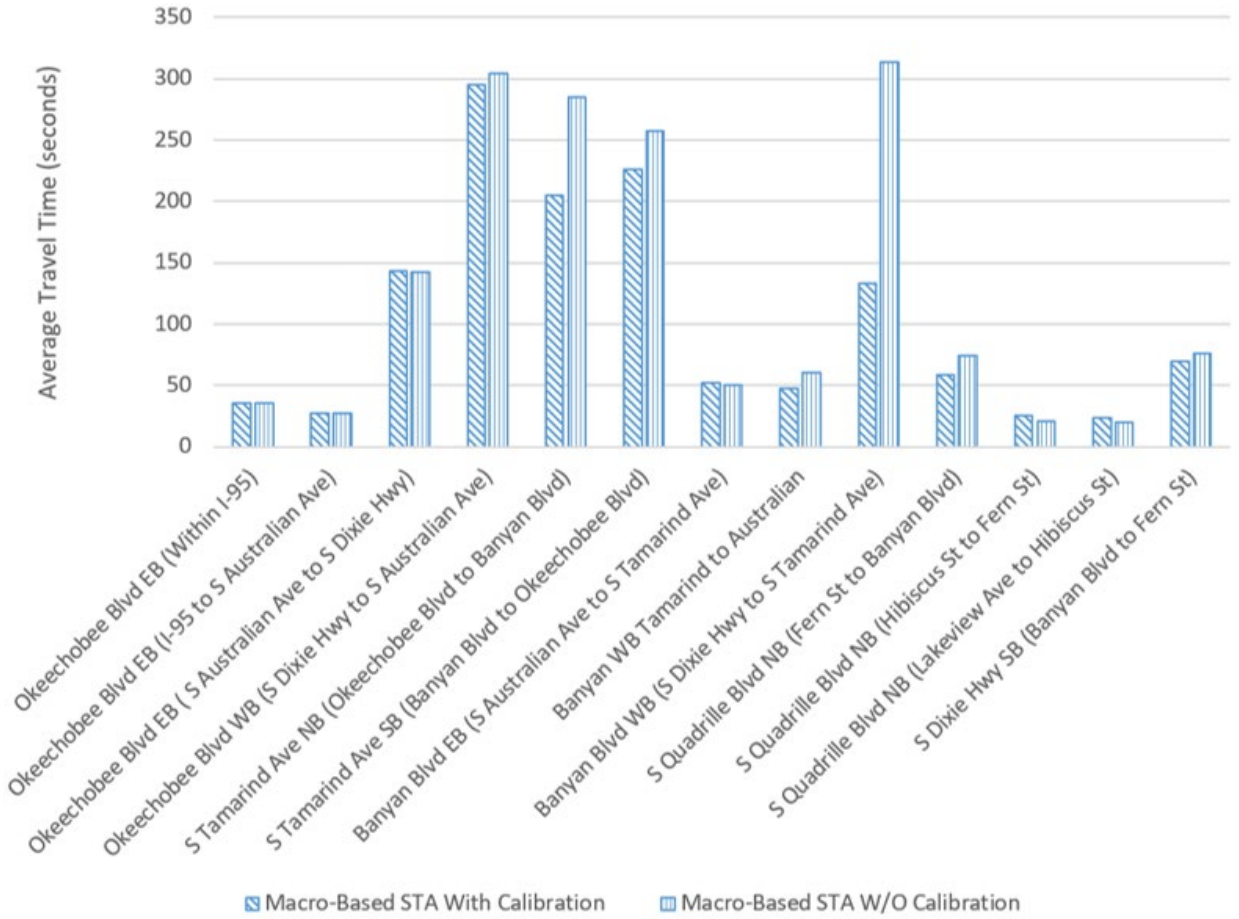

Source: FHWA.
Ave = avenue; Blvd = boulevard; Hwy = highway; S = south; St = street.

Figure 22. Bar Chart. Critical link average travel time for static assignment with and without BPR model calibration.

Benefit of MRM (Gap 3.6 and Gap 6.1)

An important investigation of this study was to determine the benefit of using mesoscopic simulation-based DTA with the SBA model in the utilized tool in comparison to using macroscopic model-based static assignment. The discussion in this section addresses gap 3.6 (feedback loop in internally consistent cross-resolution traffic representation) and 6.1 (the transportation agency valuation of the MRM implementation benefits). Whether there is a benefit to using mesoscopic simulation-based DTA with the SBA model is one of the important questions asked by analysts because the use of mesoscopic SBA will add additional cost to the modeling effort (Zhou, Hadi, and Hale 2021).

The research team's experiment involved analyzing network performance under existing demands, and also under the additional demands generated by a new development. The team assumed that the development would generate 500 vph in the modeled peak hour. The reason for conducting the comparison with the new development is that the benefits of using SBA should amplify after introducing fundamental changes to the network (e.g., a new development,

additional demands, geometric improvements, or new traffic management strategies). Another reason for the comparison is that for existing conditions, the ODME process can result in link and turn movement demands that are close to existing demands. It is notable that the investigation in this study involved assignment with an O-D matrix that was constant for the full peak period. If the analysis accounted for demand variations within the peak period, then the benefits of using SBA may have amplified even further.

Figure 23 shows that the static assignment assigned all existing and additional demands from the new development area to major zones south of the development to one path without adequately considering the delays caused by downstream intersections. This assignment resulted in blockages that prevent traffic from entering the network. Figure 24 shows that the use of SBA instead of static assignment resulted in traffic from the new development area to the major zones south of the development distributed across three routes instead of just one, as was the case with the static assignment. Figure 25 shows that the assignment using SBA results in lower network delays, specifically after introduction of the new development, when assessed using microscopic simulation. Figure 26 shows this assignment process more clearly by presenting the comparison of resulting travel times as assessed by microscopic simulation, for the streets surrounding the development. Figure 27 shows that the latent demand assessed by the microscopic simulation is much higher with the static assignment, in particular, with the introduction of the new development.

Original map: © 2021 OpenStreetMap contributors. Lines and numerical overlays added by FHWA.
A. Paths resulting from static traffic assignment without development.

Original map: © 2021 OpenStreetMap contributors. Lines and numerical overlays added by FHWA.
B. Paths resulting from static traffic assignment with development.

Figure 23. Maps. Paths resulting from static traffic assignment with and without development (OpenStreetMap B).

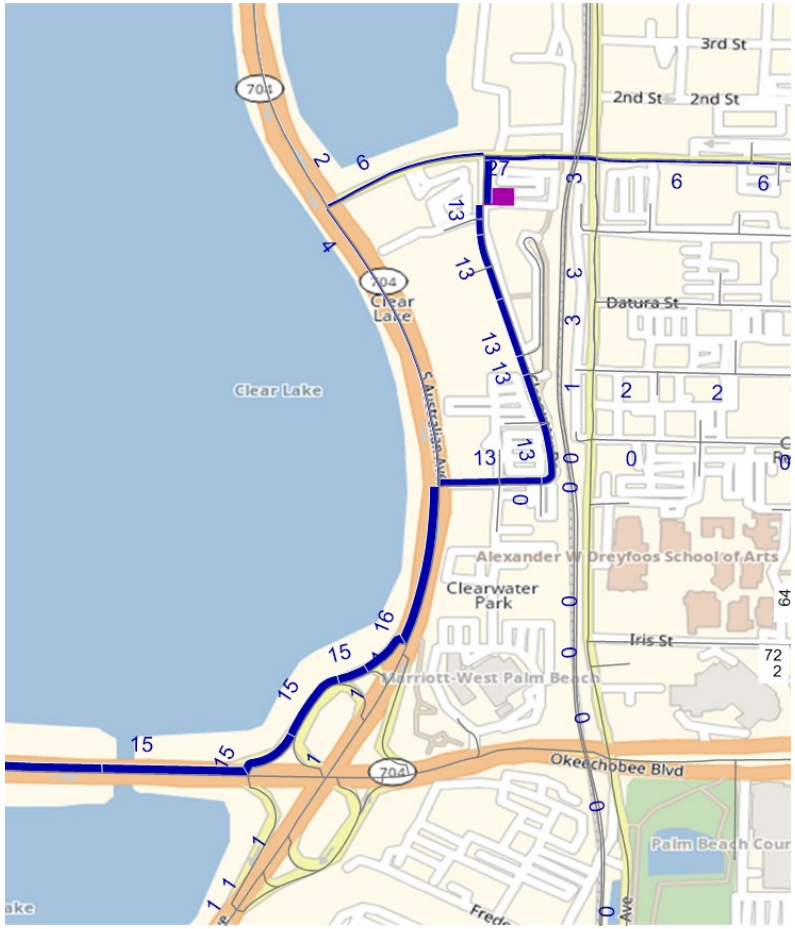

Original map: © 2021 OpenStreetMap contributors. Lines and numerical overlays added by FHWA.
A. Paths resulting from SBA without development.

Original map: © 2021 OpenStreetMap contributors. Lines and numerical overlays added by FHWA.
B. Paths resulting from SBA with development.

Figure 24. Maps. Paths resulting from SBA with and without development (OpenStreetMap B).

Source: FHWA.

Figure 25. Bar Chart. Network-wide travel time for STAs and SBAs with and without development.

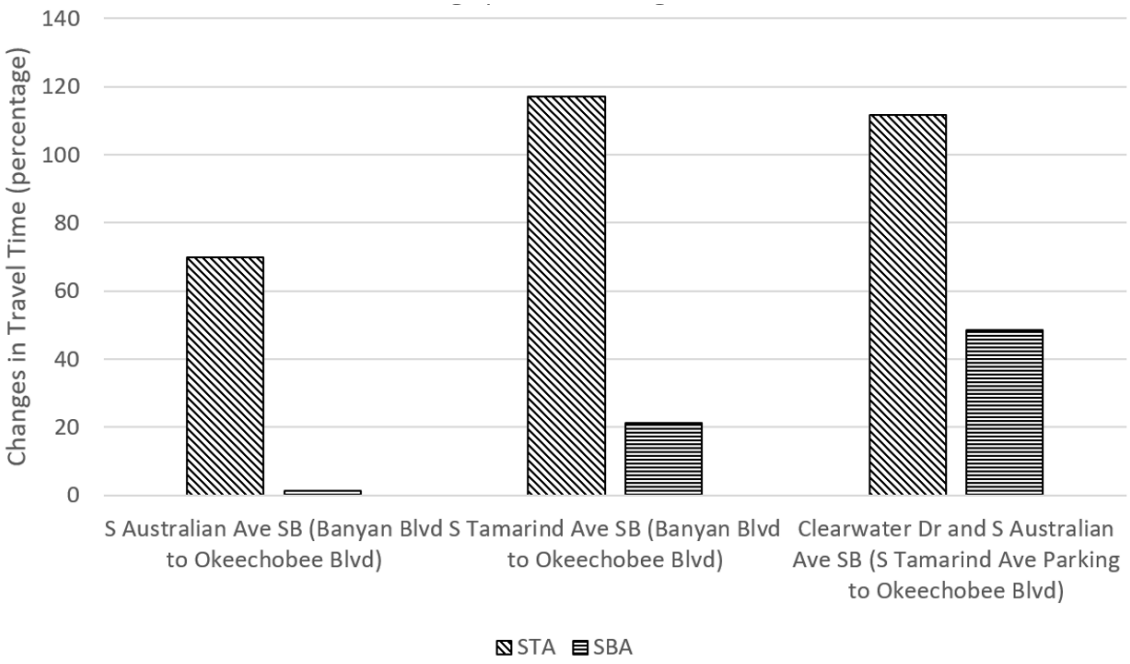

Source: FHWA.
Dr = drive.

Figure 26. Bar Chart. Changes in average travel time on critical links due to new development.

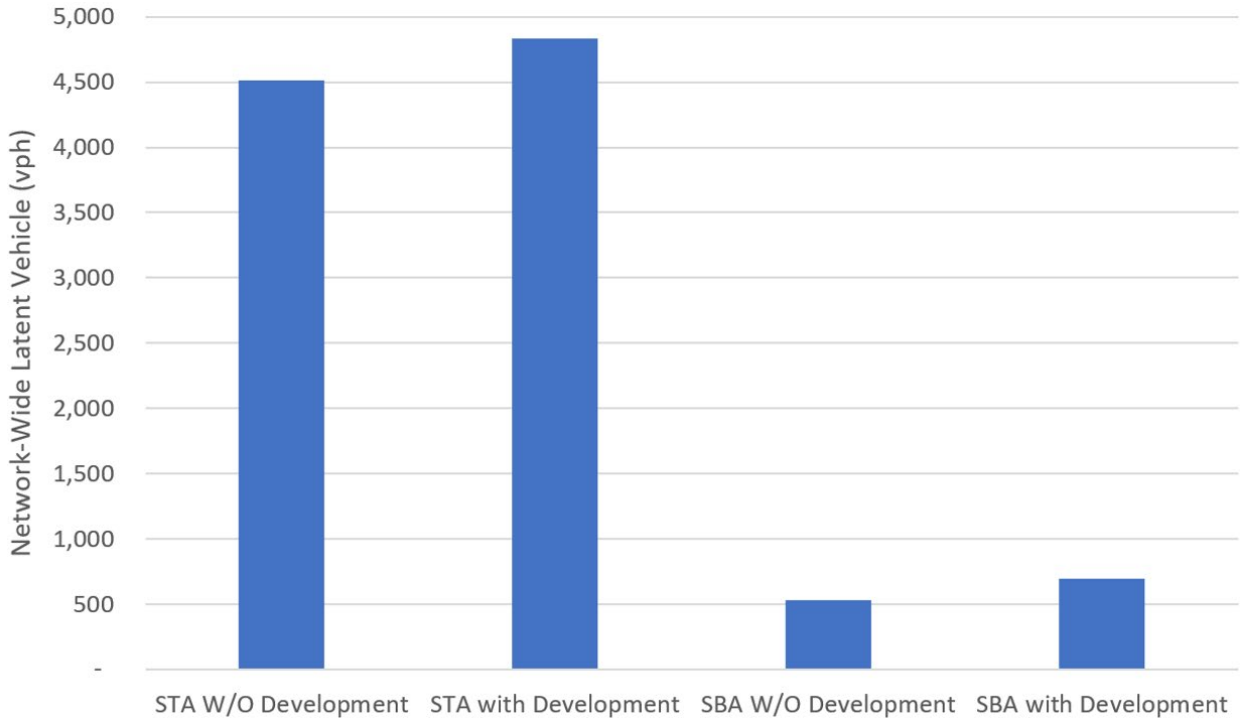

Source: FHWA.

Figure 27. Bar Chart. Comparison of network-wide latent demands with and without new development.

Cost and Time Requirements (Gap 1.3)

This section addresses gap 1.3 (allocation of funding and project time to meet the requirements for MRM). In this study, the research team used the macroscopic modeling tool as a basis to generate the microscopic simulation model. This is a common practice when using the modeling platform utilized in this study because it is easier to input the data in the macroscopic tool and convert inputs automatically to the microscopic tool format. This means that all of the inputs required to run SBA are already in the model because the microscopic simulation also requires them. This process reduces the additional cost and time significantly. Although there will be additional time required for time-variant O-D demand estimation and for ensuring realistic paths, this additional effort is justified considering the benefits of using the SBA, as discussed in the "Benefit of MRM" section.

As discussed in the "Benefit of MRM" section, the SBA results in better assignment than the static assignment, which can produce unrealistic congestion in parts of the network. The SBA results in better assignment because travel times assessed by the mesoscopic simulation model used in the SBA can produce results closer to those assessed by the microscopic simulation model than results assessed by the macroscopic model. The findings regarding the cost and time requirements discussed in this section are limited to modeling efforts similar to those of the West Palm Beach Downtown network in which the research team used all three modeling resolutions to model the same spatial and temporal network limits. This was not the case in the modeling efforts from the other case studies described in chapter 3 and chapter 4 of this report. In those

cases, the introduction of mesoscopic simulation could significantly increase the required effort, depending on the size and details of the network. The use of mesoscopic, simulation-based DTA in such cases could add several months to the project schedule when the modeled network is large in size.

Model Archiving and Maintenance (Gap 1.4)

This section addresses gap 1.4 (adoption of processes for model archiving and maintenance). One of the identified gaps in the gap analysis of this project is that many agencies do not archive and maintain the modeling files after the project ends. Palm Beach County has archived copies of the original network and data for future use. Based on discussion with the County staff, the County is planning to use the network produced by its consultant to investigate the impacts of new developments in the downtown area.

Model Conversion Effectiveness (Gap 3.1)

This section addresses gap 3.1 (methods and tools that support the integration and data conversion between different modeling levels). The conversion of networks between three modeling tools (demand forecasting, macroscopic and mesoscopic, and microscopic) was easy to use, and the converted networks had no significant issues.

Impacts of Advanced Applications (Gap 3.4)

This section discusses gap 3.4 (modeling of emerging and advanced technologies and strategies). The microscopic simulation tool allows the user to model connected and automated vehicles (AVs). Specifying a percentage of the vehicles to be equipped with this technology in the microscopic simulation level will allow for deriving an updated version of the BPR and link capacity for use in the macroscopic model, and for updating mesoscopic model parameters to consider the impact of connectivity and automation. Analysts can use these parameters in the macroscopic and mesoscopic model to determine path assignments resulting from the static assignment and SBA.

Collaboration Assessment (Gap 5.1 and Gap 5.2)

This section addresses gap 5.1 (interagency collaboration) and gap 5.2 (intra-agency collaboration). The project involved a number of departments within Palm Beach County, including Public Works, PalmTran (public transit department), Metropolitan Planning Organization, and staff of the traffic management center. The City of West Palm Beach is also a stakeholder of the project. The partner agencies collaborated on the provision of compiling data, reviewing the model calibration results, attending project presentations, and commenting on the original project report developed by a consultant for the county.

SUMMARY

This case study investigated a number of key aspects related to MRM, including the O-D demand estimation, the impact of the utilized traffic assignment, and the methods to increase the consistency between models of different resolutions in the analysis. A summary of the findings follows.

Demand Estimation

Although some users use the O-D matrix generated from the demand model, most users currently use ODME procedures to estimate the O-D matrices. These procedures minimize the deviation between volumes resulting from the model, the real-world counts, and the deviation from an initial O-D (seed) matrix. Modelers usually obtain the seed matrix from the demand model. Some users have also started utilizing partial O-D matrices that are either measured by the agency or provided by a third-party vendor if the project budget allowed obtaining such data. The West Palm Beach case study results from this chapter confirmed that using an O-D matrix directly from the demand model in the assignment does not produce realistic turning movement volumes. Using an ODME based on the counts without using a seed matrix also does not produce good results. Such use tends to produce fewer destinations and possibly shorter trips in comparison to the matrices produced by the demand model.

Some of the commercial tools have more than one ODME procedure to allow specification of different parameters and assignment procedures. The West Palm Beach case study from this chapter showed that the ODME parameters and assignment procedures affect the quality of the O-D estimation. The research team investigated using the O-D matrix produced by the demand model as a seed matrix to the ODME. The investigation compared different weights on the seed matrix with weights obtained through the turn movement volumes. The results showed improvements in the average deviations from the counts and seed matrices. However, specific turning movements continued showing higher deviations with the seed matrices than with the counts. The analyst could try to increase the weights on specific turning volumes and refine some cells within the seed matrix to address this issue. The analyst might also consider acquiring partial O-D matrices to refine the initial seed matrix. The authors also strongly recommended that the simulation modelers work with demand forecasting modelers to improve the demand forecasting model results, to increase the model's applicability for use as a seed matrix in the ODME.

In the West Palm Beach case study, the research team used turning movement counts on all signalized intersections and on some unsignalized intersections as inputs to the ODME process. Some analysts have used link counts rather than turning movement counts. The authors believe that for operational level analyses similar to this case study, it is necessary to use turning movement counts rather than link counts in the ODME process (Hadi et al. 2016).

An interesting finding is that the static assignment of traffic generated from a new development can create more congestion when estimating demands using ODME based on only the counts in comparison to using ODME based on both counts and a seed matrix. The static assignment assigned trips between an origin and a destination to only one path. Because of the low number of destinations of the generated trips when using the ODME without a seed matrix, the traffic assignment to paths can result in high demands, causing unrealistic congestion.

Impact of Assignment Method

The study found that the STA and analytical DTA produced comparable results. However, the research team performed the comparison using a fixed (non-time-variant) O-D matrix. The use of

time-variant matrices can improve the results. However, because the analytical DTA still uses a macroscopic traffic model (the BPR curve), the results are not expected to improve significantly.

The research team found that using DTA in the SBA model distributed traffic generated from the new development to more paths between each origin and destination. This assignment is more logical than the static assignment, and it can reduce traffic gridlock when transferred to the microsimulation model. However, the team found that the SBA is very sensitive to parameters coded in the model. This sensitivity could produce unrealistic assignments if the capacities as assessed in the microscopic model are lower than the capacities in the SBA. The team found this issue would occur at unsignalized intersections and at locations with heavy lane changing and weaving.

Performance Measure Consistency

A key aspect of MRM is to ensure consistency between the performance measures at different levels. This study examined the impact of utilizing microsimulation at the lower level of MRM to calibrate the BPR curve used in static assignment at the upper macroscopic level. The research team developed a network-wide BPR curve for all arterial links. In addition, the team used link capacity values that were assessed from microsimulation in the BPR curve calculation of speeds and travel times. The team found this calibration of the BPR parameters and capacities improved the assignment results, as assessed by the microsimulation. There is a potential for further improvement if analysts calibrate BPR curve parameters for each segment in the network. Results showed that the sum of travel time on the critical links is lower after calibrating the traffic assignment BPR curve (1,334 versus 1,667 s per vehicle, or 20 percent improvement). Although the BPR model calibration improved the results, the BPR curve underestimates the delays, in particular, for v/c ratios higher than 0.9.

This study also calibrated the capacity outputs from the utilized mesoscopic model (the SBA model) to be consistent with those obtained from microsimulation. Unlike the utilized macroscopic model, capacity is an output rather than an input of the SBA, which is also the case for microsimulation. The research team performed this calibration for both signalized and unsignalized intersections. The team also examined consistency of the relationship between average delay and v/c ratio in the SBA compared with the microsimulation. The analyst could further use such examination to fine-tune the model parameters, to produce consistent estimation of delays in the two models. This study showed that it is possible to fine-tune model parameters in the SBA to produce capacities close to those produced by the microsimulation.

The study also showed that the variations of delay with the v/c ratio are similar in the microscopic and mesoscopic simulation (SBA) models. However, certain traffic flow characteristics that affect capacity are not explicit inputs to microsimulation, producing inconsistency between the models. These inconsistencies occur at locations with weaving, lane changing, permissive movements, and spillovers from left-turn bays. Under such conditions, achieving 100 percent consistency between the models is difficult. However, analysts should try to improve consistency as much as possible. Without such consistency, an assignment of traffic to paths identified as optimal in the SBA may produce unrealistic gridlock in the microsimulation.

CHAPTER 3. PHOENIX METROPOLITAN AREA CASE STUDY

This chapter describes an MRM modeling effort for the Phoenix Metropolitan area, which comprises two fundamental analyses. The first analysis carries out a supply-side calibration for the static traffic assignment (STA) model parameters and their dynamic extension. The second analysis focuses on demand-side consistency by integrating a macroscopic activity-based model (ABM) with a DTA model. The case study illustrates the benefits of using speed and count data to calibrate VDF by using systematically defined demand-over-capacity ratios for congested traffic regimes, and, thus, ensuring supply-side consistency between macroscopic and mesoscopic models. To complement the other two case studies, this study performs a wide-area regional analysis and uses public domain simulation tools.

NETWORK DESCRIPTION

The research team obtained the Phoenix metropolitan regional network from the Maricopa Association of Governments (MAG) travel demand model. The travel demand model evaluates the performance of traffic systems based on VDFs for use in traffic assignment, allowing the assessment of impacts caused by transportation improvement projects. To systematically calibrate VDFs and account for the effects of traffic flow on roadway segments' capacities, the team categorized the links into different FTs and area types (ATs) with different VDF codes. The original network implements a two-way link format, that is, each link contains attributes from two directions (e.g., NB or SB). To facilitate the future extension to mesoscopic analysis, the team developed a software package to convert the two-way network to the General Modeling Network Specification (GMNS) data format (Zephyr Foundation 2020a). The GMNS defines a common human and machine-readable format for sharing routable road network files. Figure 28 shows the GMNS network for the Phoenix Metropolitan Area under consideration. The network defines five ATs: central business district (CBD), outlying CBD, mixed urban, suburban, and rural area. The network defines 17 FTs according to MAG's specification. These include high-occupancy vehicle (HOV) lanes, freeways, expressways, collectors, and six-leg arterials.

The network sets VDF codes according to a combination of AT and FT, as defined in table 10. In this region-wide case study, the research team calibrated key parameters in the VDF for each combination of AT and FT. For example, a VDF code of 101 means an AT of CBD as 1 in the first digit, and an FT of freeway as 01 in the last two digits. Using such a coding scheme, agencies can further quantify the number of sensors and measurements available in each VDF category. As the model calibration in this case study involves both speed and count measurements, an assessment on the data availability and data needs based on table 10 can further assist agencies to determine what sensor investments should be made in the future; when, where, and with what technologies (Zhou and List 2010). Essentially, agencies can locate a limited set of traffic counting stations and other types of readers in a network, across each VDF category, so as to maximize expected information gain for the subsequent capacity calibration and O-D demand estimation stages.

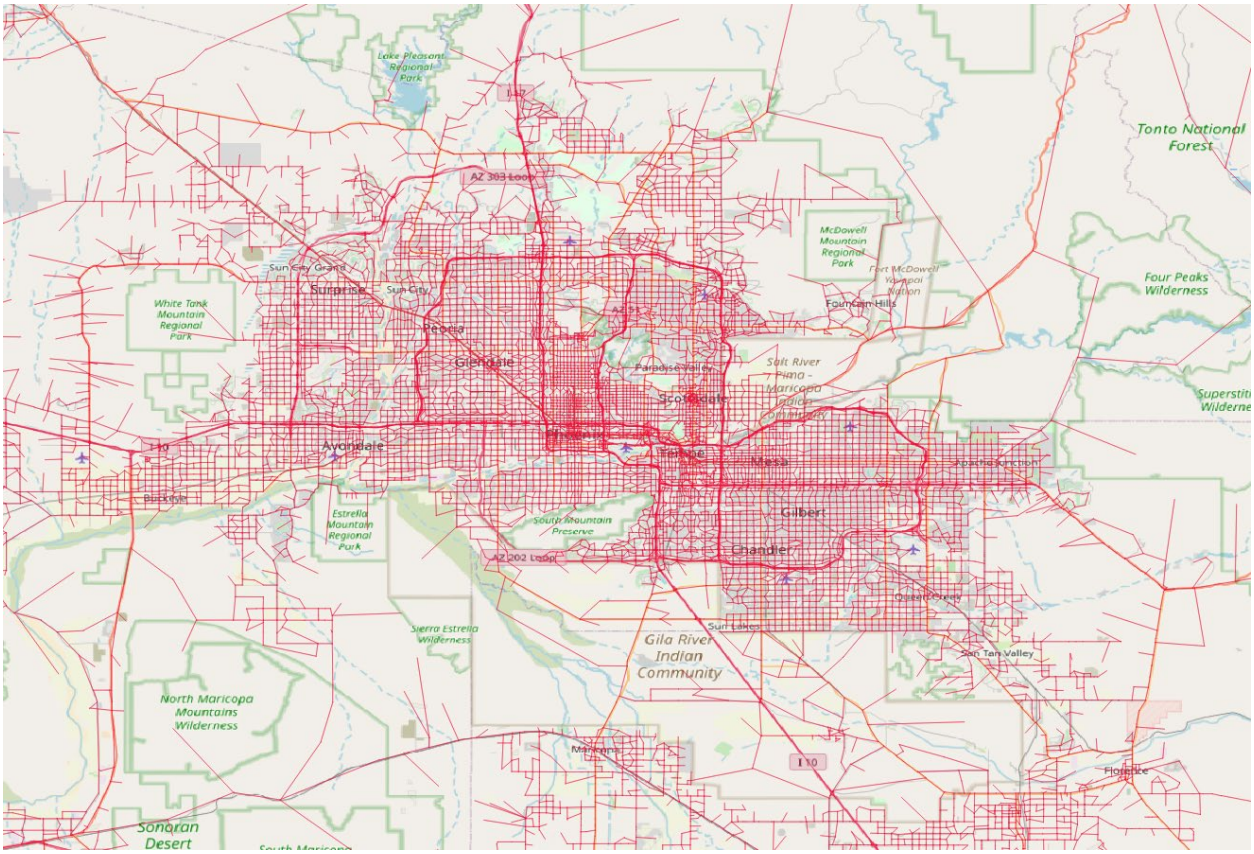

Original map: © 2021 OpenStreetMap contributors. Overlays of the modeled network added by Maricopa Association of Governments (MAG) (see Acknowledgments section).

Figure 28. Map. GMNS for the Phoenix area (OpenStreetMap C).

Table 10. Volume-delay function codes with AT and FT for a systematic assessment of data availability and data needs (gap 2.3).

AT	FT															
	HOV Lane (0)	Freeways (1)	Expressways (2)	Collectors (3)	6-Leg Arterials (4)	Centroid Connectors (5)	Major Arterials (6)	Unmetered Ramps (7)	Metered Ramps (8)	C/D Roads (9)	Arizona Parkway (10)	Unpaved Road (11)	Transit Only (12)	Light Rail (13)	Walk Only (14)	Park and Ride (15)
(1) CBD	100	101	102	103	104	105	106	107	108	109	110	111	112	113	114	115
(2) Outlying CBD	200	201	202	203	204	205	206	207	208	209	210	211	212	213	214	215
(3) Mixed urban	300	301	302	303	304	305	306	307	308	309	310	311	312	313	314	315
(4) Suburban	400	401	402	403	404	405	406	407	408	409	410	411	412	413	414	415
(5) Rural	500	501	502	503	504	505	506	507	508	509	510	511	512	513	514	515

© 2021 Maricopa Association of Governments (MAG).
C/D = collector-distributor; CBD = central business district; HOV = high-occupancy vehicle.

MODEL OVERVIEW

The MRM work tasks include the integration of ABM and traffic assignment and calibration of traffic assignment models for their underlying traffic flow models with both macroscopic and mesoscopic parameters as follows:

- Macroscopic parameters: ultimate capacity, free-flow speed, and coefficients in the VDF.
- Mesoscopic parameters: queue length, congestion period, time of queue appearance, and dissipation.

The research team collected the following data for model development and calibration:

- Network geometry data from the base year of 2018: The Phoenix Metropolitan region consists of 22,402 nodes and 32,701 links.
- Traffic speed and counts: The metro area contains 1,736 detectors and 457,000 records. Data are from two representative weekdays with 15-min intervals during 2018–2019.
- Exported O-D trip files extracted from ABM trip chain files.
- Vehicle trajectories generated by DTA.

Integration of ABM and Regional Traffic Assignment

This case study includes an integrated implementation of the ABM and regional traffic assignment. The MAG research team plans to use this integrated model to link travel behavior choices such as departure time, route choice, and mode choice under different scenarios, including the base year and future year 2040 (with or without AVs). Specifically, ABM provides trip chain files to the DTA model, while DTA tools provide a series of aggregated skims and LOS for ABM to generate trips iteratively. The MAG implementation includes an internal and an external loop in simulating activities. The external loop generates activity patterns, schedule skeletons, and individualized LOS through trajectory mining. The internal loop simulates activity patterns, adjusts schedules for realistic trip chain loading, uses individual trajectories, and evaluates "stress" measures. Table 11 specifies the inputs and outputs of ABM and DTA models in the context of an integrated model.

Table 11. Inputs and outputs of activity-based and DTA models in the MAG case study.

Model	Interfaces	Inputs	Outputs
ABM	CSV file reading and writing.	Day-to-day or minute-by-minute traffic conditions at link/path/O-D levels (skims).	Traffic request for possible departure time, destination, and mode change.
DTA	CSV file reading and writing utility. Data receiving and aggregation package.	Traffic network, vehicle O-D, existing traveled path, and real-time traffic data stream.	Information for upstream vehicles to change routes, updated travel time and queue warnings, and traffic conditions at link/path/O-D levels

ABM = activity-based model. CSV = comma-separated values. DTA = dynamic traffic assignment. O-D = origin-destination.

The original ABM produces about 1.6-million households' travel and activity participation information, and the five types of daily activities are shown in table 12. The model identifies three types of mandatory activities: home, work, and school. For each trip, the model has access to information on activity types, O-D nodes, and corresponding departure/arrival times.

Table 12. Travel activity characteristics produced by the ABM.

Activity Number	Activity Type	Mandatory or Optional
1	Work	Mandatory
2	Business	Mandatory
3	School	Mandatory
4	Shopping	Optional
5	Other	Optional

In evaluating how candidate DTA tools meet the needs of ABM-DTA integration in this pilot study, a team of researchers from MAG and multiple universities designed the following criteria to test the performance of the integrated model (INRO 2020):

- Simulation time horizon: Network modeling and simulation time horizon in DTA should both satisfy the activity trip requirements in the ABM.

- Multiresolution network: Analysts should develop consistent multilayers of networks. The macroscopic ABM and STA network should be consistent with the network for DTA models, which could be microfocused or mesofocused.

- Signal timing and control data: The mesoscopic network in DTA should cover region-wide signal timing and control data, HOV in freeways, movement restriction, transit vehicle, and shared mobility with AVs.

- Traffic flow model calibration: Analysts should calibrate different resolutions of traffic flow models in advance for macroscopic and mesoscopic networks.

- Dynamic skim computations (network accessibility calculator): Analysts should use the provided link travel times from DTA and considering 15-min time steps (aggregated travel time interval) because each of the created 96 or 48 matrices stores a number of elements.

- DTA demand generation: The DTA should distinguish between mandatory and nonmandatory trip chain files generated by the ABM. The integrated model should also consider an extended set of intrahousehold interactions and joint mobility services.

- DTA accuracy evaluation: Analysts should use the link traffic volume and speed data from MAG to check the quality of model calibration and validation for different peak periods. R^2 and root mean square error (RMSE) are key measures of comparison.

- Convergence check method and standard: The general (minimum) threshold on convergence should be considered as follows: less than 5 percent relative gap of path travel time of each O-D pair with departure time in DTA, and less than 5 percent relative

gap of travel demand of each O-D pair with departure time in ABM. In particular, DTA tools should report the number of iterations necessary for obtaining a stable skim matrix and report the percentage and number of "unfinished trips," because some trips do not complete their journeys under capacity-constrained scenarios.

- Demand calibration: In demand calibrations, analysts should integrate and utilize different levels of data sources, including household data, stated-preference surveys, GPS data, speed, and volume profiles.

The primary model integration results are as follows:

- The DTA tools under evaluation can perform multithreaded computations that provide fast DTA running speed.

- Many scripting tools automate network development. Different packages with built-in modules create traffic signal phases and optimize signal timing.

- The DTA tools demonstrate the capability to produce stable, converged DTA runs even in very highly congested scenarios.

- In general, simulation-based approaches are more flexible than analytical DTA models in accounting for various network traffic conditions such as traffic signals, incidents, or driver routing behaviors, whereas analytical DTA models provide faster computation.

- Calibrated/validated traffic flow models are essential for DTA to provide reliable travel time skims back to ABM.

In the context of MRM, the case study shows microsimulation-based DTA to be feasible for a medium-scale network, especially for the gridlock case in highly oversaturated conditions. A desirable feature in the near future is the ability to simulate traffic signals, including actuated and coordinated operations.

Traffic Assignment Periods

In the MAG STA model, there are four assignment periods corresponding to different time windows of travel demand O-D matrices:

- Morning peak (6–9 a.m.).
- Midday (9 a.m.–2 p.m.).
- Evening peak (2–6 p.m.).
- Nighttime (6 p.m.–6 a.m.).

DATA DESCRIPTION

MAG maintains and provides speed-volume data for 1,758 links on 2 representative weekdays in 15-min intervals. The research team matched speed and volume observations to directional links and link performance files using the GMNS data format. Figure 29 shows the network-wide link volume on one representative day at 4 p.m.

© 2021 Maricopa Association of Governments (MAG).
Note: Wider lines mean higher volume.

Figure 29. Map. Observed link volume for the Phoenix network.

To enable a data-driven supply-side modeling process, the research team used sensor data to calibrate key parameters in the VDF—including ultimate hourly capacity, peak hour factor, free-flow speed, and BPR coefficients—for each assignment period, AT, and FT. The ultimate goal of this supply-side calibration is to ensure consistency between ABM and DTA so that the MRM analysis can be consistent. The team obtained geographically matched speed-flow data in 15-min intervals from MAG. The team obtained third-party speed data (HERE Technologies 2021) and Arizona Department of Transportation Freeway Management System data (AZTech n.d.).

ANALYSIS DETAILS

This section describes research activities that were conducted within the case study task to fill the gaps identified in table 1. First, this section discusses research related to v/c ratios in the VDF and examines a congestion period-based calibration framework from a freeway bottleneck modeling perspective. Second, the section discusses a connection between the macroscopic speed-flow fundamental diagram with VDF curves through a well-defined demand over capacity ratio. Finally, the section examines different VDF representations using both speed and volume measurements in 15-min resolutions based on freeway data from the Phoenix metro area.

Model Conversion Effectiveness (Gap 3.1)

In this task, to support integration and data conversion between different modeling levels in MRM, especially mesoscopic tools using traffic stream models and macroscopic regional models using VDFs, the research team aimed to deliver a consistently calibrated set of traffic flow models and VDFs. As documented in the study supported by MAG (Wu et al. 2021), the challenge in calibrating VDFs comes from a lack of mathematically rigorous definitions for the v/c ratio, and more importantly, its underlying long-term planning resolution is different from the operational perspective of traffic flow theories. The following analysis attempts to demonstrate a theoretically consistent and practically effective framework for a data-driven joint traffic flow model and VDF calibration process.

The team planned to implement a refined BPR function (or other function) if necessary. The team used speed and flow data in the developed validation database to calibrate the key parameters of α and β in the BPR function. The team compared calibration outputs with results from the previous round of BPR model calibration. The team conducted a comparison analysis to demonstrate the benefits of any updated functional form to improve the predictive accuracy in the context of STA. Figure 30 illustrates the joint traffic stream model and VDF calibration process, which includes the following six major steps:

1. Traffic stream model calibration: For each VDF type, calibrate coefficients of the traffic stream model, including free-flow speed, ultimate capacity, and speed at capacity.
1. Calculate queued demand: For each link, calculate the queued demand during the congestion period.
2. VDF calibration: For different peak periods and VDF types, calibrate VDF coefficients (i.e., α and β) in the BPR function.
3. Queue demand factor (QDF): Calibrate the QDF and period capacity.
4. Traffic assignment: Given the peak period O-D matrix, perform STA using a standard transportation planning package. Compare outputs with the base year observations.
5. Further extension: Extend the static link volumes to time-dependent queue lengths.

Performance Measure Consistency (Gap 2.4)

This section describes step 1 in figure 30. To address gap 2.4 in regard to types and resolutions of measures used in model calibration and validation, the MAG team collected the following two datasets (Wu et al. 2021):

- Dataset 1 (85 sensors and 3 million records): Two months of data on freeway's HOV and general-purpose lanes at 15-min intervals. The team collected data from January 1 to February 29, 2020.

- Dataset 2 (1,736 sensors and 457 thousand records): Data in two representative weekdays with 15-min intervals in 2018–2019, covering both freeway links and arterial streets.

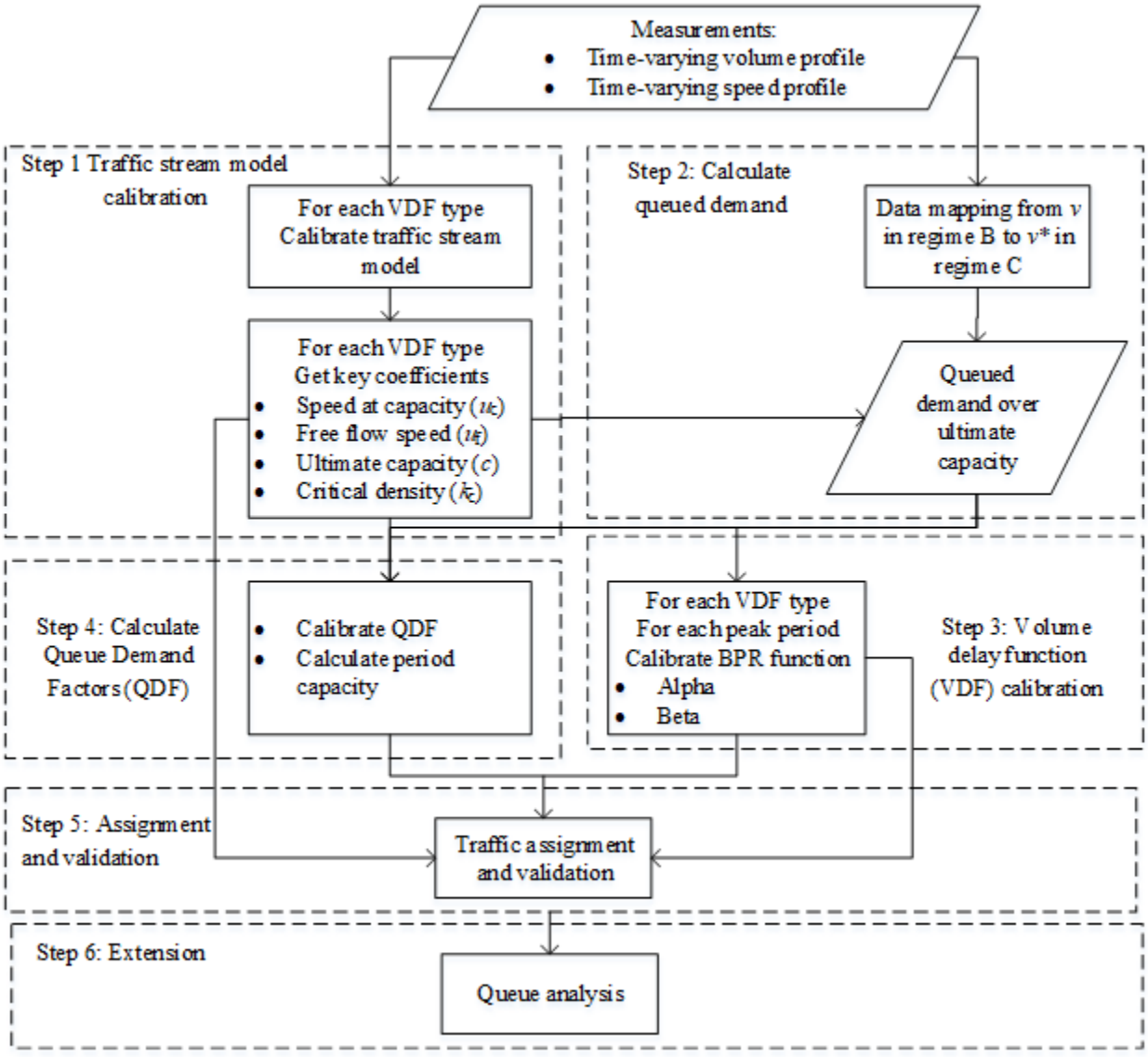

© 2021 Xin (Bruce) Wu (Wu et al. 2021).
v = observable volume; v^* = unobservable demand.

Figure 30. Flowchart. Integrated supply-side calibration process.

Performance Measure Definitions (Gap 2.1 and Gap 2.2)

This section aims to address the performance measure definitions in gap 2.1 and gap 2.2. The initial steps described here pertain to step 2 in figure 30. The standard BPR function is a normalized VDF expressed in terms of the v/c ratio. Analysts should calibrate α and β in the BPR function with the peak hour factor for FTs and ATs, using traffic sensor data. To bridge the gap between different resolutions of demand-supply relationship, and specifically to consider the oversaturated case, the research team used a queue-based method (QBM) for the BPR calibration (Belezamo 2020; Wu et al. 2021). The QBM is a demand-oriented calibration approach that aims to closely connect traffic flow measures and queue dynamics (e.g., bottleneck, evolutions, and

capacity drop). For a clear demonstration, figure 31 partitions the VDF coordinate plane into three regimes with speed at capacity:

- Regime A: Observed flow rate undersaturated with $v/c \leq 1$ and uninterrupted free speed.
- Regime B: Observed reduced flow rate saturated with $v/c = 1$ and reduced speeds.
- Regime C: Unobserved but derived "demand" volume oversaturated with $v/c \geq 1$ with reduced speeds.

The term "derived demand" is used in regime C because analysts should ensure that the traffic counts reflect demands rather than the road capacity constraints. As discussed by Huntsinger and Rouphail (2011), the demand in regime C is not simply the traffic volume measured by the detector for a given time interval (e.g., a peak hour defined as 4–5 p.m.). At a certain time interval, with the queue measured, the demand D at the bottleneck includes two elements, namely, (1) the queue length and (2) the demand at the bottleneck capacity. Accordingly, a concept of demand over capacity (D/C) ratio should be introduced when queuing occurs.

Figure 31 uses the traffic flow model and the BPR function to illustrate the three regimes. According to the traffic flow model, the observed flow falls into regime B. Comparatively, the oversaturated part of the BPR function falls in regime C. As a result, the calibration process is to map the speed-flow measurements (point *m*) from observable regime B to derived point *n* in regime C. The Phoenix case study uses the QBM, which defines the volume corresponding to point *n* as queued demand. This includes the bottleneck discharge rate and queued vehicles during a time interval. The v/c ratio in the BPR function is the D/C. A *v/c* greater than or equal to 1 implies that demand exceeds supply.

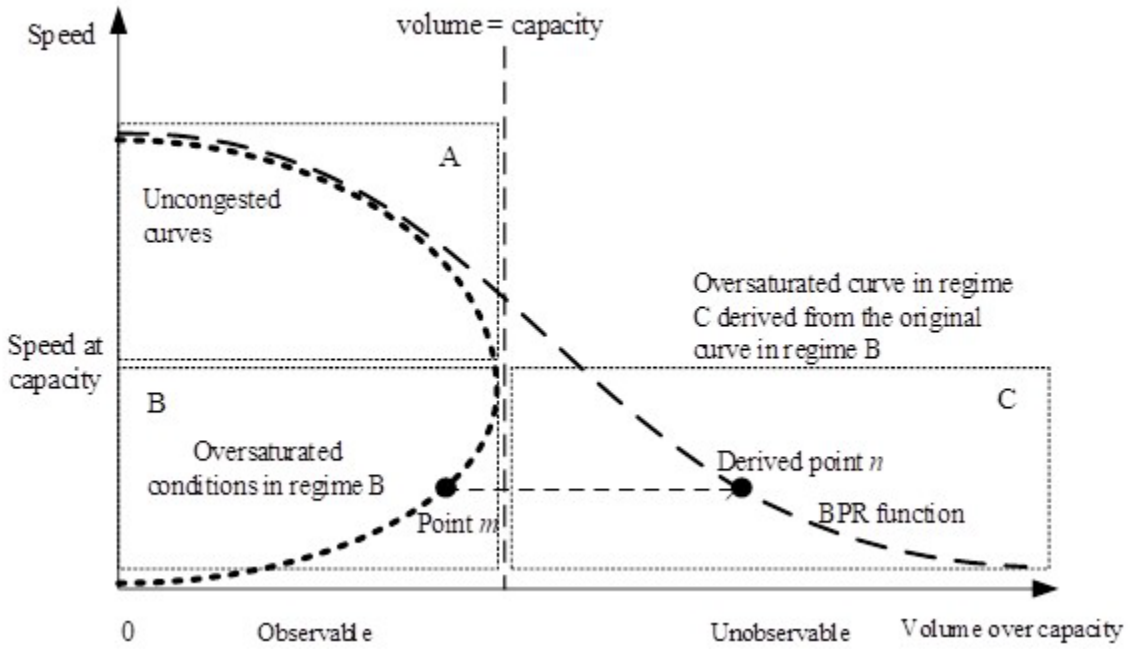

©2021 Xin (Bruce) Wu (Wu et al. 2021).
m = observed point; *n* = derived point.

Figure 31. Graph. Regimes in the speed versus v/c ratio coordinate plane.

In the example illustrated in figure 32, the morning peak assignment period covers 6–9 a.m. The minimum speed (u_{min}) happens between 8 and 8:15 a.m. The peak hour is between 7:45 and 8:45 a.m., including data collected in four 15-min periods. The research team denotes volume within the peak hour as D_h. To enable a mapping from regime B to regime C, the team first finds the lowest speed (u_{min}) during the assignment period, and then extends the congestion period range until the speed is higher than the speed at capacity (u_c), as shown in figure 33. Next, the team considers a congestion period from t_0 to t_3 containing the peak hour. The total volume D within the congestion period is equivalent to the queued demand for the peak hour's capacity under oversaturated conditions. This implies that when t_3–t_0 exceeds 1 h, D is greater than or equal to D_h, and D becomes the queued demand for the peak hour.

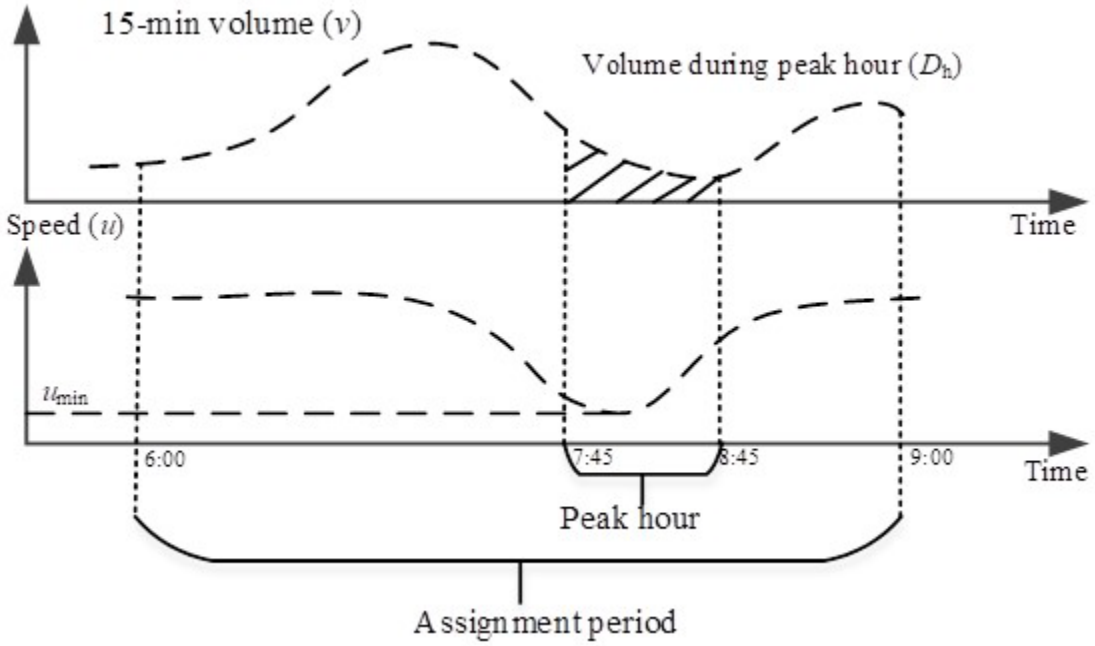

© 2021 Maricopa Association of Governments (MAG).
u_{min} = minimum speed during the assignment period.

Figure 32. Graph. Derived queued demand when congestion duration is less than 1 h.

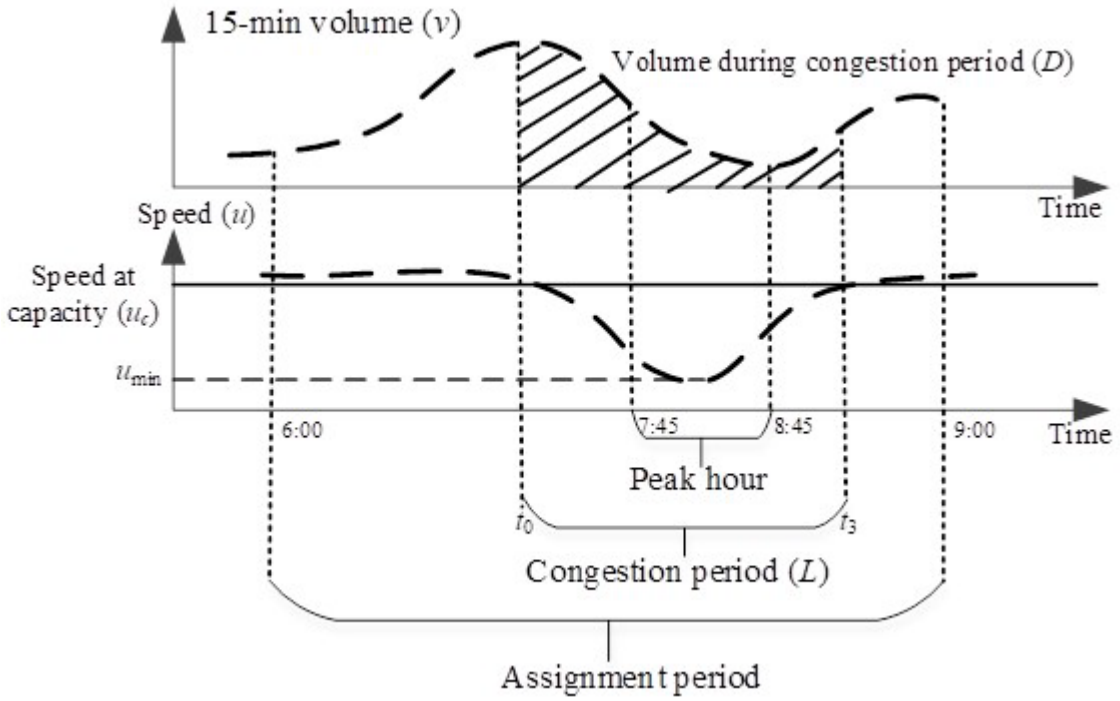

© 2021 Maricopa Association of Governments (MAG).
t_0 = start of congestion period; t_3 = end of congestion period.

Figure 33. Graph. Derived queued demand when congestion duration exceeds 1 h.

To accomplish step 3 in figure 30, the research team defined the QDF in figure 34 to convert assigned volumes to peak-hour demands in relation to the ultimate hourly capacity.

$$QDF = \frac{\text{Total volume of an assignment period}}{\text{Queued demand of a peak hour}}$$

Figure 34. Equation. QDF formula.

Where QDF = queue demand factor.

In this task, the research team also compared the QBM with the volume-based method (VBM) and the density-based method (DBM). The VBM is adapted from the Florida Standard Urban Transportation Modeling Structure (Moses et al. 2013). The DBM uses a direct approximation of density measurements to cover regimes A and C to connect fundamental diagrams with the VDF function (Drabicki, Kucharski, and Szarata 2017). The team used the mean absolute percentage error (MAPE) to evaluate the effectiveness of the calibration for all links in each FT/AT

combination. To accomplish step 4 in figure 30, the research team calibrated the VDF under the conditions and assumptions in the following list, producing the results shown in figure 35:

- CBD area.
- Evening peak period.
- $\alpha = 0.21$.
- $\beta = 4$.
- AT = 1.
- FT = 1.

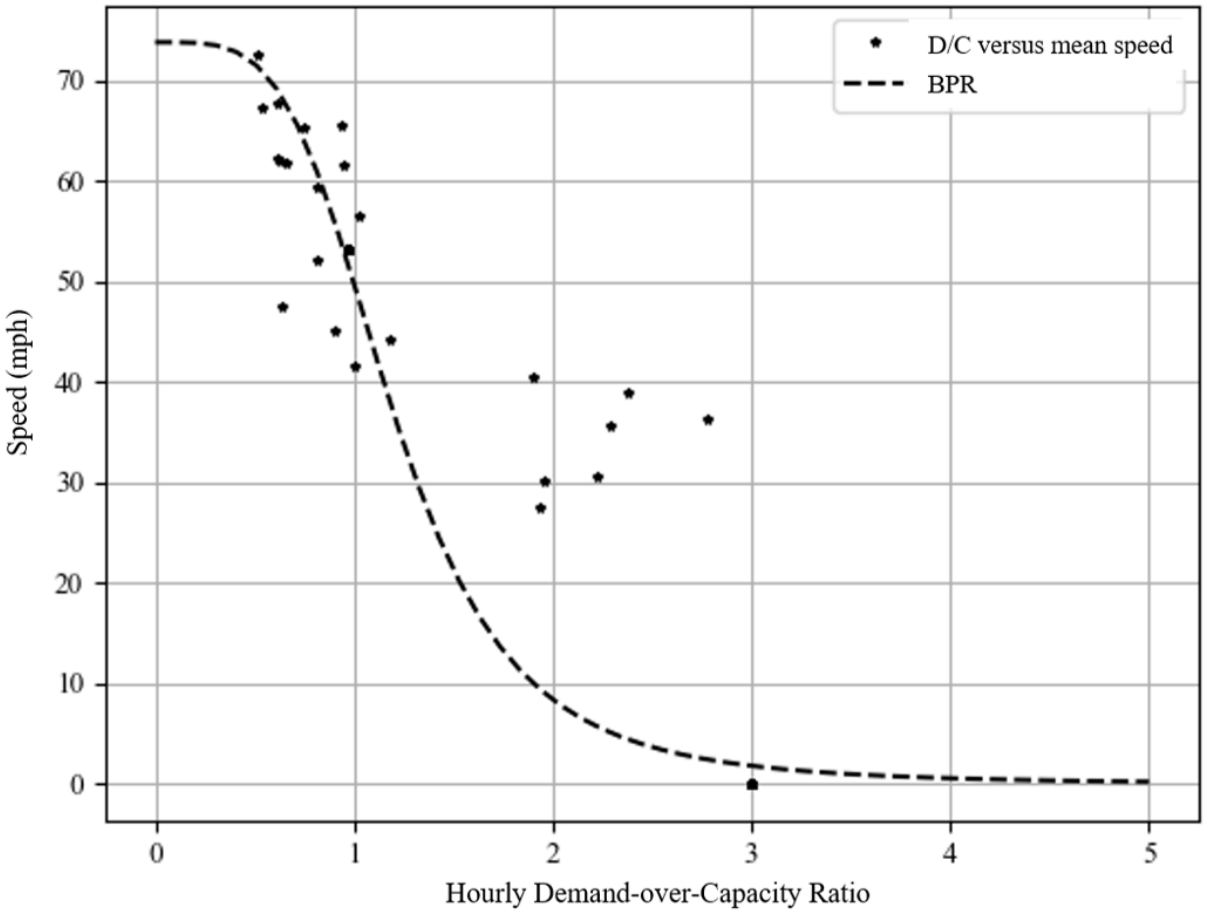

© 2021 Maricopa Association of Governments (MAG).
D/C = demand-over-capacity ratio.

Figure 35. Scatterplot. Volume-delay function calibration results for the Phoenix network.

The research community also acknowledges different perspectives within traffic flow theories and the VDF function. That is, the speed-volume relation plotted using field data has a parabolic U shape, while the fitting of the VDF requires the monotonously decreasing function. Thus, figure 35 does not use the commonly v/c ratio on the x-axis, to avoid the confusion with speed-volume relation. Instead, researchers have adopted the D/C ratio to properly address oversaturated conditions in which D/C ≥ 1 (Huntsinger and Rouphail 2011).

Feedback Loop (Gap 3.6)

In the Phoenix case study, the research team examined feedback loops between ABM, DTA, and microsimulation tools in the subarea. The team used the feedback loop mechanism to integrate ABM and DTA for demand modeling. The output of ABM includes the trip chain files to describe the personal/household travel behaviors. Analysts can use the trip chain files as input demand files for DTA models. In a real-world situation, because ABM and DTA use different models to estimate travel demand and capacity, their integration may create inconsistencies (e.g., ABM demands that are estimated from households might exceed the capacities of DTA models).

Two approaches can improve the MRM modeling consistency. First, modelers can carefully calibrate link capacities within DTA models. Second, modelers can build feedback loops between ABM and DTA to adjust O-D demands within the DTA model. Figure 36 shows a flowchart of the ABM-DTA integration provided by MAG.

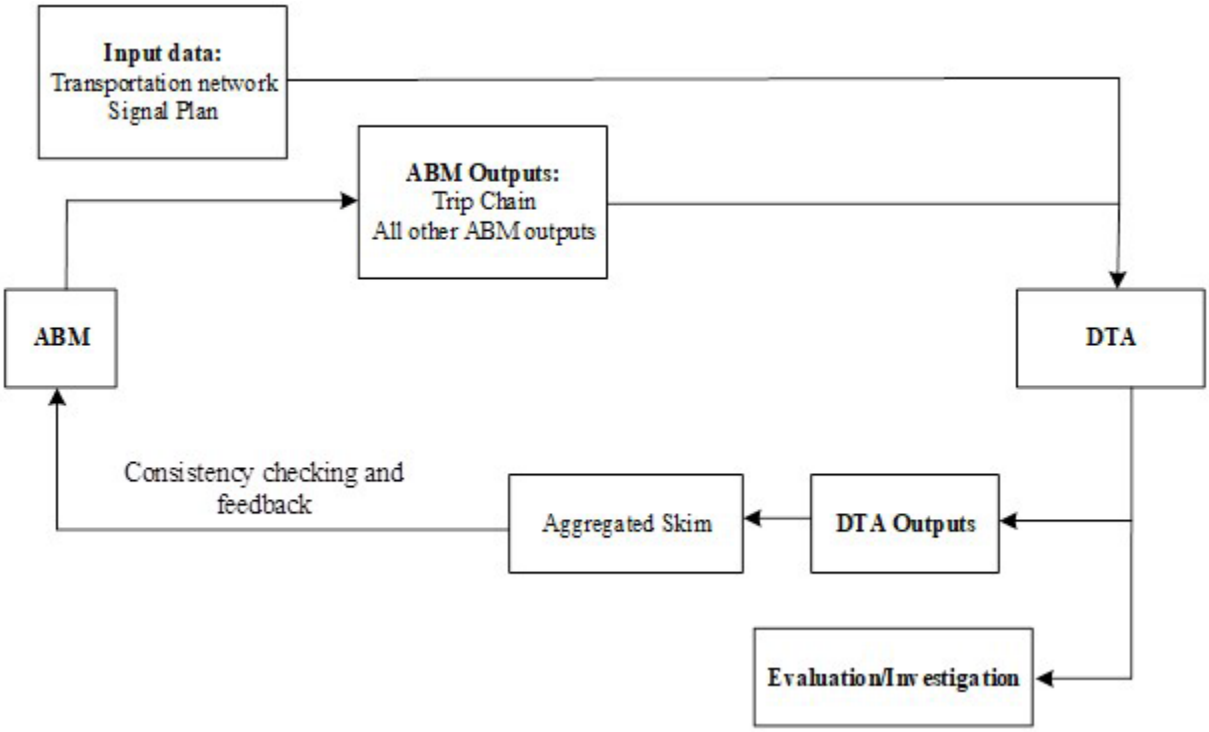

© 2021 Maricopa Association of Governments (MAG).

Figure 36. Flowchart. ABM and DTA integration.

Cost and Time Requirements (Gap 1.3)

The Phoenix case study demonstrates an application of supply-side calibration for both traffic stream models and VDFs. This streamlined process will improve the model quality of macroscopic traffic assignment, resulting mesoscopic DTA, and microscopic simulation. Other benefits for adopting the standard specification could include seamless data sharing, collaborative visualization tool development, and improved quality control for modeling data as well as simplified scenario management.

Based on the GMNS data format, the developed packages provide a baseline data inventory template for the data collection and analysis step in traffic assignment and simulation applications. By using the organized data inventory structure as a reference and a guideline, planners can develop their own customized workflow on such key MRM tasks as how to identify required data sources (both link count and speed readings), how to assemble contemporaneous data with a consistent mapping to the underlying planning network, how to verify data quality consistently across different sources, and how to further identify typical traffic conditions using cluster analysis.

Open-source software packages can automate the calibration process. Through the integrated supply-side parameter calibration package with consistent definitions from traffic flow models and macroscopic VDFs, planners can exploit this suite of open-source packages to streamline the data processing workflow. In this manner, analysts can focus on key parameter estimation steps and reasonably expect good-quality calibration based on peer agencies' results rather than simply relying on engineering judgment in the important step of error checking for all key supply-side parameters. This aspect is key: In current practice, analysts expend most of their energy on error checking for network topology and lane configuration as opposed to traffic stream model parameters (e.g., ultimate capacity, critical density, free-flow speed, and speed at capacity). The authors advise different metropolitan planning agencies to maintain consistent definitions of those parameters and ensure the transferability of supply-side models across regions and States.

In the current practice, static O-D demand estimation capabilities are readily available through the transportation planning packages from commercial vendors. However, comprehensive supply-side calibration processes and supporting packages should also be easily accessible by engineers and planners, for both stages of base model development and model calibration in traffic simulation analysis. The developed joint calibration workflow for key traffic stream models and coefficients in the VDFs could help analysts automate the data processing steps and preserve sufficient time resources and efforts for the critical error checking and validation steps. The available open-source Python® scripts can further assist users to visualize traffic flow fundamental diagrams and volume-delay relationships systematically, across different FTs, ATs, and analysis periods.

The Phoenix case study demonstrates the conversion of traditional two-way representations to the standard GMNS-directed link representation with map-matched link count and speed readings. This standardization aspect is still very important for analysts and planners to understand and adopt, especially in the context of analyzing traffic bottlenecks to calibrate VDFs. Without a consistent definition of congested periods, it is difficult to identify queued demand in the critical D/C ratio in the BPR function, especially for oversaturated conditions. This consistent definition across traffic flow theory and VDF-based planning models could bridge the gap between macroscopic and mesoscopic models and significantly reduce the cost and time associated with data sharing and model applications.

For agencies adopting this streamlined process based on their current data inventory, the authors expect planners to take from 1 to 2 w to convert the required network and sensor data into the standardized format. For example, for each link in the planning model, analysts can match speed measurements to corresponding volume measurements at the same time interval during a typical weekday. Once the inventoried data have been standardized to the community specification,

agencies can leverage existing work significantly, especially for utilizing tools to validate, edit, and manage networks across different projects.

It could take 1 w to calibrate the capacities and other coefficients for major FTs, given sufficient measurements are available across different areas of the region (e.g., CBD area, outlying CBD, mixed urban area, suburban area, and rural area). It is notable that to gain a reliable estimate of ultimate capacity, valid data samples in both free-flow and congested regimes should be sufficiently available. Otherwise, the default theoretical capacity values provided by the *HCM* must be used (Transportation Research Board 2010). Finally, it is important to remark that analysts should not view the comprehensive calibration of supply-side parameters as additional or increased modeling efforts in place of current practices. Instead, analysts should view the calibration as a key step for reaching quality standards for model completeness. Agencies might define different tiers of completeness in their model validation and calibration processes so they can plan careful assessments of the additional levels of effort required to reach higher levels of model accuracy.

Analysis Results

Figure 37 through figure 42 depict the speed-flow, speed-density, and flow-density relationships based on dataset 1 and dataset 2, respectively (Wu et al. 2021). Corresponding to table 10, VDF type 101 indicates freeways in the CBD area based on MAG's VDF code definitions.

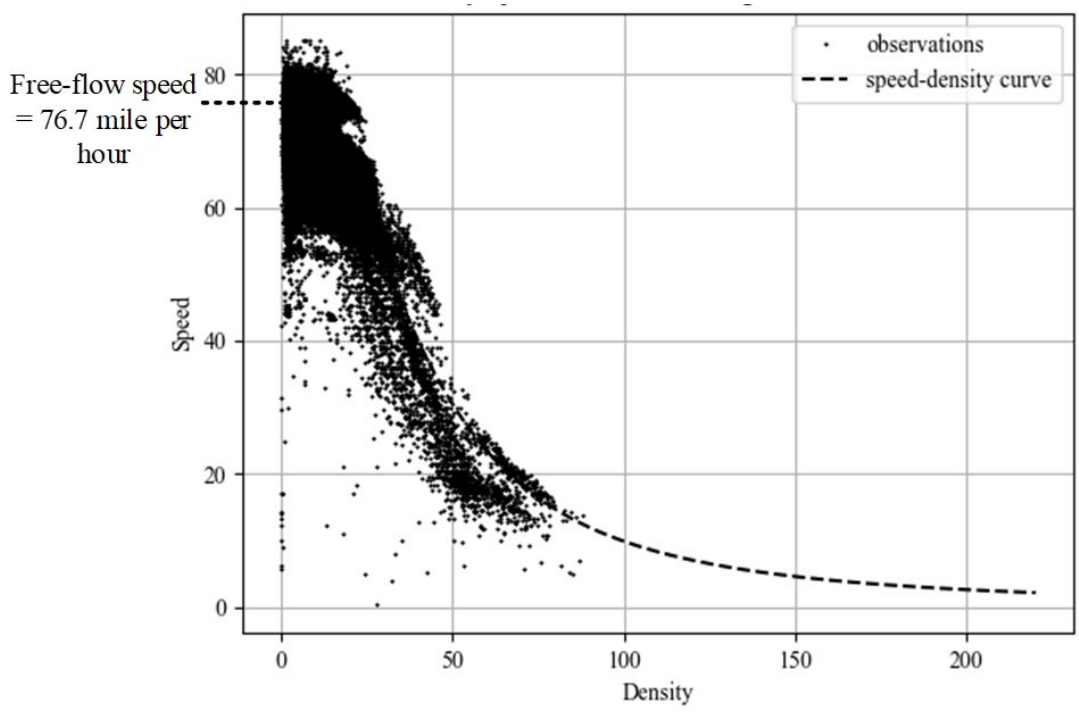

© 2021 Maricopa Association of Governments (MAG).

Figure 37. Graph. Calibrated speed-density relationship using data from freeways in the CBD (dataset 1).

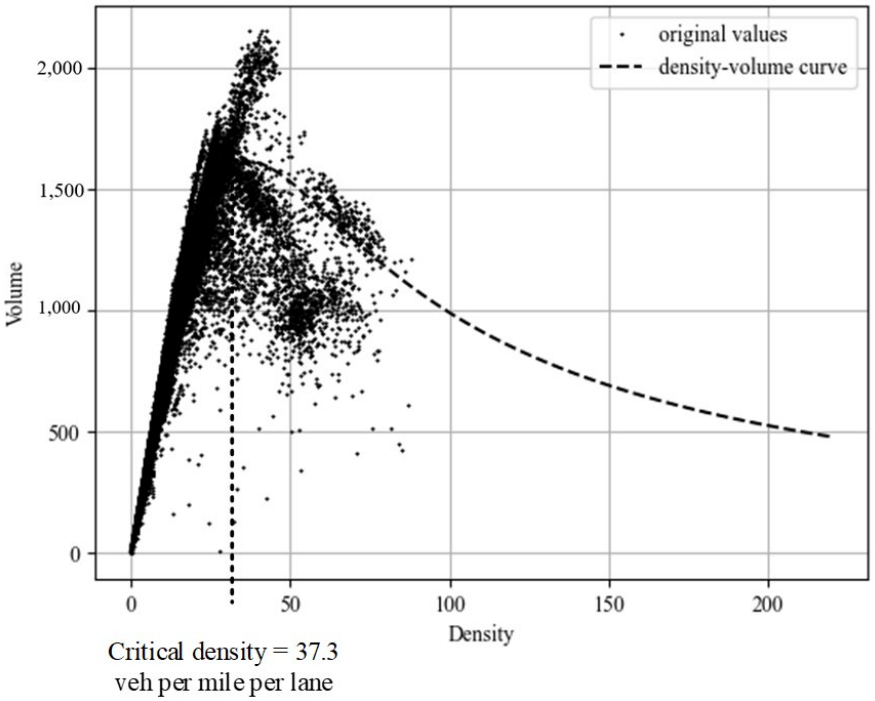

© 2021 Maricopa Association of Governments (MAG).

Figure 38. Graph. Calibrated volume-density relationship using data from freeways in the CBD (dataset 1).

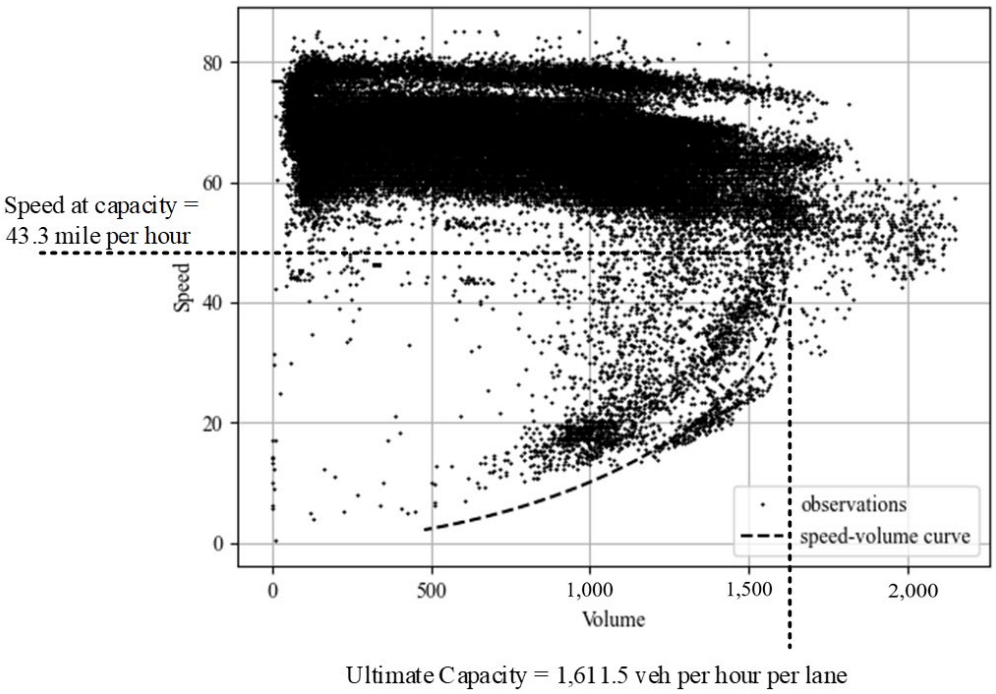

© 2021 Maricopa Association of Governments (MAG).

Figure 39. Graph. Calibrated speed-volume relationship using data from freeways in the CBD (dataset 1).

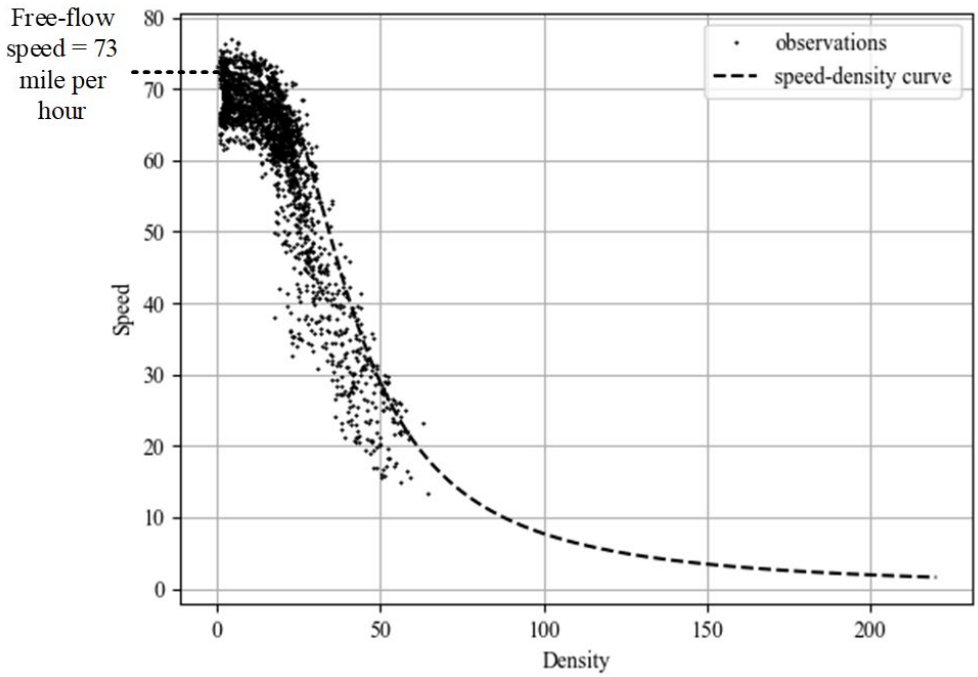

© 2021 Maricopa Association of Governments (MAG).

Figure 40. Graph. Calibrated speed-density relationship using data from freeways in the CBD (dataset 2).

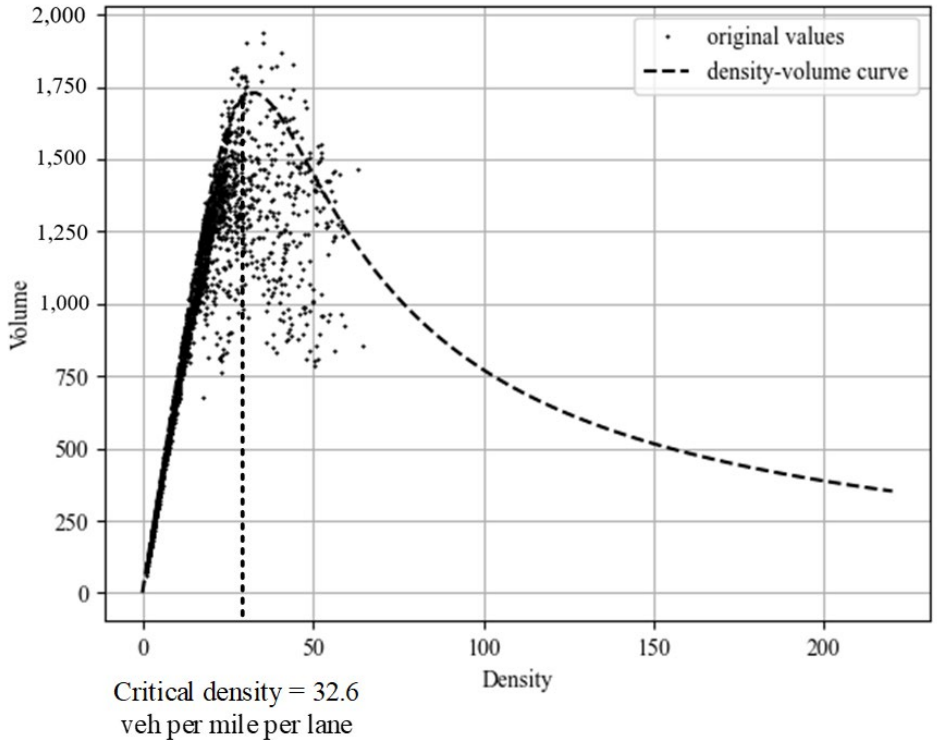

© 2021 Maricopa Association of Governments (MAG).

Figure 41. Graph. Calibrated volume-density relationship using data from freeways in the CBD (dataset 2).

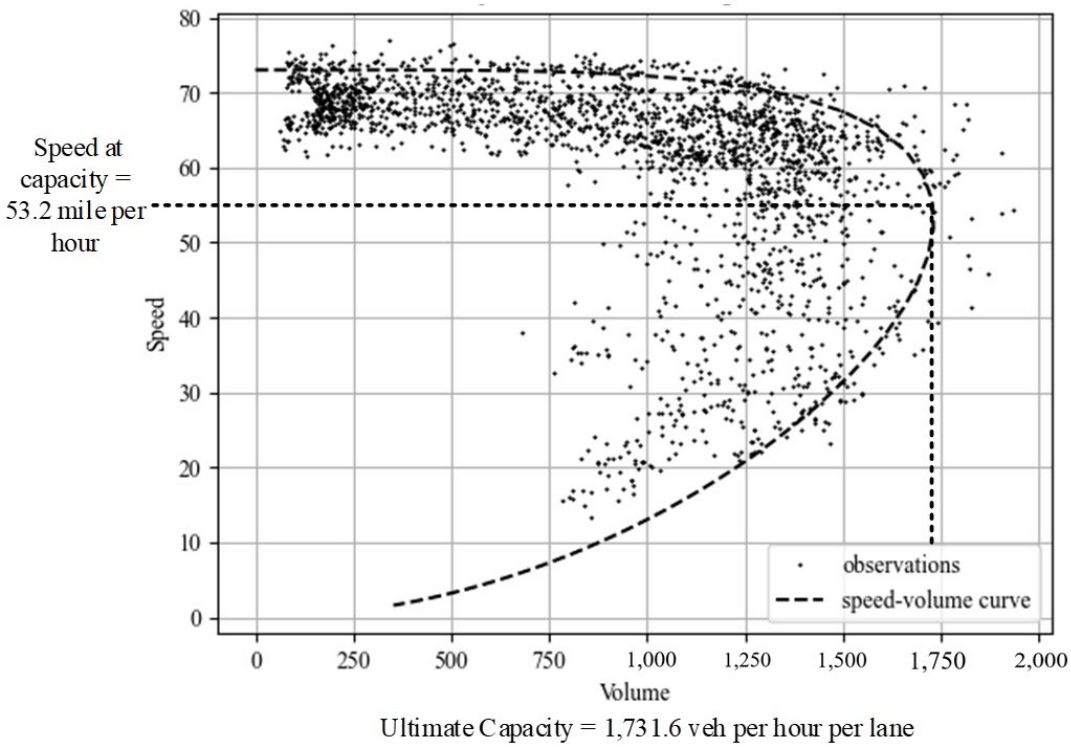

© 2021 Maricopa Association of Governments (MAG).

Figure 42. Graph. Calibrated speed-volume relationship using data from freeways in the CBD (dataset 2).

Table 13 further shows the calibrated traffic stream parameters for different VDF types including freeways (FT = 1) in the CBD area (AT = 1), outlying CBD (AT = 2), and mixed urban (AT = 3) in the MAG modeling network (Wu et al. 2021).

Table 13. Calibrated traffic stream model parameters for different datasets.

FT	AT	Dataset	Speed at Capacity (u_c)	Ultimate Capacity (c)	Density at Capacity (k_c)	Free-Flow Speed (u_f)
Freeway	CBD	1	49.0	1,571	32.1	70.0
Freeway	Outlying CBD	1	50.6	1,715	33.9	69.4
Freeway	Mixed urban	1	56.3	1,679	29.8	71.0
Freeway	CBD	2	51.5	1,695	32.9	70.0
Freeway	Outlying CBD	2	52.1	1,848	35.5	70.0
Freeway	Mixed urban	2	58.9	2,064	35.0	70.9

Using figure 31, the research team mapped the derived point *n* in the calibrated D/C curve back to point *m* in the calibrated traffic stream model and compared it with the ground truth speed and volume measures (which can be slightly different from point *n* due to the traffic stream model calibration errors). table 14, table 15, table 16, and table 17 report the average MAPE of speed and assignment period volume for different VDF types based on three different methods.

Overall, the QBM consistently performs well in terms of link volume estimation in both datasets because it can capture the dynamic relationship between excess demand during the congestion period and the observed volume in the given assignment period, as illustrated in figure 33. In terms of link speed estimation errors, three methods offer similar performance within a 10 percent error range, while DBM produces the smallest error. The team expected such results because traffic flow theory indicates a linear relationship between speed and density. Overall, the QBM provides a balanced estimation performance across both speed and volume measures.

Table 14. MAPE of volume for dataset 1.

FT	AT	Assignment Period	QBM	VBM	DBM
Freeway	CBD	Morning peak	13.3	13.7	45.0
Freeway	CBD	Midday	6.0	18.7	57.5
Freeway	CBD	Afternoon peak	26.0	16.9	33.7
Freeway	Outlying CBD	Morning peak	28.6	21.2	34.7
Freeway	Outlying CBD	Midday	8.4	21.1	48.8
Freeway	Outlying CBD	Afternoon peak	31.0	20.8	29.2
Freeway	Mixed urban	Morning peak	8.4	21.5	46.0
Freeway	Mixed urban	Midday	3.1	19.8	52.5
Freeway	Mixed urban	Afternoon peak	2.6	12.0	38.0
Average	N/A	N/A	14.2	18.4	42.8

Adapted from Wu et al. 2021.

Table 15. MAPE of volume for dataset 2.

FT	AT	Peak Period	QBM	VBM	DBM
Freeway	CBD	Morning peak	31.7	30.7	17.6
Freeway	CBD	Midday	15.1	35.5	15.3
Freeway	CBD	Afternoon peak	51.8	26.8	27.4
Freeway	Outlying CBD	Morning peak	22.5	45.0	21.8
Freeway	Outlying CBD	Midday	8.9	48.4	15.6
Freeway	Outlying CBD	Afternoon peak	33.5	29.1	19.0
Freeway	Mixed urban	Morning peak	21.5	47.0	29.9
Freeway	Mixed urban	Midday	11.9	46.8	25.3
Freeway	Mixed urban	Afternoon peak	21.9	32.8	20.5
Average	N/A	N/A	24.3	38.0	21.4

Adapted from Wu et al. 2021.

Table 16. MAPE of speed for dataset 1.

FT	AT	Assignment Period	QBM	VBM	DBM
Freeway	CBD	Morning peak	8.0	9.4	7.3
Freeway	CBD	Midday	6.0	5.8	4.6
Freeway	CBD	Afternoon peak	14.0	9.9	8.1
Freeway	Outlying CBD	Morning peak	11.0	9.4	9.0
Freeway	Outlying CBD	Midday	7.0	5.9	6.1
Freeway	Outlying CBD	Afternoon peak	15.0	10.9	9.9
Freeway	Mixed urban	Morning peak	9.0	7.8	6.5
Freeway	Mixed urban	Midday	7.0	7.0	6.1
Freeway	Mixed urban	Afternoon peak	8.0	7.5	6.7
Average	N/A	N/A	9.4	8.2	7.1

Adapted from Wu et al. 2021.

Table 17. MAPE of speed for dataset 2.

FT	AT	Peak Period	QBM	VBM	DBM
Freeway	CBD	Morning peak	12.0	12.0	9.6
Freeway	CBD	Midday	6.0	6.9	5.2
Freeway	CBD	Afternoon peak	17.0	16.3	13.1
Freeway	Outlying CBD	Morning peak	11.0	9.3	9.7
Freeway	Outlying CBD	Midday	5.0	4.2	3.8
Freeway	Outlying CBD	Afternoon peak	12.0	11.7	9.5
Freeway	Mixed urban	Morning peak	13.0	8.6	7.7
Freeway	Mixed urban	Midday	4.0	3.6	3.3
Freeway	Mixed urban	Afternoon peak	7.0	7.2	6.3
Average	N/A	N/A	9.7	8.9	7.6

Adapted from Wu et al. 2021.

After performing traffic assignments based on the calibrated coefficients, the team compared the assignment results with the observations to calculate performance measures in terms of R^2, percent of RSME (RMSE%), and percent of differential (Diff%), for both speed and volume measurements. First, the results indicate that the R^2 values did not significantly change before and after the parameter updating. Second, the results indicate that the volume estimation during the congested afternoon peak period in the CBD area can significantly improve. Table 18 shows the suggested comparison between observed and assigned volumes across different ATs for links with a specific combination of AT and FT.

Table 18. Suggested performance measures for the traffic assignment validation step.

Measurement Type	Validation Criteria
Volume	Compare assigned volume with observed volume on both two-way links and one-way links based on VDF type of AT/FT combination. Measures: • R^2 • RMSE% • Diff% The assignment period is afternoon peak.
Speed	Compare assigned speed with observed speed on one-way links based on VDF type of AT/FT combination. Measures: • R^2 • RMSE% • Diff% The assignment period is afternoon peak.

To systematically assess possible error sources from both demand and supply sides, as shown in figure 43, the research team used quadrants of the coordinate plane to systematically compare observed speed and volume measurements with the assigned solution. The horizontal line on the x-axis shows system-wide average volume. The vertical line on the y-axis shows the system-wide average speed. The ground truth is located at the center. A perfectly calibrated VDF would intersect at each line's center and divide the plane into four sections. Starting in the upper-right section of the graph, counterclockwise Roman numerals label the four quadrants. For assignment results in quadrant II or quadrant IV, the signs of volume and speed differences are opposite each other. Thus, one can further adjust the demand flow loaded into the DTA simulator or STA program to consistently reduce the underestimated or overestimated demand and congestion level. If the assignment results appear at quadrant I or quadrant III, then simply changing the externally loaded demand might move the assignment solution toward the center as the ground truth. As a result, analysts should carefully examine capacity settings and VDF parameters, such as alpha and beta, to remove possible supply-side system representation errors.

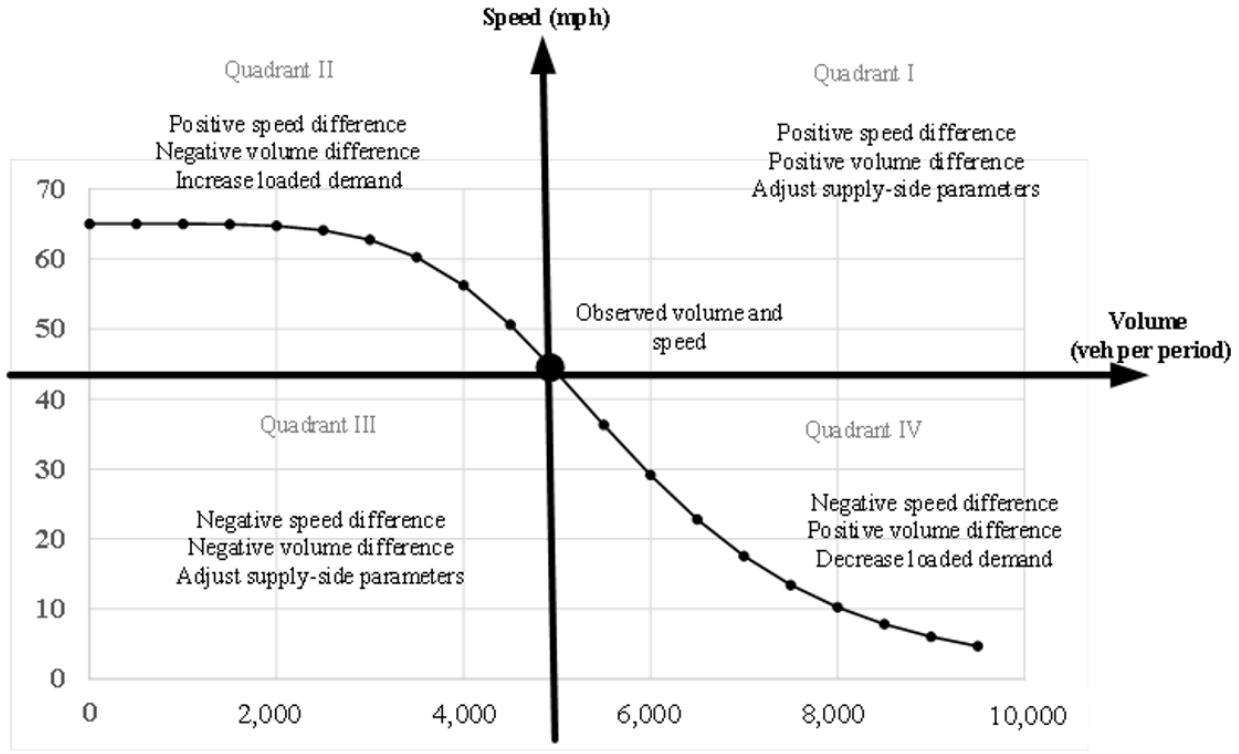

Source: FHWA.
veh = vehicle.

Figure 43. Graph. Comparison of observations and assignment results to assess possible demand-side or supply-side estimation errors.

SUMMARY

In the iterative traffic assignment process of macroscopic and mesoscopic travel demand models, analysts primarily evaluate the performance of road systems via traffic stream models and VDFs. This case study attempts to systematically examine different ways of representing v/c ratios with definitions consistent with queueing-based traffic flow theory. The developed joint traffic stream model and VDF calibration framework allow modelers to estimate the congestion period during which both speed and flow drop because of oversaturation. This MRM approach can better characterize the volume term in the traditional v/c ratio as the queued demand after a bottleneck. The case study calibrates different v/c representation methods using both speed and volume measurements in 15-min resolutions in the Phoenix metropolitan area. The authors hope to shed new light on the following aspects:

- A data-driven process that allows joint estimation of traffic stream parameters and period-based demand flows for oversaturated traffic conditions.
- A more systematic definition of the v/c (more precisely D/C) ratio in the VDF by bridging the gap between the different temporal resolutions of the demand-supply relation.
- A congestion-period, demand-oriented calibration framework that closely connects traffic flow measures and queue dynamics (e.g., bottleneck, evolutions, and capacity drop).

CHAPTER 4. MARYLAND I–95 NETWORK

In comparison to the other two case studies, this case study focuses more on the next-generation model development approach. It illustrates the benefits of using GMNS as the base to represent macroscopic, mesoscopic, and microscopic networks to achieve a new level of consistency in MRM (Zephyr Foundation 2020a). The case study further demonstrates enhanced calibration of traffic bottleneck capacities using probe data and efficient generation of traffic signal timing data for all scenarios. For all modeling resolutions, GMNS allows a more consistent definition of bottleneck locations and intersection turning movements. This case study builds on an existing integrated ABM and DTA system, namely, AgBM-DTALite, which aims to capture agent-based travel behavior and transportation network dynamics (Xiong, Zhou, and Zhang 2018).

NETWORK DESCRIPTION

The test network used in this study consists primarily of the corridor network between Washington, DC, and Baltimore, MD. This network includes two interstate freeways, namely I–95 and the Washington–Baltimore Parkway, U.S. Route 29, and U.S. Route 1. The corridor network contains approximately 200 O-D demand zones. The research team extracted corresponding zonal scheme from an existing statewide transportation planning dataset that covers the greater Washington, DC, area. The team calibrated dynamic O-D demand tables, using a static planning O-D table, and archived time-dependent link flow and speed observations. The network in figure 44 includes several signalized intersections.

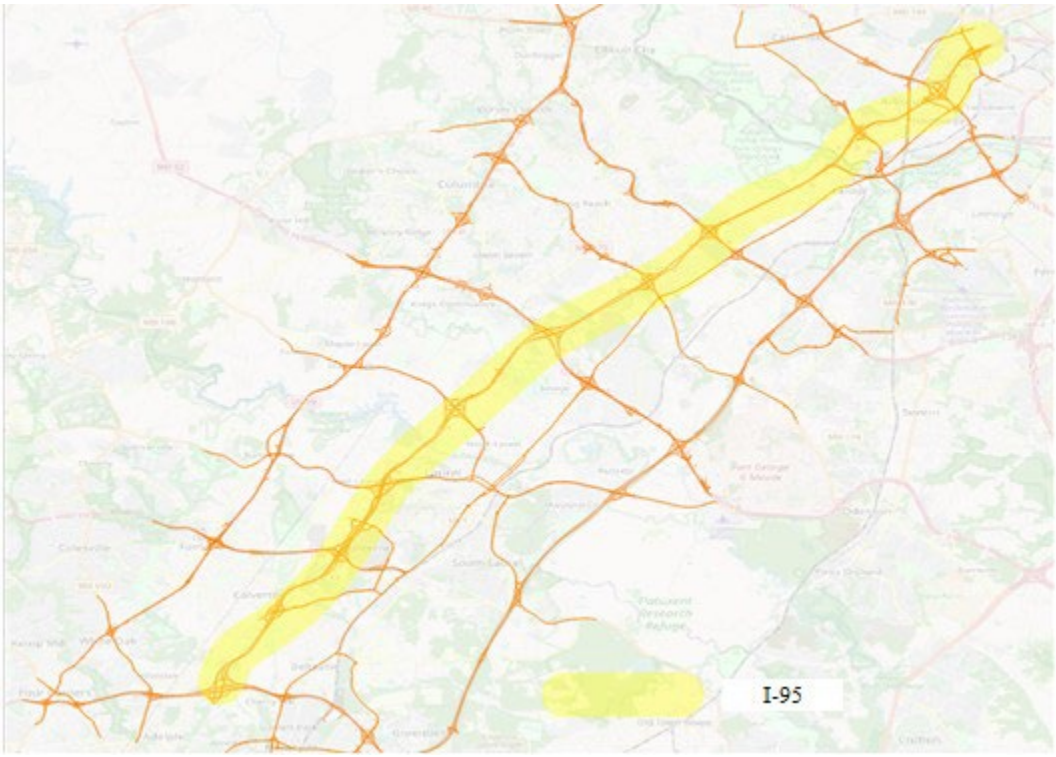

Original map: © 2021 OpenStreetMap contributors. Overlays added by FHWA.

Figure 44. Map. Maryland I–95 network (OpenStreetMap D).

MODEL OVERVIEW

The regional planning model covers the entire region of Washington, DC; counties in Maryland, including Montgomery, Prince George's, and Frederick; and parts of Arlington and Fairfax Counties in Virginia. Some of the network statistics are as follows:

- Regional network: 3,722 TAZs, 17,605 nodes, and 48,973 links with 3,387,446 vehicles simulated in the model.
- Subarea network: 2,040 TAZs, 9,535 nodes, and 27,188 links with 2,330,849 vehicles simulated in the model.

All interstate freeways, highways, major and minor arterials, and most connectors and local roadways are included in the network. The research team coded the DTA model in the lightweight, open-source software package, DTALite (Zhou and Taylor 2014). The team chose DTALite because its built-in parallel computing capability dramatically speeds up the traffic assignment and O-D estimation process by using multicore central processing unit hardware. The team extracted the baseline model directly from a macroscopic travel demand model, and thus, it may not be directly applicable for mesoscopic DTA modeling. The team calibrated the base model's supply and demand based on real-world observations. Table 19 provides the traffic network statistics for the different modeling resolutions.

Table 19. Maryland traffic network statistics for different modeling resolutions.

Network Type	Number of Nodes	Number of Links (Ways)
Original OpenStreetMap network	1,389,653	177,400
Macroscopic network	21,099	45,826
Mesoscopic network	86,882	119,999
Microscopic network	1,202,959	1,689,994

Note: The GMNS denotes links as "ways" in OpenStreetMap.

DATA DESCRIPTION

All of the geographic and traffic infrastructure information for this network comes from the Metropolitan Washington Council of Governments.

ANALYSIS DETAILS

This case study focused on optimizing MRM data exchange between the macroscopic, mesoscopic, and microscopic levels of analysis. It is important to systematically identify internal and external functional interfaces to exchange the performance measures of higher-level models with lower-level models. The research team considered the following three types of consistency to ensure seamless data conversion: network interfaces, demand interfaces, and supply interfaces. Typical network interfaces involve data conversion from a macroscopic network to a microscopic network. To perform consistent analysis across different layers, the team used a mesoscopic, lane-based network representation as a unique data bridge. This method enabled unique mapping of macroscopic links to mesoscopic lane elements. It also enabled the team to further discretize mesosegments into cells and map them to a space-continuous road representation. Demand interfaces contain the tools to convert different levels of trip desire data.

As an important example of supply interfaces, scalable and consistent representation of junction control data (i.e., signal timing) is critically needed for the success of MRM. Because there are inherent connections between macroscopic capacity measures and microscopic headway and reaction times, analysts should also pay attention to ensure the consistency in supply-side representations across different resolutions.

Model Conversion Effectiveness (Gap 3.1)

To demonstrate the MRM process, this study used open-source tools osm2gmns and net2cell to build a multiresolution I–95 network (Python Package Index 2021a; Python Package Index 2021b). The research team first downloaded original map data for the subarea network from OpenStreetMap, then converted it via osm2gmns to macroscopic GMNS network files. The team generated corresponding mesoscopic and microscopic networks by using the net2cell tool. Figure 45 and figure 46 show examples of mesoscopic and microscopic network representation in OpenStreetMap.

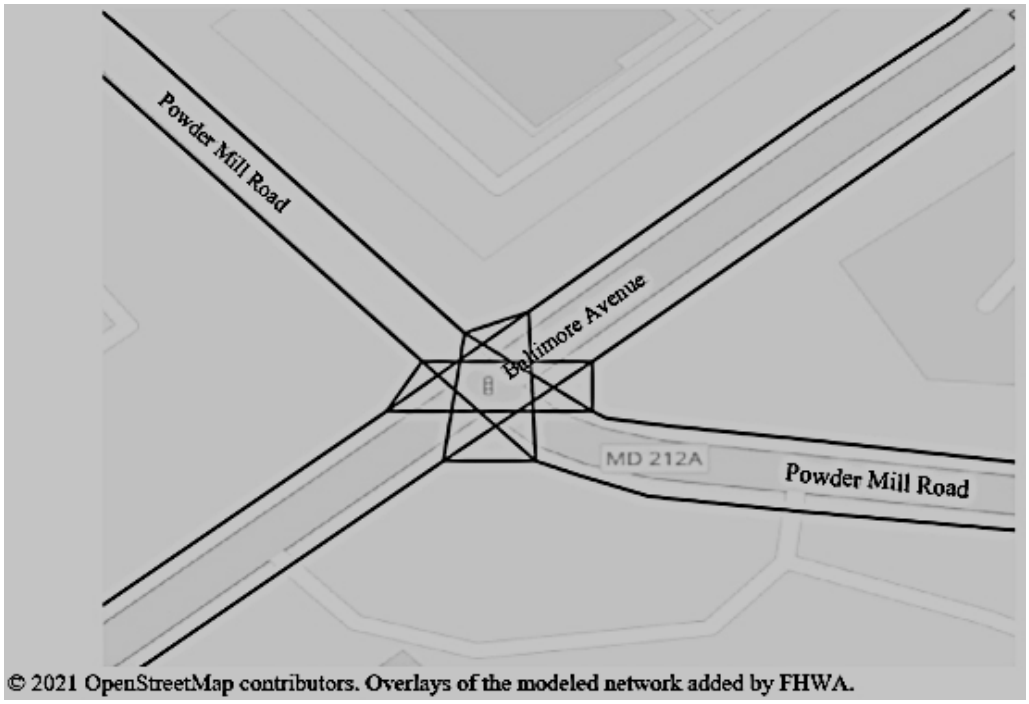

© 2021 OpenStreetMap contributors. Overlays of the modeled network added by FHWA.

Figure 45. Map. Mesoscopic network representation near node 10643 (OpenStreetMap E).

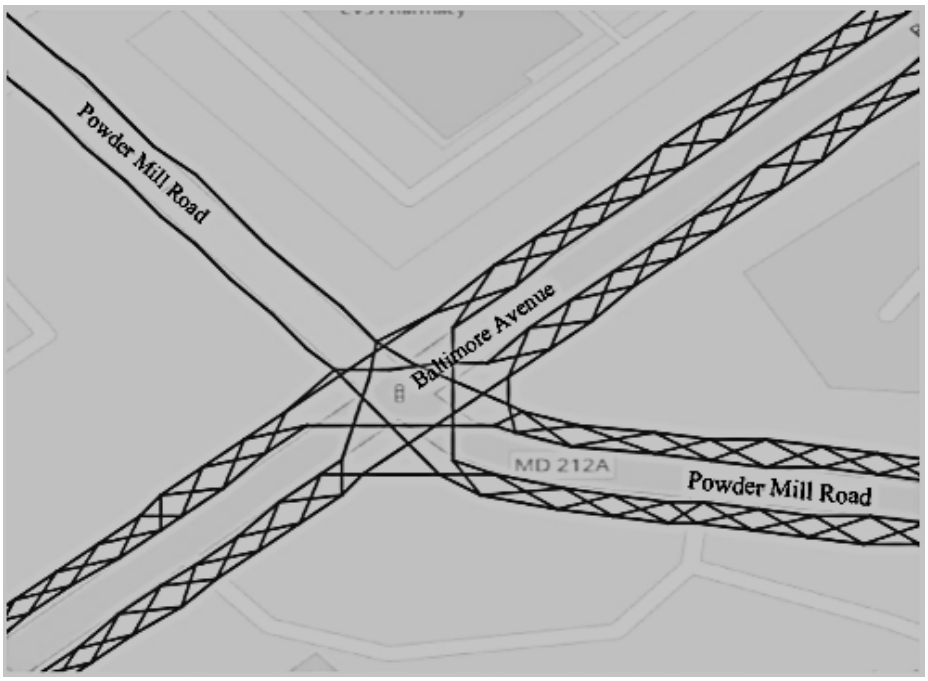

© 2021 OpenStreetMap contributors. Overlays of the modeled network added by FHWA.

Figure 46. Map. Microscopic network representation near node 10643 (OpenStreetMap E).

Regarding MRM functions in the osm2gmns tool, osm2gmns can parse the map data and output to GMNS comma-separated values (CSV) files with a few lines of Python code. Analysts can perform this function after downloading map data for the target region from OpenStreetMap. The following three simple lines of Python code can be used to perform this function:

```
>>> import osm2gmns as og

>>> net = og.getNetFromOSMFile('map.osm')

>>> og.outputNetToCSV(net)
```

It is notable that OpenStreetMap often represents one large intersection with multiple nodes to allow flexibility of user input. However, this structure makes the simulation of traffic signal timing very difficult. Accordingly, the research team developed a function to consolidate intersection nodes, that is, generate a new node to replace existing nodes for each intersection within a certain buffer, as shown in figure 47.

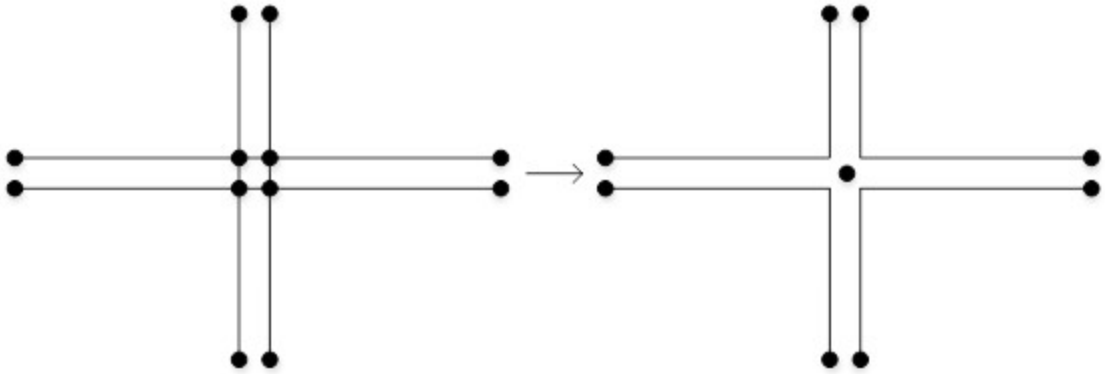

Source: FHWA.

Figure 47. Illustration. Automated consolidation of complex intersections from OpenStreetMap.

To facilitate multimodal modeling, the osm2gmns tool supports five different network types, including auto, bike, walk, railway, and aeroway. The osm2gmns can also import point-of-interest nodes and create connectors, as shown in figure 48.

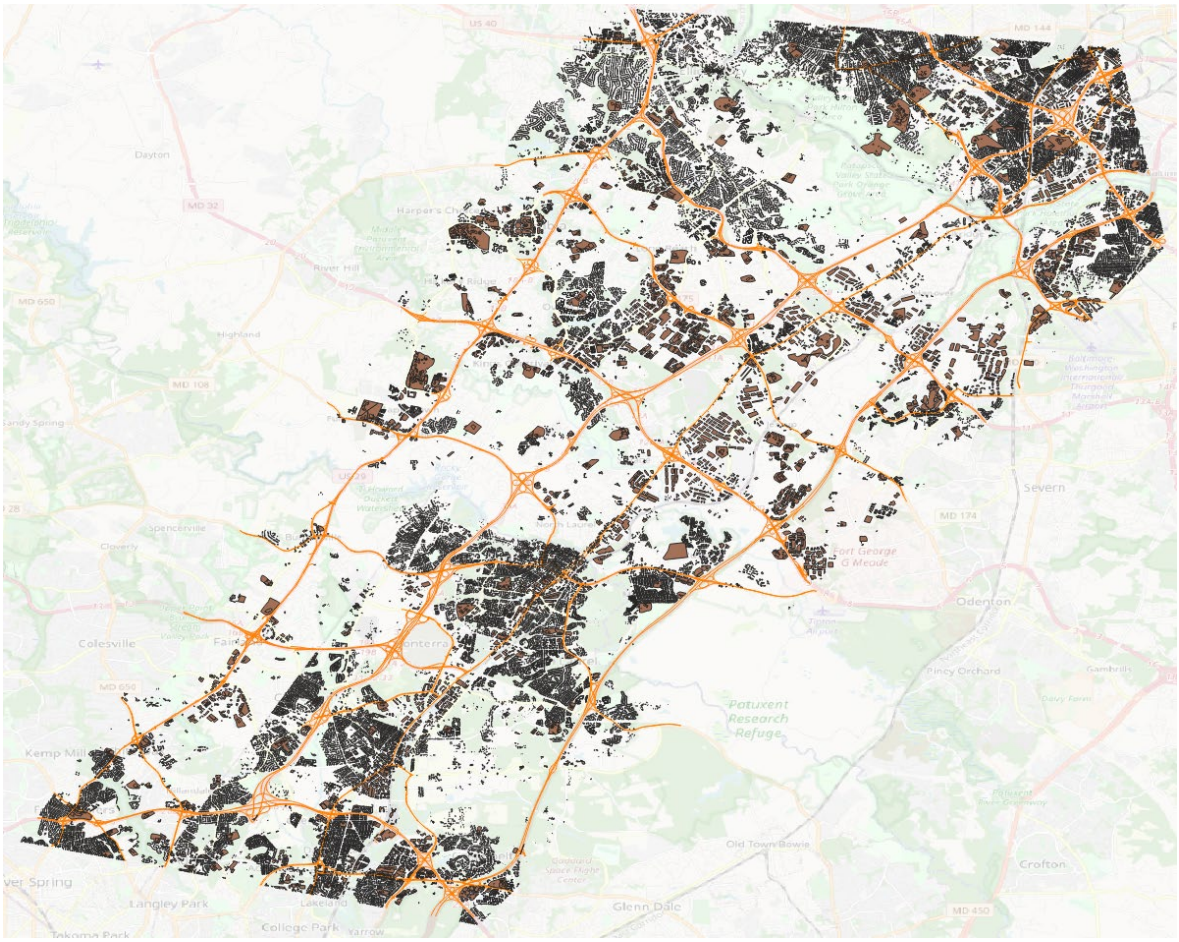

© 2021 OpenStreetMap contributors. Overlays of the points of interest added by FHWA.

Figure 48. Map. Maryland network with points of interest (OpenStreetMap D).

The research team applied a three-stage iterative calibration and validation approach to the base-year model. In the first stage, the team calibrated seed O-D matrices using an iterative path-based O-D adjustment algorithm for the time interval 4–11 a.m. The team used the 4–6 a.m. and 9–11 a.m. time intervals for warm-up and cool-down periods, respectively. Stage 1 includes the ODME procedure in DTALite to perform traffic assignment and achieve user equilibrium (Zhou and Taylor 2014). In stage 2, the team adjusted supply-side link parameters regarding link-level inflow, outflow and speed, and network bottleneck locations. Stage 3 includes the model consistency check where the team thoroughly inspected model performance metrics, to conduct local adjustments for both O-D and supply-side attributes.

The research team used travel time and speed validation to verify the model accuracy. Specifically, the output files of DTALite provide time-dependent travel time and the speed information for links and every individual's trip trajectory. The team systematically examined the corridor travel times and congestion heat maps based on spatiotemporal speed data.

This case study adopted and extended the GMNS-based representation for ABM, macrolayers, mesolayers, and microlayers of representation to achieve a hybrid-resolution network construction. The study adopted the GMNS standard for multiresolution transportation network representation even though the developers mainly designed GMNS for macroscopic networks. As a result, this MRM-oriented study extends the GMNS-based representation for both mesoscopic and microscopic networks.

Mesoscopic Network Representation

The mesoscopic network has more detailed information in the intersections than the original macroscopic network. In the mesoscopic network, the research team expanded each intersection represented by a node in the macroscopic network. The team built a connector link for each movement in the intersections to facilitate intersection modeling, especially for signalized intersections.

Macroscopic and mesoscopic networks have different link-level coding schemes. Macroscopic networks often represent a road segment between two adjacent intersections as a link. However, lane changes sometimes occur within a link, especially when close to intersections. Changes in terms of the number of lanes result in capacity changes, but the link attributes cannot properly reflect these changes. This issue may bring inconvenience or even potential errors when performing network modeling. In the GMNS standard, the segment.csv file stores lane changes. For each link with lane changes from a macroscopic network, the research team split and converted it to multiple mesoscopic links, so that each mesoscopic link has a homogeneous capacity.

Microscopic Network Representation

In the Maryland case study, microscopic networks use a lane-by-lane cell-based representation. Instead of a conceptual line segment, lanes now represent each link. To accurately describe vehicle motion status when moving on the road, the research team further discretized lanes into small cells, as shown in figure 49. The team lane also created changing cells to enable vehicles to

switch trajectories between lanes. Users can customize the length of cells to accommodate different modeling needs.

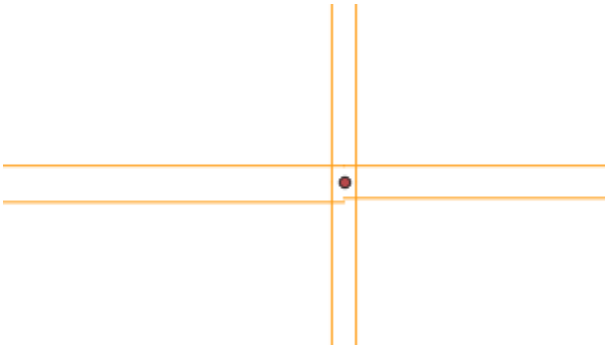

Source: FHWA.
A. Macroscopic network representation.

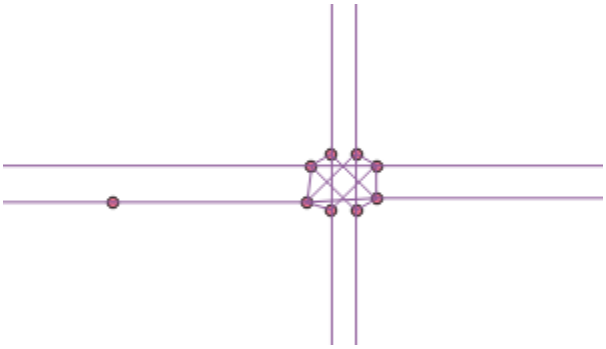

Source: FHWA.
B. Mesoscopic network representation.

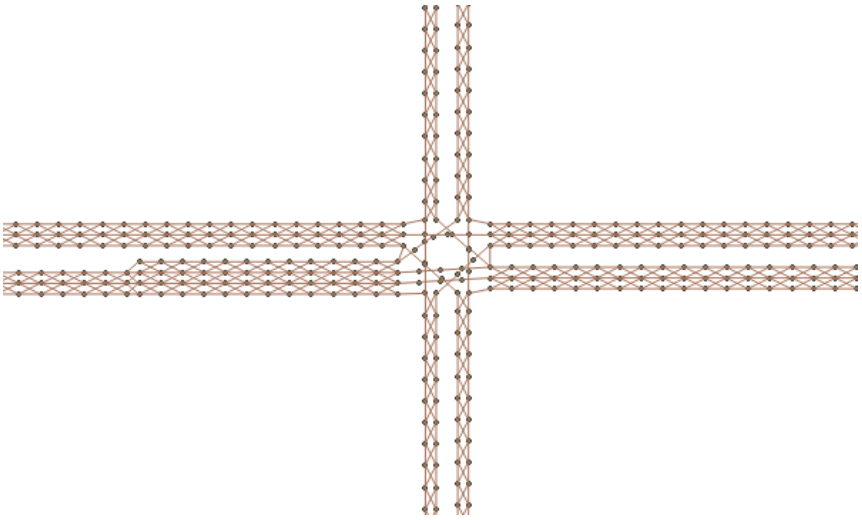

Source: FHWA.
C. Microscopic network representation.

Figure 49. Illustrations. Multiresolution network representations.

Enhancement of Tools (Gap 3.2)

To address gap 3.2 on enhancement of MRM tools, this case study adopted the GMNS format in a new analysis, modeling, and simulation (AMS) data hub framework. Table 20 illustrates a seven-step workflow process using GMNS. In this table:

- A/B Street is a traffic simulation game that explores how small changes to roads affect cyclists, transit users, pedestrians, and drivers (GitHub 2021).
- DTALite is a queue-based mesoscopic traffic simulator (Zhou and Taylor 2014).

- grid2demand is a data conversion tool to generate zone-to-zone travel demand based on grid cells (Python Package Index 2021c).
- GTFS2GMNS is a data conversion tool to directly convert GTFS data into the GMNS format (Arizona State University Transportation Artificial Intelligence Laboratory 2021).
- net2cell is a data conversion tool to automatically generate hybrid transportation networks to accommodate different modeling needs (Python Package Index 2021b).
- osm2gmns is a data conversion tool to directly convert OSM map data to node and link network files into the GMNS format (Python Package Index 2021a).
- QGIS is a free, open-source geographic information system (QGIS 2021).
- Sigma-X is a spreadsheet-based computational engine for signalized intersections (Zlatkovic 2021).
- vol2timing is a GMNS-based signal timing generation tool for multi-resolution modeling (Python Package Index 2021d).

Table 20. AMS workflow process involving the GMNS.

Step	Description	Software	Input Files	Output Files
0	OSM data download	OSM	N/A	map.osm
1	Convert OSM data to GMNS	osm2gmns	map.osm	node.csv, link.csv, poi.csv
2	Convert GTFS data to GMNS	GTFS2GMNS	Open transit data GTFS	node.csv, link.csv, poi.csv
3	Expand macroscopic network data to micro, meso	net2cell	node.csv, link.csv	Mesonetworks, and micronetworks in node.csv and link.csv
4	Zone-to-zone travel demand	grid2demand	node.csv, link.csv, poi.csv, poi_trip_rate.csv	demand.csv, zone.csv, accessibility.csv, input_agent.csv
5	Traffic signal for timing	vol2timing, Sigma-X	node.csv, link.csv, movement.csv	timing.csv
6	AMS simulation	A/B Street, DTALite	demand.csv, node.csv, link.csv, input_agent.csv	agent.csv, link_performance.csv
7	Visualization	QGIS, NeXTA	node.csv, link.csv, movement.csv, zone.csv, demand.csv	N/A

GTFS = General Transit Feed Specification OSM = OpenStreetMap.

Performance Measure Consistency (Gap 2.4 and Gap 3.6)

To address gap 2.4 and gap 3.6 in terms of performance measure consistency, the research team also used the congestion and bottleneck identification (CBI) tool (Hale et al. 2016, 2021) to identify bottlenecks and estimate the congestion duration by following these steps: First, one can visit the Regional Integrated Transportation Information System website, click “Tool Catalog” in

the horizontal navigation bar, and then use the find function (Ctrl-F) to search for the massive data downloader (CATT Lab 2021). Second, one can search the road name, and then select data attributes with a data averaging level. The downloaded data are available within data readings.csv and TMC_identification.csv, which the CBI tool can read directly. Figure 50 shows the interface and the speed heat map in the CBI tool.

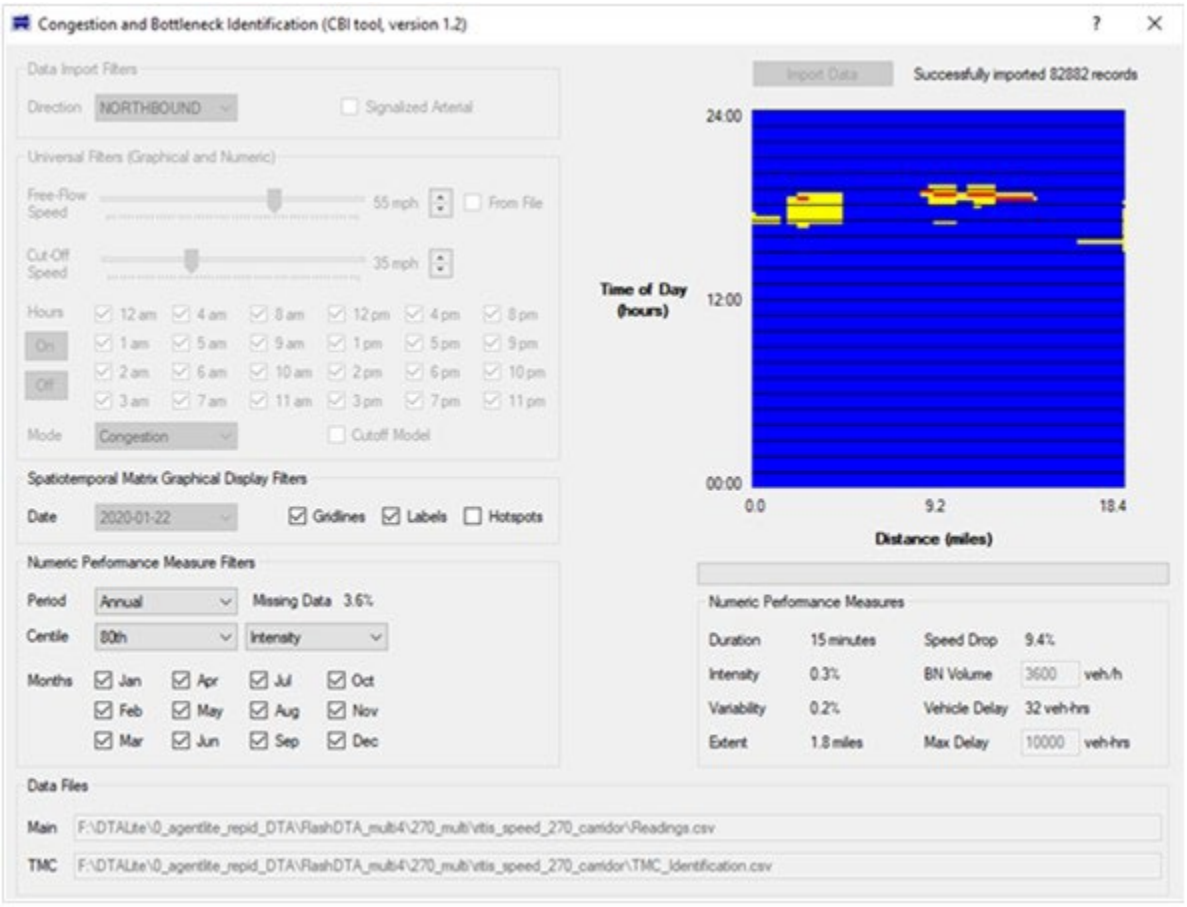

Source: FHWA.
BN = bottleneck; veh/h = vehicles per hour; veh-hrs = vehicle-hours.

Figure 50. Screenshot. Field-measured speed heat map in the CBI tool.

Signal Timing Methods and Tools (Gap 3.1 and Gap 3.2)

The Maryland case study demonstrates the efficient transfer of signal timing data between the different resolutions of MRM. Although different modeling resolutions involve fundamentally different inputs for traffic signal timings, the case study addresses gap 3.1 by converting signal timings to multiple formats. And although certain analyses involve estimating or optimizing the signal timings as a function of limited available data, the case study addresses gap 3.2 by implementing enhanced signal timing tools designed for MRM. For a large-scale network, it is typically difficult to collect all signal control data in the MRM system. The research team used a traffic signal timing configuration tool, Sigma-X, to generate default signal plans for intersections (Zlatkovic and Zhou 2015; Zlatkovic 2021). Sigma-X adopts the *HCM* 2010 methodology for signalized intersection analysis (Transportation Research Board 2010).

Sigma-X is also extendable to other methodologies for computing parameters of signalized intersections, as described in the *Traffic Signal Timing Manual* (Koonce and Rodegerdts 2008). Analysts can use Sigma-X as a stand-alone application or integrate it with the MRM data hub. Analysts can collect additional timing data from the operating agencies that manage the arterial and freeway corridors, and then input additional data such as green wave band and offsets for complex intersections and corridor-level signal timing coordination.

Benefit of MRM (Gap 3.6 and Gap 6.1)

The effective integration of different AMS tools should carefully address gap 3.6 (feedback loop in internally consistent cross-resolution traffic representation). For example, the integration of microsimulation tool outputs into macroscopic demand models could provide improved accessibility indicators from the agent-based traffic simulation model to the upper-level demand model. Accordingly, the macroscopic demand model could further adjust the demand to be loaded in the lower-level representation.

Without systematic O-D demand calibration and supply-side calibration as shown in chapter 2 and chapter 3, simply loading initial demand into a microsimulation network could lead to unrealistic oversaturated conditions. In addition, analysts and planners should also address gap 6.1 (the transportation agency valuation of the MRM implementation benefits), because the exchange of accurate roadway attributes across open data and existing planning models could be mutually beneficial.

Multimodal Modeling (Gap 3.3)

An important investigation of this study is to determine the benefit of using an open-data format to enable the effective integration of existing microsimulation tools, as stated in step 6 in table 20. There are many challenges in preparing a microsimulation network based on available macroscopic maps. Specifically, coding networks, preparing O-D demand, and preparing traffic signal timing data could be very time consuming and prone to errors, which could still require a significant amount of consulting resources and planning staff time. In this study, the research team built a system prototype of MRM based on A/B Street (Carlino, Li, and Kirk 2021). Rather than focusing on simulation model calibration with available data, the goal in this task is to demonstrate how to utilize available open-source or commercial simulation platforms through open-data and open-specification ecosystems.

Unlike traditional microsimulation tools in the highway engineering field, A/B Street aims to help planners work with community partners to evaluate the benefit of multimodal decisionmaking. The scenarios that A/B Street can evaluate relate to road configuration changes that affect cyclists, transit users, pedestrians, and drivers. The A/B Street user interface and graphical animation screens can provide subarea maps that show which modes of travel (e.g., passenger cars, bicycles, transit vehicles, and pedestrians) are using each roadway segment. The user can also zoom in to intersections to view transit routes, buses, trains, bus lanes, transit stops, pedestrians, and passenger cars.

As stated in table 20, the AMS tool A/B Street utilizes open multimodal network data from OpenStreetMap (OpenStreetMap Contributors 2021). The research team used the open standard

of GMNS to create and share the demand and signal timing data for generic macroscopic and mesoscopic GMNS networks. The developers of A/B Street follow GMNS principles to import both demand scenarios and signal timing data from this open-data ecosystem. Through this streamlined process, community stakeholders and planners can use such integrated MRM models for quick, inexpensive prototyping of new traffic management scenarios. This process further provides a potential for creating new forms of citizen engagement by communities, and new approaches to city operations and management by city planners. In the long run, the proposed open-data and open-source framework also intends to create a user community of software developers and users in this emerging area across different geographically distributed communities.

Cost and Time Requirements (Gap 1.3)

A free open package and open-data ecosystem could dramatically reduce the cost and complexity of managing computers and simulation models, bringing benefits within the traditional domains of city planning, and community policy analysis. This paradigm could provide a cost effective and customized, but coordinated, way to create a digital representation. This representation would enable different communities to build their own versions of a high-fidelity virtual model from different open and user-contributed data sources.

Analysis Results

The research team used the weighted mean squared error (WMSE), shown in figure 51, to calculate the difference between simulation results and the observed data.

$$WMSE = \sqrt{\frac{\sum_{i=1}^{N}\sum_{t=1}^{T}\left(y_{i,t}^{*} - y_{i,t}\right)^2}{\sum_{i=1}^{N}\sum_{t=1}^{T} y_{i,t}^2}}$$

Figure 51. Equation. WMSE formula.

Where:

N = total number of sensors.
T = total number of time intervals.
$y_{i,t}$ = observed traffic volume or travel time for link i at time t.
$y^{*}_{i,t}$ = simulated traffic volume or travel time for link i at time t.

Table 21 and table 22 summarize the calibration results for traffic link counts and corridor travel times in both directions of travel.

Table 21. Traffic count calibration results for the Maryland case study.

Corridor Direction	WMSE (Percent)	Average Observed Counts per Hour	Average Simulated Counts per Hour	Number of Count Sensors
I–95 NB	9.5	5,990	5,766	15
I–95 SB	18.3	6,063	5,218	18

Table 22. Travel time calibration results for the Maryland case study.

Corridor Direction	Seed Model WMSE (Percent)	Calibrated WMSE (Percent)
I–95 NB	15.9	5.7
I–95 SB	143.4	7.9

SUMMARY

Based on an existing ABM-DTA modeling system, the Maryland I–95 case study demonstrates a next-generation traffic model development procedure, using a common data format to seamlessly represent all three levels of analysis (i.e., macroscopic, mesoscopic, and microscopic). The development of a streamlined workflow enables the effective integration of AMS tools across various domains and scales. The streamlined workflow also enables information and data to be easily exchanged at both the input and output levels. To succeed in meeting the MRM objectives, the authors suggest that the following principles should guide the building of open-data and open-source ecosystems:

- Open-source data specifications, which can precisely represent a multiresolution physical traffic system and support secure data sharing, lay the foundation for guiding the AMS method and tool development. Other teams in the transportation planning area should work with the Zephyr Foundation to promote use of the General Travel Network Specification, which aims to advance the field through flexible and efficient support, education, guidance, encouragement, and incubation (Zephyr Foundation 2020b).

- Effective AMS integration requires enterprise-grade open-source tools and coordinated MRM data sharing among public sectors, including metropolitan planning organizations and State departments of transportation, private software vendors, community citizens, and planners.

- The feedback loops between MRM computational engines, demand-side and supply-side calibration across different resolution levels, are the theoretical foundation in the effective integration of a wide range of software packages.

CHAPTER 5. CONCLUSION

During the FHWA MRM project, the research team spent a few months on literature reviews and stakeholder meetings to identify gaps that could be preventing a wider adoption of MRM. The authors of this report also developed an MRM state-of-practice and gap analysis report, which will be published separately (Zhou, Hadi, and Hale 2021). The identified gaps helped to inform the MRM case studies described in this report. Chapter 1 of this report summarized the ways in which the three case studies (i.e., West Palm Beach downtown, Phoenix metropolitan area, and Maryland I–95) addressed these gaps.

In most instances, the case studies did not attempt to address high-level institutional activities such as procurement, staff training, and shifting the culture, although chapter 2 briefly touched on a few such items. Instead, the case studies focused on several of the key technical challenges that analysts face when contemplating or conducting MRM analyses. Chapter 2, chapter 3, and chapter 4 supply many of the details for addressing these challenges, with each chapter focusing on one of the three case studies. The technical challenges include how to:

- Develop an MRM model.
- Estimate the benefits and costs of MRM.
- Select and apply the right tools to facilitate use of MRM.
- Select and apply the right options for demand estimation and traffic assignment.
- Efficiently develop realistic and effective traffic signal timings for all modeling resolutions.
- Estimate the impacts of feedback and convergence among the different modeling resolutions.
- Reconcile fundamental differences in the performance measures used by different modeling resolutions.

The authors of this report also developed an MRM guidebook, which will be published separately.[1] The case studies helped to inform the guidebook material. The authors developed a generalized MRM methodology and devoted a chapter to this in the guidebook. Table 1 in this report summarizes the connections between the identified MRM gaps, the case studies that address those gaps, and steps of the MRM methodology that address those gaps. The MRM guidebook also contains a chapter to summarize the case study outcomes, albeit in much less detail than is given in this report.

WEST PALM BEACH LESSONS LEARNED

In the West Palm Beach Downtown case study, the research team used all three modeling resolutions to model the same spatial and temporal network limits. The team also used the commercial modeling tool—which includes macroscopic, mesoscopic, and microscopic models—to automatically generate their microscopic simulation model from the lower resolution models. These steps significantly decreased the required effort for MRM, particularly

[1]Zhou, X., M. Hadi, and D. Hale. Forthcoming. *Multiresolution Modeling for Traffic Analysis Guidebook*. Washington, DC: Federal Highway Administration.

considering that the temporal and spatial limits of the models in the three resolutions were the same. The team generally found that SBA and DTA were more effective than STA for achieving consistent and realistic results across all modeling resolutions, although they cautioned that SBA and DTA effectiveness are highly dependent on choosing the right parameters. The team strongly recommended using intersection turn movement counts to calibrate the O-D demands for operational studies and working closely with demand forecasting modelers to improve the demand forecasting model results. The team also found that increasing the consistency between the three resolutions was helpful in improving the modeling results. This increase in consistency involved updating the macroscopic and mesoscopic models to use the link capacities, as assessed by the microscopic simulation model, and to use traffic flow model parameters derived from the microscopic model.

PHOENIX LESSONS LEARNED

In the Phoenix metropolitan area case study, the research team demonstrated a robust VDF calibration process that exploits speed and volume data from the field. This robust calibration enabled the VDF to accurately reflect a variety of congestion regimes, time periods, ATs, and FTs. By explicitly considering the D/C ratio rather than the traditional v/c ratio, the robust process is more effective for analyzing and modeling oversaturated traffic conditions. Finally, by explicitly incorporating speed and volume data from the field, the demonstrated calibration process can help to increase users' confidence in the final results, relative to the more traditional approaches.

MARYLAND LESSONS LEARNED

In the Maryland I–95 case study, the research team demonstrated the use of open-source tools for efficiently building MRM networks. The tools can convert map data available through OpenStreetMap to macroscopic GMNS network files. They can further generate corresponding mesoscopic and microscopic networks. The GMNS format facilitates enhanced calibration of traffic bottleneck locations, durations, and capacities using probe data. GMNS also facilitates generation of traffic signal timing data for all scenarios. For all modeling resolutions, GMNS allows a more consistent definition of bottleneck locations and intersection turning movements. Although GMNS is not yet compatible with all simulation tools, and does not yet support all types of simulation input data, the open-source tools described in chapter 4 can help users of all tools to generate and/or transfer some of the most challenging MRM data (e.g., O-D demands, signal timings, bottleneck parameters).

ACKNOWLEDGMENTS

For figure 1, the original map is the copyright property of OpenStreetMap contributors and can be accessed from https://www.openstreetmap.org.

For figure 23, the original maps are the copyright property of OpenStreetMap contributors and can be accessed from https://www.openstreetmap.org. The lines and numerical overlays were added by FHWA as a part of this project.

For figure 24, the original maps are the copyright property of OpenStreetMap contributors and can be accessed from https://www.openstreetmap.org. The lines and numerical overlays were added by FHWA as a part of this project.

For figure 28, the original maps are the copyright property of OpenStreetMap contributors and can be accessed from https://www.openstreetmap.org. The lines were added by MAG based on a screenshot of the QGIS software package.

For figure 44, the original maps are the copyright property of OpenStreetMap contributors and can be accessed from https://www.openstreetmap.org. The overlays were added by FHWA as a part of this project.

For figure 45, the original map is the copyright property of OpenStreetMap contributors and can be accessed from https://www.openstreetmap.org. Overlays of the modeled network were added by FHWA as part of this project.

For figure 46, the original map is the copyright property of OpenStreetMap contributors and can be accessed from https://www.openstreetmap.org. Overlays of the modeled network were added by FHWA as part of this project.

For figure 48, the original map is the copyright property of OpenStreetMap contributors and can be accessed from https://www.openstreetmap.org. Overlays of the modeled network were added by FHWA as part of this project.

REFERENCES

Akçelik, R. 1991. "Travel Time Functions for Transport Planning Purposes: Davidson's Function, Its Time Dependent Form and Alternative Travel Time Function." *Australian Road Research*, 21, no. 3: 44–59.

Arizona State University Transportation Artificial Intelligence Laboratory. "GTFS2GMNS" (web page). https://githubmemory.com/repo/asu-trans-ai-lab/GTFS2GMNS, last accessed March 16, 2021.

AZTech. n.d. "ADOT Freeway Management System" (web page). http://www.aztech.org/Projects/ADOTFMS, last accessed March 15, 2021.

Belezamo, B. 2020. "Data-Driven Methods for Characterizing Transportation System Performances Under Congested Conditions: A Phoenix Study." Doctoral dissertation. Arizona State University.

Bentley Systems, Inc. 2021. "Transportation and Land-use Modeling" (web page). https://www.bentley.com/en/products/brands/cube, last accessed March 6, 2021.

Bureau of Public Roads. 1964. *Traffic Assignment Manual: For Application with a Large, High Speed Computer*. Washington, DC: U.S. Department of Commerce, Urban Planning Division.

Carlino, D., Y. Li, and M. Kirk. 2021. "A traffic simulation game exploring how small changes to roads affect cyclists, transit users, pedestrians, and drivers" (web page). https://github.com/a-b-street/abstreet, last accessed March 16, 2021.

CATT Lab. "Regional Integrated Transportation Information System CATT Lab" (web page). https://www.cattlab.umd.edu/?portfolio=ritis, last accessed March 10, 2021.

Dowling, R, W. Kittelson, J. Zegeer, and A. Skabardonis. 1997. *Planning Techniques to Estimate Speeds and Service Volumes for Planning Applications.* Report No. NCHRP 387. Washington, DC: Transportation Research Board of the National Academies. http://onlinepubs.trb.org/Onlinepubs/nchrp/nchrp_rpt_387.pdf, last accessed December 9, 2021.

Dowling, R., A. Horowitz, and W. McShane. 1999. *Planning Applications for the Year 2000 Highway Capacity Manual*. Report No. NCHRP 3-55(2)A. Washington, DC: Transportation Research Board of the National Academies. http://onlinepubs.trb.org/onlinepubs/archive/NotesDocs/finerep.pdf, last accessed December 9, 2021.

Dowling, R. 2007. *Traffic Analysis Toolbox Volume VI: Definition, Interpretation, and Calculation of Traffic Analysis Tools Measures of Effectiveness*. Report No. FHWA-HOP-08-054. Washington, DC: Federal Highway Administration.

Drabicki, A., R. Kucharski, and A. Szarata. 2017. "Modelling the Public Transport Capacity Constraints' Impact on Passenger Path Choices in Transit Assignment Models." *Archives of Transport* 43, no. 3. http://www.archivesoftransport.com/eaot/2017/03/001.pdf, last accessed December 8, 2021.

Federal Highway Administration. 2012. *Creating an Effective Program to Advance Transportation Systems Management and Operations: Primer*. Report No. FHWA-HOP-12-003. Washington, DC. https://ops.fhwa.dot.gov/publications/fhwahop12003/index.htm, last accessed December 15, 2021.

Florida Department of Transportation. 2014. *Traffic Analysis Handbook: A Reference for Planning and Operations*. Tallahassee, FL: Florida Department of Transportation.

FSUTMSOnline. "Southeast Florida Regional Planning Model (SERPM)" (web page). https://www.fsutmsonline.net/index.php?/model_pages/modD44/index/, last accessed April 23, 2021.

Hadi, M., S. Shabanian, H. Ozen, and Y. Xiao, M. Doherty, C. Segovia, and H. Ham. 2013. *Application of Dynamic Traffic Assignment to Advanced Managed Lane Modeling*. Report Submitted to Florida Department of Transportation. Miami, FL: Florida International University.

Hadi, M., Y. Xiao, T. Wang, S. Qom, L. Azizi, J. Jia, A. Massahi, and M.S. Iqbal. 2016. *Framework for Multi-Resolution Analyses of Advanced Traffic Management Strategies*. Report Submitted to Florida Department of Transportation. Miami, FL: Florida International University.

Hadi, M., Y. Xiao, M. Iqbal, T. Wang, M. Arafat, and F. Hoque. 2019. *Estimation of System Performance and Technology Impacts to Support Future Year Planning*. Report Submitted to Florida Department of Transportation. Miami, FL: Florida International University.

Hale, D., G. Chrysikopoulos, A. Kondyli, and A. Ghiasi. 2021. "Evaluation of Data-Driven Performance Measures for Comparing and Ranking Traffic Bottlenecks." *IET Intelligent Transportation Systems* 15, no. 4: 504–513. https://doi.org/10.1049/itr2.12040, last accessed December 10, 2021.

Hale, D., R. Jagannathan, M. Xyntarakis, P. Su, X. Jiang, J. Ma, J. Hu, and C. Krause. 2016. *Traffic Bottlenecks: Identification and Solutions*. Report No. FHWA-HRT-16-064. Washington, DC: Federal Highway Administration.

HERE Technologies. 2021. "All your location data and software in one platform" (web page). https://www.here.com/, last accessed March 15, 2021.

Horowitz, A., T. Creasey, R. Pendyala, and M. Chen. 2014. *Analytical Travel Forecasting Approaches for Project-Level Planning and Design*, National Cooperative Highway

Research Program Report 08-83. Washington, DC: Transportation Research Board of the National Academies.

Huntsinger, L. F., and N. M. Rouphail. 2011. "Bottleneck and Queuing Analysis: Calibrating Volume–Delay Functions of Travel Demand Models." *Transportation Research Record* 2255, no. 1: 117–124.

INRO. 2020. "MAG Selects Dynameq for Multimodal ABM-DTA Initiative." *INRO* (blog), October 29, 2020, https://info.inrosoftware.com/blog/dynameq-selected-by-mag, last accessed May 5, 2021.

Koonce, P., and L. Rodegerdts. 2008. *Traffic Signal Timing Manual*. Report No. FHWA-HOP-08-024. Washington, DC: Federal Highway Administration.

Lin, W. 2006. "A Robust Model for Estimating Freeway Dynamic Origin-Destination Matrices." Doctor of Philosophy dissertation. College Park, MD: University of Maryland.

Mahut, M. 2001. "A Discrete Flow Model for Dynamic Network Loading." Doctor of Philosophy dissertation. University of Montreal.

Martin, W. 1998. *Travel Estimation Techniques for Urban Planning*. National Cooperative Highway Research Program Report 365. Washington, DC: Transportation Research Board of the National Academies.

McTrans. 2021. "HCS™ Highway Capacity Software™" (web page). https://mctrans.ce.ufl.edu/mct/index.php/hcs/, last accessed March 11, 2021.

Moses, R., E. Mtoi, S. Ruegg, and H. McBean. 2013. *Development of Speed Models for Improving Travel Forecasting and Highway Performance Evaluation*. Project No. BDK83. Tallahassee, FL: Florida Department of Transportation.

OpenStreetMap Contributors. 2021. "OpenStreetMap" (web page). https://www.openstreetmap.org/, last accessed August 18, 2021.

OpenStreetMap A. West Palm Beach, FL. August 19, 2021. Scale: 1:12,000 ft. https://www.openstreetmap.org/search?query=west%20palm%20beach#map=15/26.7142/-80.0646, last accessed August 19, 2021.

OpenStreetMap B. West Palm Beach, FL. August 19, 2021. Scale: 1:6,000 ft. https://www.openstreetmap.org/search?query=west%20palm%20beach#map=16/26.7101/-80.0669, last accessed August 19, 2021.

OpenStreetMap C. Phoenix, AZ. August 19, 2021. Scale: 1:633,600 ft. https://www.openstreetmap.org/search?query=Phoenix%20Arizona#map=9/33.4727/-112.0473, last accessed August 19, 2021.

OpenStreetMap D. Maryland Interstate 95, Laurel, MD, August 19, 2021. Scale: 1:190,080 ft. https://www.openstreetmap.org/search?query=maryland%20interstate%2095#map=11/39.0996/-76.9063, last accessed August 19, 2021.

OpenStreetMap E. Beltsville, Maryland. August 19, 2021. Scale: 1:600 ft https://www.openstreetmap.org/search?query=Beltsville%20Maryland#map=19/39.03483/-76.90740, last accessed August 19, 2021.

Palm Beach County. 2020. *Intermodal Transit Center Relocation—West Palm Beach Traffic Modeling and Analysis Project #2020-026787 Final Report*. West Palm Beach, FL: Palm Beach County.

Palm Tran. "myStop" (web page). http://www.palmtran.org/igo, last accessed April 29, 2021.

PTV Group. 2021a. *PTV Vissim 11 User Manual*. Karlsruhe, Germany: PTV AG.

PTV Group. 2021b. *PTV Visum 2020 - Manual*. Karlsruhe, Germany: PTV AG.

Python Package Index. 2021a. "osm2gmns" (web page). https://pypi.org/project/osm2gmns/, last accessed March 16, 2021.

Python Package Index. 2021b. "net2cell" (web page). https://pypi.org/project/net2cell/, last accessed March 16, 2021.

Python Package Index. 2021c. "grid2demand" (web page). https://pypi.org/project/grid2demand/, last accessed March 16, 2021.

Python Package Index. 2021d. "vol2timing" (web page). https://pypi.org/project/vol2timing/, last accessed March 16, 2021.

QGIS. 2021. "Welcome to the QGIS Project!" (web page). https://www.qgis.org/en/site/, last accessed March 16, 2021.

Spiess, H. 1984. "Contributions à la Théorie et aux Outils de Planification de Réseaux de Transport Urbain." Doctor of Philosophy thesis. Université de Montréal, publication 382.

Tisato, P. 1991. "Suggestions for an Improved Davidson Travel Time Function." *Australian Road Research* 21, no. 2: 85–100.

Transportation Research Board. 2010. *Highway Capacity Manual: HCM2010*. Washington, DC: Transportation Research Board of the National Academies.

Virginia Department of Transportation. 2020. *VDOT VISSIM Microscopic Simulation Tool User Guide, Version 2.0*. Richmond, VA: Virginia Department of Transportation. https://www.virginiadot.org/business/resources/VDOT_Vissim_UserGuide_Version2.0_Final_2020-01-10.pdf, last accessed January 10, 2022.

Wiedemann, R. 1974. “Simulation des Strassenverkehrsflusses.” Doctor of Philosophy dissertation. Karlsruhe, Germany: Universitaet Karlsruhe.

Wisconsin Department of Transportation. 2018. “Traffic Forecasting, Travel Demand Models and other Planning.” In *Transportation Planning Manual*. Madison, WI: Wisconsin Department of Transportation.

Wisconsin Department of Transportation. 2019. “Traffic Analysis and Modeling: Microscopic Simulation Traffic Analysis.” Chapter 16, section 20 in *Traffic Engineering, Operations, & Safety Manual*. Madison, WI: Wisconsin Department of Transportation. https://wisconsindot.gov/dtsdManuals/traffic-ops/manuals-and-standards/teops/16-25.pdf, last accessed December 20, 2021.

Wu, X. B., A. Dutta, Z. Wang, H. Zhu, V. Livshits, and X.S. Zhou. 2021. *Characterization and Calibration of Volume-to-Capacity Ratio in Volume-Delay Functions on Freeways Based on a Queue Analysis Approach*. Report No. TRBAM-21-04304. Washington, DC: Transportation Research Board of the National Academies.

Xiong, C., X. Zhou, and L. Zhang. 2018. “AgBM-DTALite: An Integrated Modelling System of Agent-Based Travel Behaviour and Transportation Network Dynamics.” *Travel Behaviour and Society* 12: 141–150.

Zephyr Foundation. 2020a. “Network Data Standard and Management Tools” (web page). https://zephyrtransport.org/projects/2-network-standard-and-tools/, last accessed March 14, 2021.

Zephyr Foundation. 2020b. “General Travel Network Specification” (web page). https://zephyrtransport.org/trb17projects/7-general-travel-network-specification/, last accessed May 6, 2021.

Zhou, X., and G.F. List. 2010. “An Information-Theoretic Sensor Location Model for Traffic Origin-Destination Demand Estimation Applications.” *Transportation Science* 44, no. 2: 254–273.

Zhou, X, M. Hadi, and D. Hale. 2021. *Multiresolution Modeling for Traffic Analysis: State-of-Practice and Gap Analysis Report.* Report No. FHWA-HRT-21-082. Washington, DC: Federal Highway Administration. https://www.fhwa.dot.gov/publications/research/operations/21082/index.cfm, last accessed December 16, 2021.

Zhou, X., and J. Taylor. 2014. “DTAlite: A Queue-Based Mesoscopic Traffic Simulator for Fast Model Evaluation and Calibration.” *Cogent Engineering* 1, no 1: 961345. https://doi.org/10.1080/23311916.2014.961345, last accessed December 10, 2021.

Zlatkovic, M. 2021. “Excel-based computational engine for signalized intersections” (web page). https://github.com/milan1981/Sigma-X, last accessed March 16, 2021.

Zlatkovic, M., and X. Zhou. 2015. “Integration of Signal Timing Estimation Model and Dynamic Traffic Assignment in Feedback Loops: System Design and Case Study.” *Journal of Advanced Transportation* 49, no. 6: 683–699.

Recycled
Recyclable

Recommended citation: Federal Highway Administration,
Multiresolution Modeling for Traffic Analysis: Case Studies Report
(Washington, DC: 2022) https://doi.org/10.21949/1521855.

HRSO-50/2-22(WEB)E